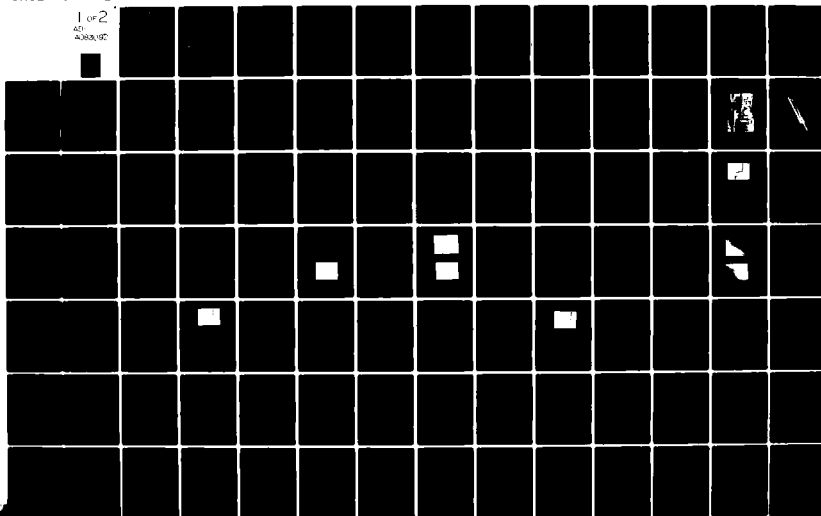


AD-A083 092

RESEARCH TRIANGLE INST RESEARCH TRIANGLE PARK N C F/G 10/2
DEVELOPMENT OF HIGH EFFICIENCY STACKED MULTIPLE BANDGAP SOLAR C--ETC(U)
OCT 79 S M BEDAIR, J R HAUSER, M F LAMORTE F33615-78-C-2077
RTI-41U-1678 AFAPL-TR-79-2116 NL

UNCLASSIFIED

1 of 2
40
4088/9C



ADA 083092

AFAPL-TR-79-2116

LEVEL II

(2)
4

DEVELOPMENT OF HIGH EFFICIENCY, STACKED MULTIPLE BANDGAP SOLAR CELLS

*RESEARCH TRIANGLE INSTITUTE
POST OFFICE BOX 12194
RESEARCH TRIANGLE PARK, NC 27709*

OCTOBER 1979

TECHNICAL REPORT AFAPL-TR-79-2116
Final Report for period 1 August 1978 - 30 September 1979

Approved for public release; distribution unlimited.

AIR FORCE AERO PROPULSION LABORATORY
AIR FORCE WRIGHT AERONAUTICAL LABORATORIES
AIR FORCE SYSTEMS COMMAND
WRIGHT-PATTERSON AIR FORCE BASE, OHIO 45433

DTIC
ELECTE
S APR 15 1980
E

DDC FILE COPY.


80 4 14 051

NOTICE


When Government drawings, specifications, or other data are used for any purpose other than in connection with a definitely related Government procurement operation, the United States Government thereby incurs no responsibility nor any obligation whatsoever; and the fact that the government may have formulated, furnished, or in any way supplied the said drawings, specifications, or other data, is not to be regarded by implication or otherwise as in any manner licensing the holder or any other person or corporation, or conveying any rights or permission to manufacture, use, or sell any patented invention that may in any way be related thereto.

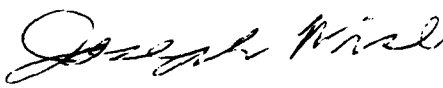
This report has been reviewed by the Information Office (OI) and is releasable to the National Technical Information Service (NTIS). At NTIS, it will be available to the general public, including foreign nations.

This technical report has been reviewed and is approved for publication.


W. PATRICK RAHILLY
Project Engineer
Energy Conversion Branch

FOR THE COMMANDER


JAMES D. REANS
Chief, Aerospace Power Division
Aero Propulsion Laboratory


JOSEPH F. WISE
TAM, Solar Energy Conversion
Energy Conversion Branch

"If your address has changed, if you wish to be removed from our mailing list, or if the addressee is no longer employed by your organization please notify AFWAL/POOC-2, W-PAFB, OH 45433 to help us maintain a current mailing list".

Copies of this report should not be returned unless return is required by security considerations, contractual obligations, or notice on a specific document.

REPORT DOCUMENTATION PAGE		READ INSTRUCTIONS BEFORE COMPLETING FORM
1. REPORT NUMBER AFAPL-TR-79-2116 ✓	2. GOVT ACCESSION NO.	3. RECIPIENT'S CATALOG NUMBER
4. TITLE (and Subtitle) Development of High Efficiency Stacked Multiple Bandgap Solar Cells.		5. TYPE OF REPORT & PERIOD COVERED Technical 8/1/78 to 9/30/79
7. AUTHOR(s) S. Bedair, J. R. Hauser, M. F. Lamorte, S. Phatak, M. L. Timmons, J. E. Andrews, M. Simons		6. PERFORMING ORG. REPORT NUMBER -41U-1678
9. PERFORMING ORGANIZATION NAME AND ADDRESS Research Triangle Institute Research Triangle Park, NC 27709;		8. CONTRACT OR GRANT NUMBER(s) F33615-78-C-2077 ew
11. CONTROLLING OFFICE NAME AND ADDRESS Air Force Aero-Propulsion Laboratory Attn: AFAPL/POE-2; Rahilly Wright-Patterson AFB, Ohio 45433		10. PROGRAM ELEMENT, PROJECT, TASK AREA & WORK UNIT NUMBERS 15/1021
14. MONITORING AGENCY NAME & ADDRESS (if different from Controlling Office)		12. REPORT DATE Oct 1979
		13. NUMBER OF PAGES 99
		15. SECURITY CLASS. (of this report) Unclassified
		15a. DECLASSIFICATION/DOWNGRADING SCHEDULE
16. DISTRIBUTION STATEMENT (of this Report) Approved for public release; distribution unlimited.		
17. DISTRIBUTION STATEMENT (of the abstract entered in Block 20, if different from Report) Final 1.1 10-79 5/1/79		
18. SUPPLEMENTARY NOTES		
19. KEY WORDS (Continue on reverse side if necessary and identify by block number) Cascade Solar Cells, Multi-junction Solar Cells, III-V Compound Semiconductors, Gallium Arsenide		
20. ABSTRACT (Continue on reverse side if necessary and identify by block number) The objective of this research was to develop the technology required to fabricate two-junction, cascade solar cell assemblies having conversion efficiencies exceeding 25 percent when operating at 25°C under 1 sun, AM 0 conditions. The experimental effort has focused on several different III-V ternary and quaternary materials that show promise for use in fabricating a cascade cell. These include GaAlAs, GaInAs, GaInP, GaAsSb, and GaAlAsSb. The work also includes theoretical calculations of cascade solar cell performance over a wide range of operating temperatures.		

FOREWORD

The work described in this report involved a cooperative effort between the Research Triangle Institute, Research Triangle Park, North Carolina and North Carolina State University, Raleigh, North Carolina. The work was conducted between August 1, 1978 and September 30, 1979 under the direction of the Air Force Aero-Propulsion Laboratory, Wright-Patterson Air Force Base, Ohio. W. Patrick Rahilly (AFAPL/POE-2) was the Air Force Project Engineer.

The authors of this report were S. M. Bedair, J. R. Hauser, M. F. Lamorte, S. Phatak, M. L. Timmons, J. E. Andrews, and M. Simons. Others participating in the experimental effort were T. R. Howell, R. W. Sillmon, T. S. Colpitts, R. A. Connor, D. H. Abbott (programming), S. Varadargan, M. K. Kim, J. P. C. Chiang, A. D. Brooks, and D. G. Denton. Work on Ge substrates was performed under subcontract to TRW by W. Von Der Ohe and R. S. Whitte. The program was managed by M. Simons with the valuable assistance of J. J. Wortman and R. D. Alberts.

Accession For	
NTIS GMA&I	<input checked="checked" type="checkbox"/>
DDC TAB	<input type="checkbox"/>
Unannounced	<input type="checkbox"/>
Justification	
By	
Distribution/	
Classification Codes	
Dist	Standard/or Special
A	

TABLE OF CONTENTS

1.0	INTRODUCTION	1
2.0	EVALUATION OF VARIOUS MATERIAL SYSTEMS FOR CASCADE SOLAR CELLS	3
2.1	The Cascade Cell	3
2.2	General Material and Device Requirements	4
2.3	III-V Semiconductor Systems	7
2.3.1	GaInAs/AlGaAs/AlGaAs System	10
2.3.2	GaInAs/GaInP/AlAsSb	10
2.3.3	GaInAs/AlGaAsSb/AlGaAsSb Material System	13
2.3.4	GaAsSb/AlGaAsSb/AlGaAsSb Material System	15
2.4	Summary	15
3.0	EXPERIMENTAL STUDIES OF MATERIAL SYSTEMS	19
3.1	Introduction	19
3.2	Growth Techniques	19
3.3	Measurement Techniques	23
3.4	AlGaAs/GaAs Studies	24
3.5	AlGaAs/GaInAs Studies	31
3.6	Inverted GaInAs/AlGaAs Structure	35
3.7	AlGaAs Tunnel Diode	40
3.8	AlGaAsSb/GaAsSb Studies	44
3.9	GaInP Studies	60
4.0	PREDICTED CASCADE SOLAR CELL PERFORMANCE CHARACTERISTICS BETWEEN 83 K and 600 K	65
4.1	Introduction	65
4.2	Computer Modeling Results	67
5.0	REDUCED EQUIVALENT CIRCUIT OF A TWO-JUNCTION SOLAR CELL	77
5.1	Introduction	77
5.2	Reduced Equivalent Circuit	78
5.3	Summary	83
6.0	PREPARATION AND EVALUATION OF GaAs EPILAYERS ON Ge SUBSTRATES	85
6.1	Introduction	85
6.2	Spreading Resistance Measurement	85
6.3	Etching/Dislocation Experiment	86
6.4	Discussion	92
6.5	RTI Evaluation of GaAs/Ge Samples	93
6.5.1	Surface Characteristics	93
6.5.2	X-Ray Diffraction	93
6.5.3	Photoluminescence	96
6.5.4	Summary	96
	REFERENCES	97

LIST OF ILLUSTRATIONS

2.1	Simplified cascade solar cell	3
2.2	Use of tunneling interface for monolithic cascade cell . .	5
2.3	Bandgap and lattice constant values for the III-V semiconductors	8
2.4	GaInAs/AlGaAs/AlGaAs material system	11
2.5	GaInAs/GaInP/AlAsSb material system	12
2.6	GaInAs/AlGaAsSb/AlGaAsSb material system	14
2.7	GaAsSb/AlGaAsSb/AlGaAsSb material system	16
3.1	Liquid phase epitaxy system	20
3.2	The seven-well graphite boat and slider assembly	21
3.3	GaInAsP VPE system	22
3.4	Bottom cell in GaAs plus top n^+ - p^+ tunnel contact	24
3.5	Spectral response of three GaAs cells with n^+ - p^+ tunnel contacts	26
3.6	Spectral response of GaAs cell with wide bandgap tunnel junction	27
3.7	AlGaAs structure for tests of top cell	28
3.8	Spectral response of AlGaAs top cell	29
3.9	Spectral response of Be ion implanted top cell of AlGaAs .	30
3.10	V-I characteristics of AlGaAs/GaInAs cascade structure . .	34
3.11	Inverted GaInAs/AlGaAs cell structure	36
3.12	Lattice parameter profile for inverted structure	38
3.13	Bandgap profile for inverted structure	39
3.14	Voltage current characteristics of AlGaAs tunnel diode . .	41
3.15	I-V characteristics of the cascade cell structure with and without light, showing no evidence of any appreciable series resistance due to the tunnel diode	43
3.16	I-V characteristics of the cascade cell structure with and without light, showing the tunnel junction is present- ing an appreciable nonlinear series resistance	43
3.17	Diffraction pattern for layers of $\text{GaAs}_{0.88}\text{Sb}_{0.12}$ grown on GaAs using isothermal, etchback-regrowth method to grow this continuously graded, matching layer	47
3.18	Demonstration of efficacy of continuously graded layers . .	48
3.19	Portion of GaAsSb phase diagram	49
3.20	X-ray diffraction pattern for GaAsSb five step-graded layers on GaAs substrate	51
3.21	Photoluminescence spectra for GaAsSb sample	52
3.22	V-I characteristics of GaAsSb p-n junction	53
3.23	V-I characteristic for GaAsSb diode	54
3.24	X-ray diffraction scan of T50A showing FWHM of three grown layers comparable to GaAs substrate	56
3.25	X-ray diffraction pattern for AlGaAsSb on GaAsSb	58
3.26	V-I characteristics of AlGaAsSb p-n junction	59
3.27	Photoluminescence spectra of GaInP sample	61
3.28	GaInP sample configuration	62
3.29	V-I characteristics for GaInP sample (44.8% InP in GaInP) .	63
4.1	Bandstructure of a two-junction, voltage aiding, two- terminal cascade solar cell optimized for operation at 300 K, AM 0, 10^6 cm sec^{-1} surface recombination velocity, and unity solar concentration ratio	66

4.2	Cascade solar cell V-I family of curves with temperature a parameter; conversion efficiency maximized for operation at 300 K, AM 0, unity solar concentration ratio, and 10^6 cm sec ⁻¹ surface recombination velocity	68
4.3	Conversion efficiency vs. temperature of a cascade cell designed for maximum efficiency under the operating conditions of 300 K, AM 0, unity solar concentration ratio, and 10^6 cm sec ⁻¹ surface recombination velocity	69
4.4	Voltage at the maximum power point of the cascade cell V-I curve vs. temperature of a cascade cell designed for maximum efficiency under the operating conditions of 300 K, AM 0, unity solar concentration ratio, and 10^6 cm sec ⁻¹ surface recombination velocity	71
4.5	Dark current of the top and bottom cells vs. temperature of a cascade cell designed for maximum efficiency under the operating conditions of 300 K, AM 0, unity solar concentration ratio, and 10^6 cm sec ⁻¹ surface recombination velocity	74
4.6	Spectral response of electrons and holes for top and bottom cells and the total spectral response of the cascade cell at 83 K and 300 K of a cascade cell designed for maximum efficiency under the operating conditions of 300 K, AM 0, unity solar concentration ratio, and 10^6 cm sec ⁻¹ surface recombination velocity	75
5.1	(a) Energy bandstructure of a two-junction, monolithic cascade solar cell; (b) equivalent circuit of two-junction cascade solar cell; (c) reduced equivalent circuit	79
6.1	Spreading resistance curve of GaAs/Ge heteroepitaxial wafer	87
6.2	Ruby laser pulse energy	91
6.3	Cleaved and stained cross-section of GaAs/Ge wafer	94
6.4	Diffraction pattern for GaAs/Ge as-grown samples	95

1.0 INTRODUCTION

The basic objective of this research has been to develop the technology required to fabricate two-junction cascade solar cell assemblies having conversion efficiencies exceeding 25 percent when operating at 25°C under 1 sun, AM 0 conditions. A long-range objective of the work is to develop the cascade cell to the point where the theoretical conversion efficiency of 30 to 35 percent is approached. The first year's work has been oriented toward the study of several different III-V materials systems that show promise for use in fabricating the cascade cell. This report describes the work performed on cascade solar cell development between August 1, 1978 and September 30, 1979.

As an introduction to cascade solar cells, Section 2.0 provides some background discussion of cascade cells as compared with conventional single-junction cells. Also included is a general discussion of the material and device parameters that must be considered in selecting material systems for use in a cascade solar cell. Finally, an evaluation is given of the most promising III-V materials for use in a two-junction cascade solar cell.

Research has been undertaken in several major areas. First, a number of ternary and quaternary material systems that have potential application to the cascade solar cell have been studied and improved in quality. Additionally, p-n junctions have been made and evaluated in materials appropriate to the top and bottom cells in a two-junction cascade structure. These experimental results are reported in Section 3.0.

The computer modeling of cascade solar cells has been valuable in helping to decide on particular material systems to explore and in demonstrating the validity of the cascade cell concept under varying temperature conditions. Recent theoretical calculations on cascade solar cell performance between 83 K and 600 K are reported in Section 4.0. A reduced equivalent circuit model of the cascade cell is represented in Section 5.0.

Section 6.0 summarizes the work performed under subcontract by TRW in preparing GaAs epitaxial layers on Ge substrates and provides data on RTI's evaluation of these samples.

2.0 EVALUATION OF VARIOUS MATERIAL SYSTEMS FOR CASCADE SOLAR CELLS

2.1 The Cascade Cell

Conventional single-crystal solar cells appear to be rapidly approaching the ultimate intrinsic limits to conversion efficiency. For AM 0, one sun operation, silicon solar cells appear to be limited in efficiency to the 20 to 21 percent range [1-5]. For GaAs cells, the efficiency limit is slightly higher, around 21 to 23 percent [5-7]. These intrinsic limits arise because of the finite lifetime of minority carriers and because of the intrinsic energy bandgap of a given semiconductor material.

The cascade solar cell approach makes use of two or more cells to utilize the solar spectrum more efficiently. The cells of a cascade system are connected in optical and electrical series as illustrated in Figure 2.1. In this approach, the wide bandgap cell is located above the narrow bandgap cell. The high energy photons are absorbed in the wide bandgap top cell while the low energy photons (below the bandgap of the top cell) pass to the bottom cell. In Figure 2.1 a simple ohmic connection is indicated between the two cells. This connection is one of the

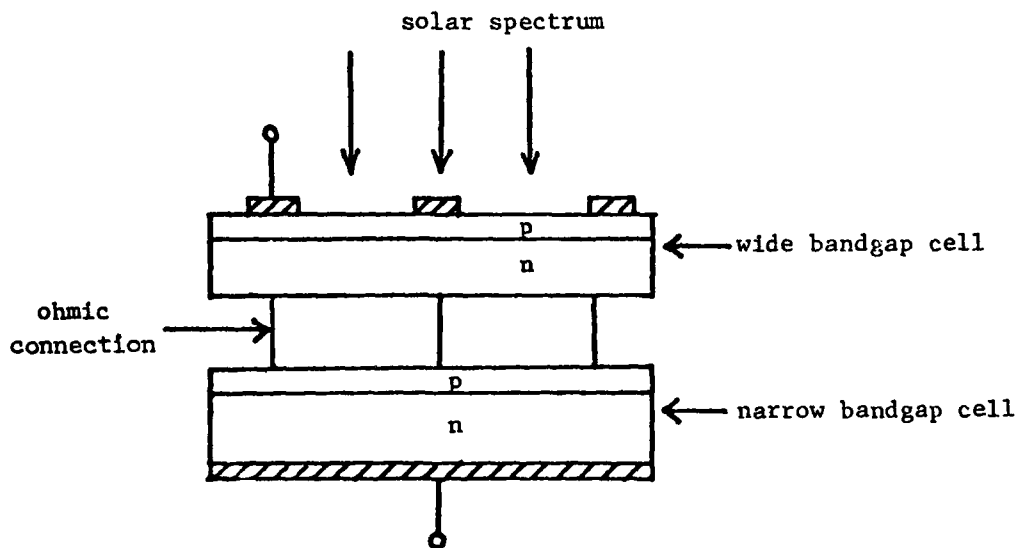


Figure 2.1. Simplified cascade solar cell.

most critical parts of the cascade solar cell concept. If the two cells are simply made with the four semiconductor layers in series, an additional p-n junction results at the interface of the two cells. This is not acceptable, and some means must be found to produce a low impedance interface.

A monolithic cascade structure which uses a heavily doped tunneling interface as shown in Figure 2.2 is the major approach being explored for interconnecting the cascade cells [8,9]. With this approach the entire cascade cell can be made in monolithic form on a single-crystal substrate.

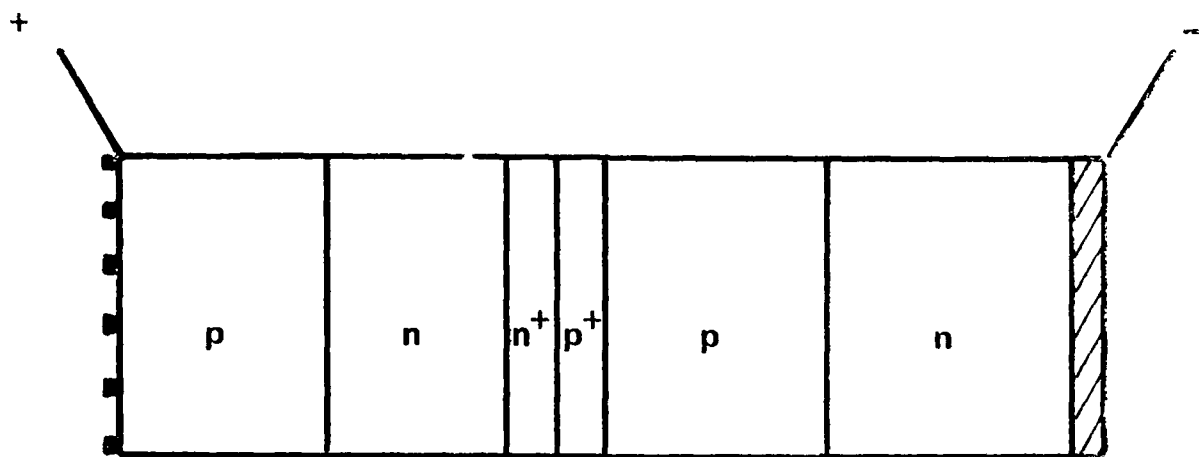
The feasibility of using a tunneling interface to connect two optically active cells has been demonstrated using an AlGaAs/GaAs cell structure [10]. The major requirement on the heavily doped interface is that the layers be as large as or larger than that of the top cell.

The advantages of the monolithic cascade cell are not, of course, obtained free but are obtained at the expense of a more complex cell. Many more layers must be reproducibly grown on a single substrate for the cascade cell, and this will make the cell more expensive than a single-junction cell.

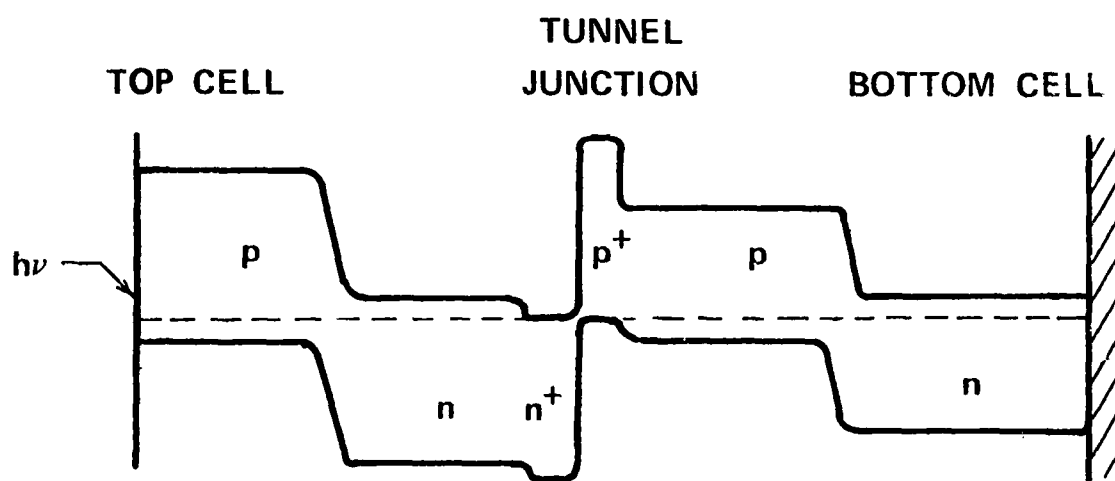
In addition to two-junction cascade cells, various speculations have appeared in the literature about three- or more junction cells [11]. Such cells can theoretically give even higher efficiencies than two-junction cells. However, until a high efficiency two-junction cell has been demonstrated experimentally, such cell concepts must remain mainly of academic interest.

2.2 General Material and Device Requirements

The general requirements for a high efficiency cascade solar cell are now fairly well established. The most critical factor in the selection of materials for the two cells is the bandgaps of the two cells. Because of the series connection of the two cells, a good first-order approximation for optimum designs requires the short circuit currents of the two cells to be equal. With some reasonable assumptions regarding collection efficiency of the two cells, this design constraint can be used to obtain a required relationship between the bandgaps of the two cells [8,11,12].



(a) PHYSICAL STRUCTURE



(b) ENERGY BAND STRUCTURE

Figure 2.2. Use of tunneling interface for monolithic cascade cell.

As in single-junction cells, an optimum bandgap combination exists for maximum efficiency of a two-junction cascade cell. Both simple approaches [11,12] and detailed computer studies have been performed to determine the optimum bandgap combinations at various temperatures, various air mass conditions, and various concentration ratios [8]. A detailed computer optimization study, using AlGaAs parameters as model parameters for the wide bandgap cell and using GaInAs parameters as model parameters for the narrow bandgap cell, has established the optimum bandgaps for 1 sun, AM 0 conditions as 0.95 eV and 1.6 eV [8]. Both of these values increase somewhat for designs optimized at elevated temperatures. For example, at 150°C the optimum bandgaps are approximately 1.20 eV and 1.80 eV. If one is willing to sacrifice slightly in efficiency, a range of bandgap values can be found near the optimum design values which still give high efficiency.

In addition to the optimum bandgap values, a monolithic cascade cell requires that all materials used in both cells form a compatible system such that all layers can be grown in a monolithic structure. This requires that the two cells have ideally the same lattice constants, and in a practical sense the two cells should be as closely lattice matched as possible.

In addition to the proper bandgaps and lattice matching materials, a cascade cell must have other desirable electrical properties. The minority carrier lifetime must be long enough to give a low dark current and high collection efficiency. For direct bandgap III-V semiconductors, this means a diffusion length of several μm . The materials must, of course, be stable, easily grown, and easily doped. The doping requirements are not trivial since a degenerately doped tunneling junction must be fabricated to provide a low impedance connection between the two cells. This must also be accomplished in a wide bandgap semiconductor (1.6 eV or larger) where large doping densities become a severe problem.

The choice of material systems must also be influenced somewhat by the available substrates on which to grow the cell. At present, available substrates in their order of preference are Si, GaAs, Ge, InP, InAs, and GaAs. At present, substrates with lattice constants different from these semiconductors must be grown by some step grading or linearly grading

technique. For example, GaInAs has been successfully step graded onto GaAs substrates up to InAs compositions of about 40 percent. Such step-graded layers can be considered as substrates onto which a cascade cell can be fabricated.

From the general requirements for a monolithic cascade solar cell discussed above, one can conclude that no combination of elementary semiconductors is suitable for such a cell. Of all the common semiconductors, only silicon has a bandgap close to that required for the narrow bandgap cell. Of all the III-V elementary semiconductors, AlSb has a bandgap closest to that required of the wide bandgap cell. However, its lattice constant (6.14 Å) differs so greatly from that of silicon (5.42 Å) that a monolithic structure of these two semiconductors appears impossible.

In fact, it is extremely difficult to grow any heterojunction on silicon because of its low lattice constant and high melting point. For these reasons silicon does not appear to be a good choice for the lower bandgap of a cascade cell even though its bandgap is close to the desired value.

As discussed above, none of the elementary Group IV or III-V semiconductors have the required properties for a monolithic cascade solar cell. This leaves the III-V ternary and quaternary systems of more exotic materials such as the II-VI semiconductors or the chalcopyrites [13]. These materials are not developed to the extent of the III-V materials so the ternary and quaternary III-V materials are the only logical present choices for a cascade solar cell design.

2.3 III-V Semiconductor Systems

The two fundamental requirements for materials for a monolithic cascade solar cell are a close lattice match between the materials and appropriate bandgaps for the two cells. Figure 2.3 shows energy bandgap and lattice constants for the various III-V semiconductors. Also shown are values for silicon and germanium as well as various solid lines representing selected ternary III-V semiconductors. The two crosshatched areas represent the desired bandgap ranges for the bottom and top cells in a two-junction cascade cell. The optimum bandgaps range from the low range combinations (0.95 eV and 1.6 eV) to the high range combinations

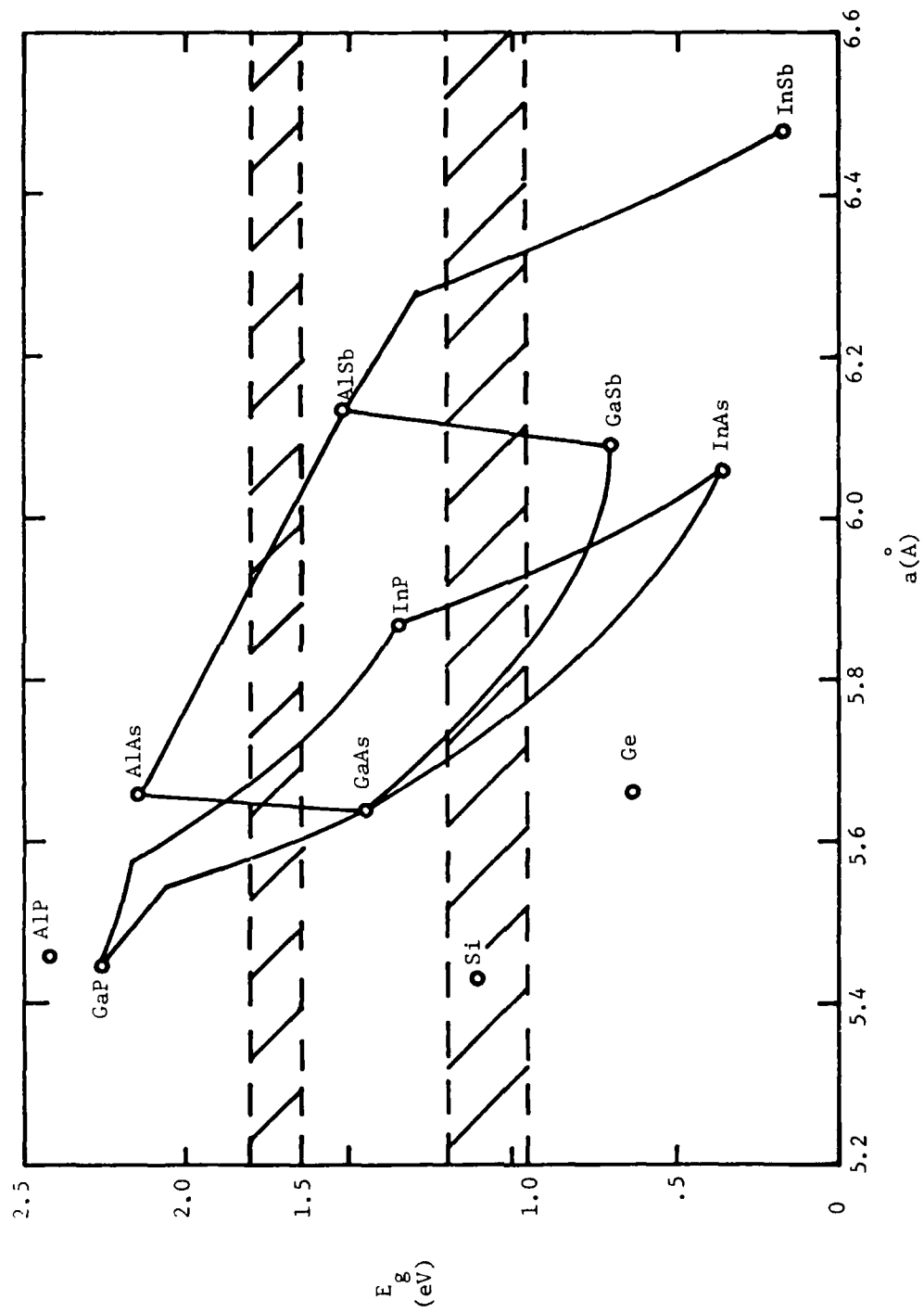


Figure 2.3. Bandgap and lattice constant values for the III-V semiconductors.

for high temperature optimization (1.2 eV and 1.8 eV). The selected semiconductors should ideally fall on a vertical line in Figure 2.3.

From a careful inspection of Figure 2.3, it can be seen that there is no one combination of materials that is obviously superior to all other combinations. Choices for the narrow bandgap cell include the ternaries GaInAs, GaAsSb, InPAs, AlGaAs, GaInP, and AlAsSb. However, there is no ideal lattice match between any ternary with the correct lower bandgap value and any other ternary with the correct upper bandgap value. All potential cascade cell designs using the ternary III-V materials involve some lattice mismatch.

The ternary systems are worthy of consideration even though they involve some degree of lattice mismatch. If the lattice mismatch can be confined in Figure 2.3 to the tunneling junction or to the heavily doped connecting regions, then some degree of lattice mismatch might be tolerated between the top and bottom cells.

Four material systems for use in fabricating a two-junction monolithic cascade solar cell were examined in detail during this study. Two of these systems involve only the ternary III-V semiconductors for the active elements while the other two involve a quaternary III-V semiconductor. Although the quaternary systems are more complex and less explored systems, they are the only III-V material systems that offer the possibility of a completely lattice-matched cascade cell from a window layer to top cell to connecting junction to bottom cell. The four material systems examined during the study are shown in Table 2.1 and are discussed in Sections 2.3.1 through 2.3.4.

Table 2.1. Cascade Solar Cell Materials Systems.

Bottom Cell	Top Cell and Tunnel Junction	Window Layer
1. GaInAs	AlGaAs	AlGaAs
2. GaInAs	GaInP	AlAsSb or AlGaAsSb
3. GaAsSb	AlGaAsSb	AlGaAsSb
4. GaAsSb	AlGaAsSb	AlGaAsSb

2.3.1 GaInAs/AlGaAs/AlGaAs System

This material system, as illustrated in Figure 2.4, uses GaInAs as the bottom cell and AlGaAs as the top cell and window layer. Of all the ternary III-V materials, AlGaAs is the most extensively explored and characterized, and GaInAs is the next most extensively studied. The electrical properties such as diffusion length of both of these materials are suitable for high efficiency solar cells. P-n junctions have been demonstrated separately in both AlGaAs and GaInAs, and the tunnel junction has been successfully fabricated in AlGaAs.

However, the major problem with the system illustrated in Figure 2.4 is the relatively large lattice mismatch between the bottom and top cells. The mismatch is smallest for cells optimized for high temperature operation. For a 1.8 eV top cell and a 1.2 eV bottom cell, the mismatch is about 1.01 percent while the mismatch becomes 2.30 percent for bandgaps of 1.64 eV and 0.96 eV. The lattice mismatch also causes the top cell to be under tensile stress. Experimentally it has been found that considerably less lattice mismatch can be tolerated in layers grown under tension than layers grown under compression [14]. Microcracks tend to form in layers grown under tension. This problem has thus far thwarted efforts to grow high quality GaAlAs top cell and connecting junction structures on the GaInAs bottom cell.

A special case of this system is the GaAs/GaAlAs/GaAlAs cell in which GaAs is substituted for the GaInAs lower cell. Though not an optimized system from the standpoint of overall conversion efficiency (about 24 to 25 percent theoretical), this system is lattice matched and has been utilized to demonstrate concept feasibility [10]. Work in this system has been directed toward improving experimental efficiency values.

2.3.2 GaInAs/GaInP/AlAsSb

This material system has GaInAs for the lower cell, in common with the previous system, but uses GaInP for the upper cell and a lattice-matched AlAsSb combination for a wide bandgap window layer (see Figure 2.5). The advantage of using GaInP for the wide bandgap cell is a smaller lattice mismatch between the cells, especially for cells designed for low

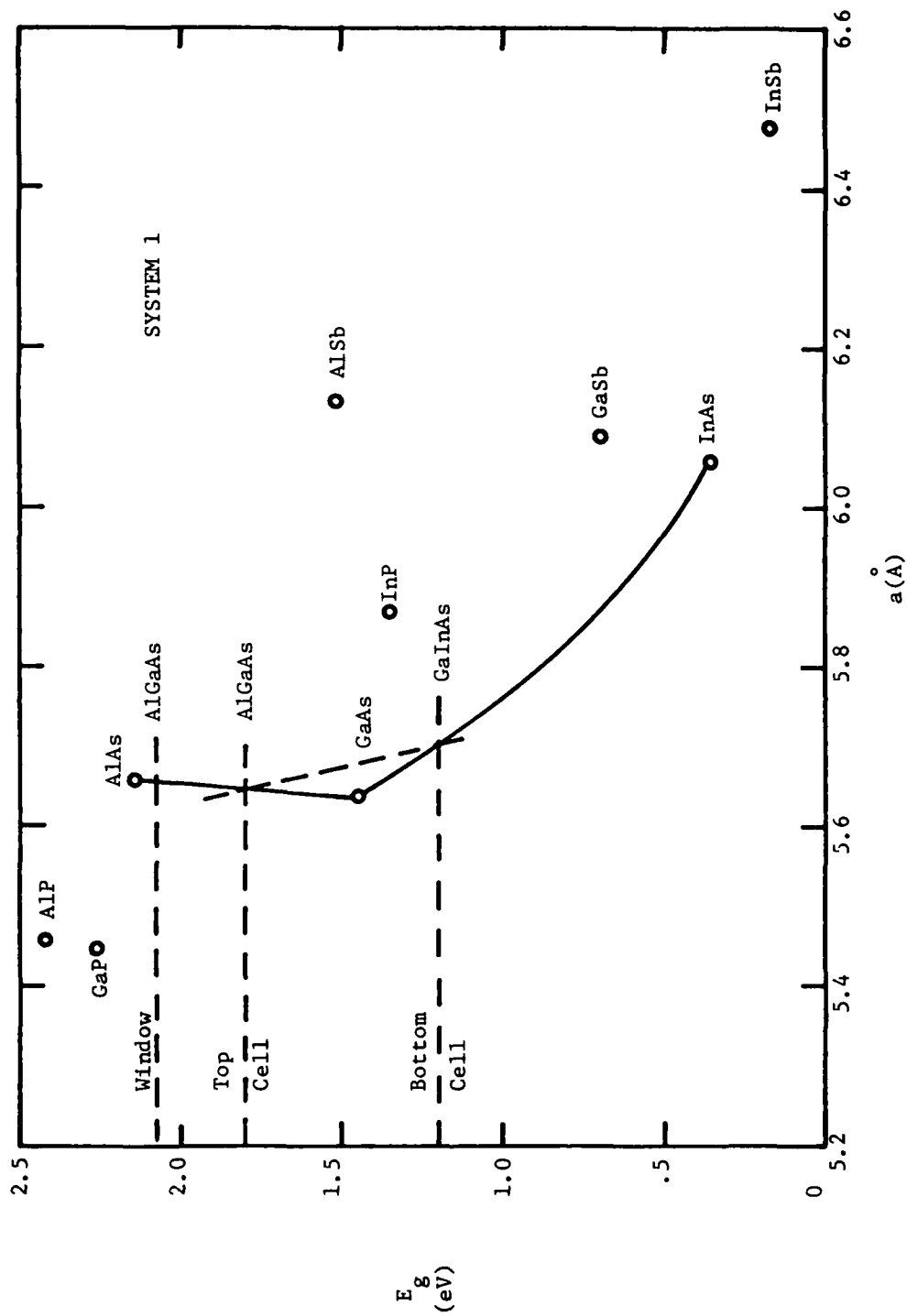


Figure 2.4. GaInAs/AlGaAs material system.

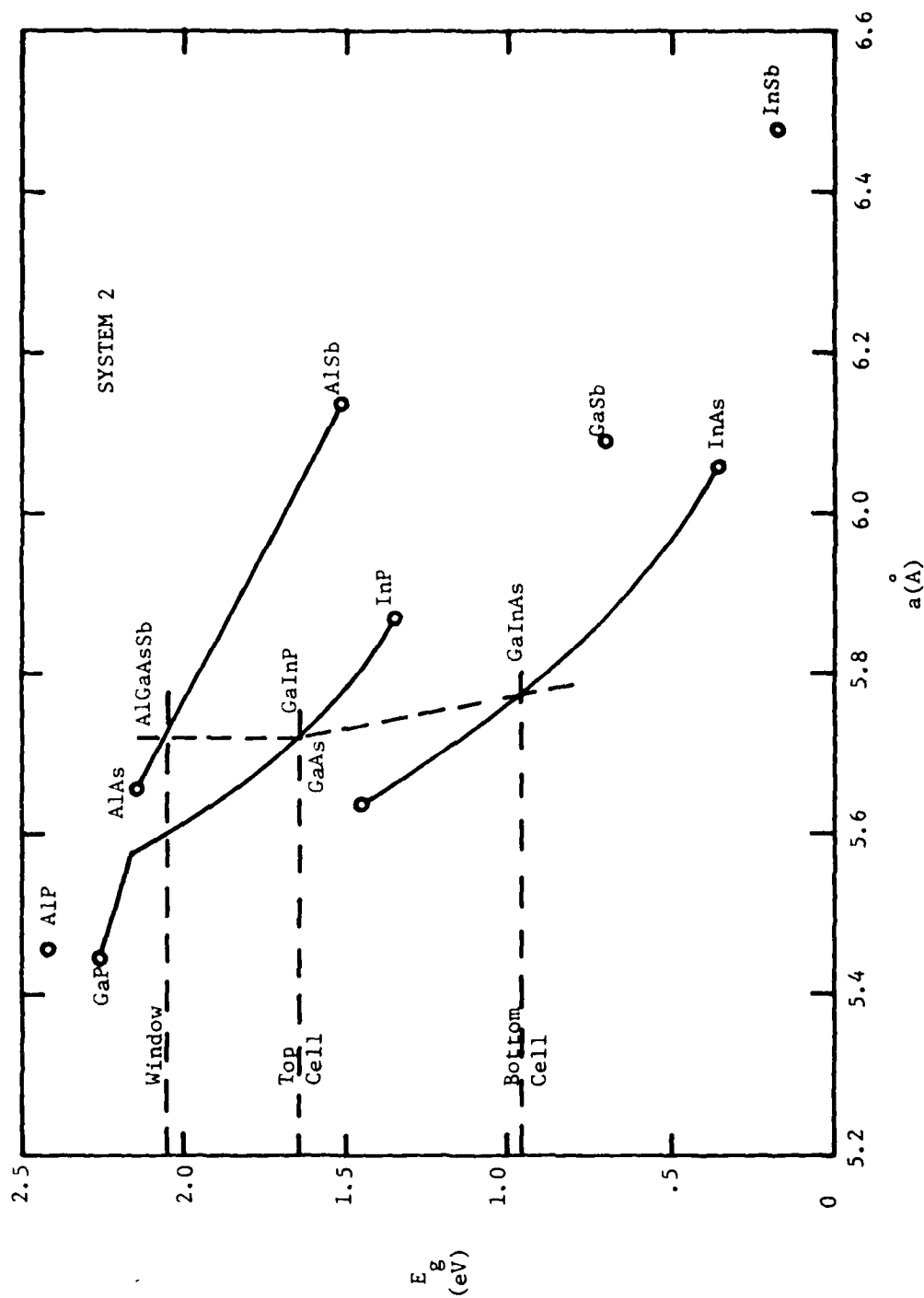


Figure 2.5. GaInAs/GaInP/AlAsSb material system.

temperature operation. For the room temperature optimized design (0.95 eV and 1.6 eV), this system has a lattice mismatch of 0.83%, which is much less than that of the first system for the same bandgaps. However, the lattice mismatch (and the fact that the upper cell is under tension) is still a potential problem with this material system.

Other considerations are the relatively unknown properties of the GaInP layers and the difficulty in growing the desired GaInP layers [15]. The GaInP layers are much more difficult to grow using liquid phase epitaxy (LPE) techniques than AlGaAs layers because of the high distribution coefficient of GaInP and because of a lattice-pulling effect [16]. During this work efforts have been directed toward the growth of GaInP using vapor phase epitaxy (VPE) techniques. Although a p-n junction has now been achieved in GaInP, the ability to heavily dope this material with both n- and p-type dopants needed for the connecting junction remains to be demonstrated.

An alternative to AlAsSb for the window layer is the quaternary AlGaAsSb with a small percentage of Ga. This can also have the same lattice constant as the GaInP top cell.

2.3.3 GaInAs/AlGaAsSb/AlGaAsSb Material System

This system uses the quaternary AlGaAsSb for the upper cell and window layer (see Figure 2.6). While this is a more complex material system, it is only by considering quaternary material systems that a lattice-matched cascade design can be obtained in the III-V materials. Figure 2.6 shows a lattice-matched combination for a 25°C optimum design. By moving along the GaInAs curve toward GaAs, bandgap combinations can be found for cells optimized at higher temperatures. The attractive feature of this system, as well as other quaternary systems, is that along a vertical line of constant lattice constant, all the desired bandgaps can be obtained within the quaternary plane.

The unknown factors associated with this system involve the ability to reproducibly obtain AlGaAsSb layers having adequate diffusion lengths. P-n junctions have been obtained during this work in AlGaAsSb having a bandgap in the 1.4 to 1.5 eV range. Additional work is needed to explore this quaternary in the compositional range of interest. Growth of AlGaAsSb

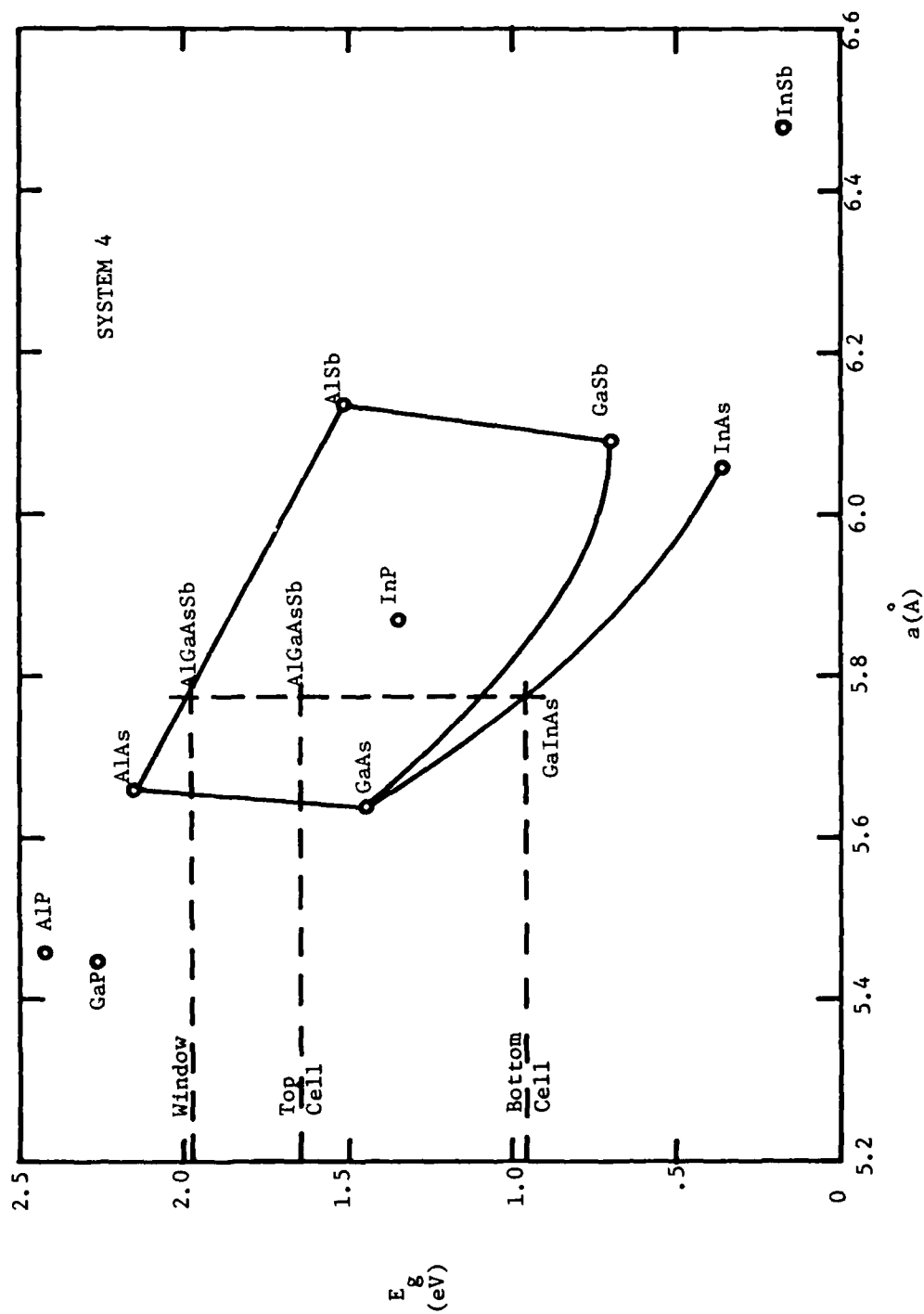


Figure 2.6. GaInAs/AlGaAsSb material system.

directly on the GaInAs bottom cell remains to be explored and will require some care since this quaternary compound has no In component.

The window layer should have as wide a bandgap as possible. This leads to the ternary AlAsSb as the best choice from purely a bandgap viewpoint. However, some Ga in the layer may make the window layer easier to grow and should be acceptable as long as the material is an indirect bandgap material.

2.3.4 GaAsSb/AlGaAsSb/AlGaAsSb Material System

This system, shown in Figure 2.7, is similar to the previous system with the substitution of GaAsSb for GaInAs for the bottom cell. Because of the larger bandgap of GaAsSb as compared with GaInAs for a given lattice constant, this system is also attractive for cells optimized for high temperature operation. The bandgap combinations in Figure 2.7 are 1.2 eV and 1.8 eV for the two cells. Lower bandgap combinations require AlGaAsSb layers nearer the center of the quaternary plane where a miscibility gap may be present. However, the predicted efficiency of a 1.2/1.8 eV cell at 25°C is still around 30 percent or more.

For this system the connecting junction and upper cell of AlGaAsSb may be easier to grow on the GaAsSb lower cell since all elements of the lower cell appear in the quaternary alloy. P-n junctions have been fabricated during this work in both GaAsSb and AlGaAsSb of compositions near the desired values.

2.4 Summary

The preceding section has discussed four potential material systems for use in fabricating a high efficiency cascade solar cell. Only the III-V material systems have been considered since these appear to be the only systems with sufficient flexibility with regard to bandgaps and with sufficient previous development to make possible a cascade solar cell in the near future.

All ternary systems that give optimum bandgap combinations involve some lattice mismatch. The GaInAs/AlGaAs/AlGaAs system appears to be more suitable for cells optimized for high temperature operation (150°C or above) while the GaInAs/GaInP/AlAsSb system is more applicable to

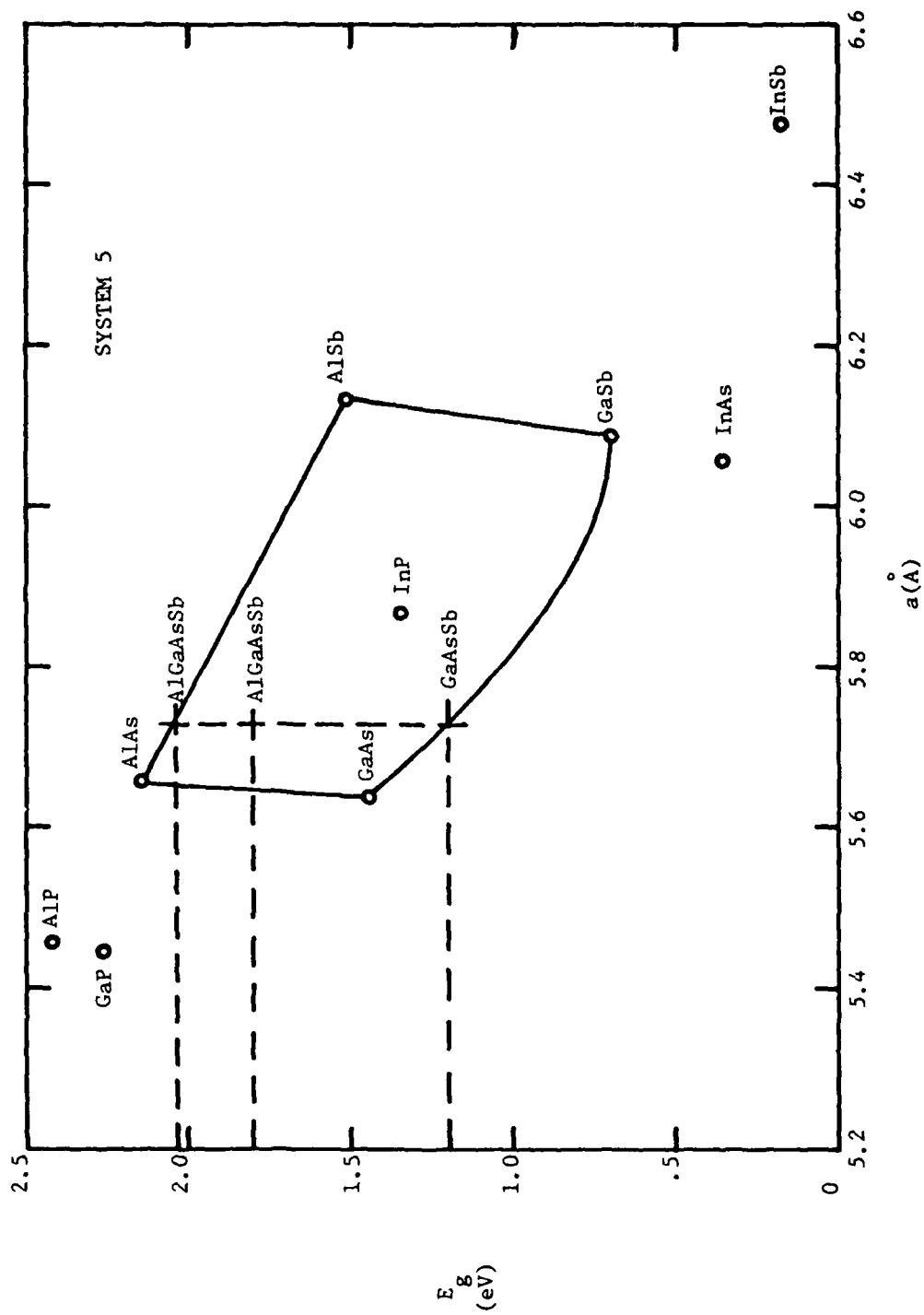


Figure 2.7. GaAsSb/AlGaAsSb material system.

cells optimized for near room temperature operation. The GaInAs/AlGaAs system involves a relatively large lattice mismatch, but the GaInP system, in addition, involves several potential problems with respect to doping and materials growth.

The quaternary systems are attractive because of the possibility of achieving a completely lattice-matched structure. However, the growth technology of these materials must be further advanced in order to demonstrate a cascade cell in either of these systems.

All of the proposed material systems have certain common features and problems. The lattice constant of the bottom cell for each proposed system differs from that of available substrates such as GaAs, Ge, InP, etc., so all systems require lattice grading to match the substrate. For the systems that use GaInAs as the bottom cell, a suitable technology has been developed and is available to grade from GaAs to the required lattice constant of the lower cell. For the system that uses GaAsSb, continuous grading by an isothermal growth technique has been used successfully to obtain good quality GaAsSb layers on GaAs substrate material.

The achievement of a heavily doped, low impedance connecting junction is a requirement for all the proposed material systems. This must be achieved in a wide bandgap semiconductor with a bandgap in the range of 1.6 eV to 1.8 eV. As the bandgap of the semiconductor increases, it becomes more and more difficult to achieve the required heavily doped connecting junction. The only material system in which a tunnel-connecting junction has been studied extensively is the AlGaAs system. The achievement of low impedance AlGaAs junctions for bandgaps up to 1.8 eV gives hope that the connecting junction can be achieved in other materials as well.

3.0 EXPERIMENTAL STUDIES OF MATERIAL SYSTEMS

3.1 Introduction

Experimental studies have been underway to explore and develop the four cascade material systems discussed in Section 2.0. The work has been directed toward determining the material parameters required for these cascade solar cell designs and has concentrated on GaInAs, GaInP, GaAsSb, AlGaAs, and AlGaInAs. Research in each of these materials, as well as in various materials combinations required for the cascade cell, is discussed in detail in the following sections.

3.2 Growth Techniques

The ternary and quaternary layers have been grown primarily by the LPE technique. Usual LPE procedures and techniques have been employed in a horizontal LPE furnace as shown in Figure 3.1. The furnace uses a 24-inch heat pipe which gives excellent temperature uniformity over the entire length of the furnace. Graphite boats and sliders were used for growing epitaxial layers on 1-cm by 1-cm substrates. Multiple-well boats with as many as seven wells, as shown in Figure 3.2, have been used to grow the multiple layers.

A VPE technique was used to grow GaInP layers since previous attempts to grow this material via LPE resulted in difficulties in obtaining heavily doped p-type layers [10]. The VPE growth system is based on the HCl-hydride open tube technique [17] and is designed to grow quaternary GaInAsP alloys (as well as any binary or ternary alloy of these elements) over any desired compositional range. Growth rates of from 1 to 10 $\mu\text{m/hr}$ and system response times on the order of 1 to 5 seconds (selected to produce 100 to 200 Å p-n junction transitions) can be achieved. This system is depicted schematically in Figure 3.3.

The substrates for all growth studies were GaAs layers. For most of the work the (111) orientation has been used with experiments on both the A and B faces. The (111) orientation was selected because this orientation is able to accommodate a larger lattice mismatch than the (100) direction for the material combinations under study.

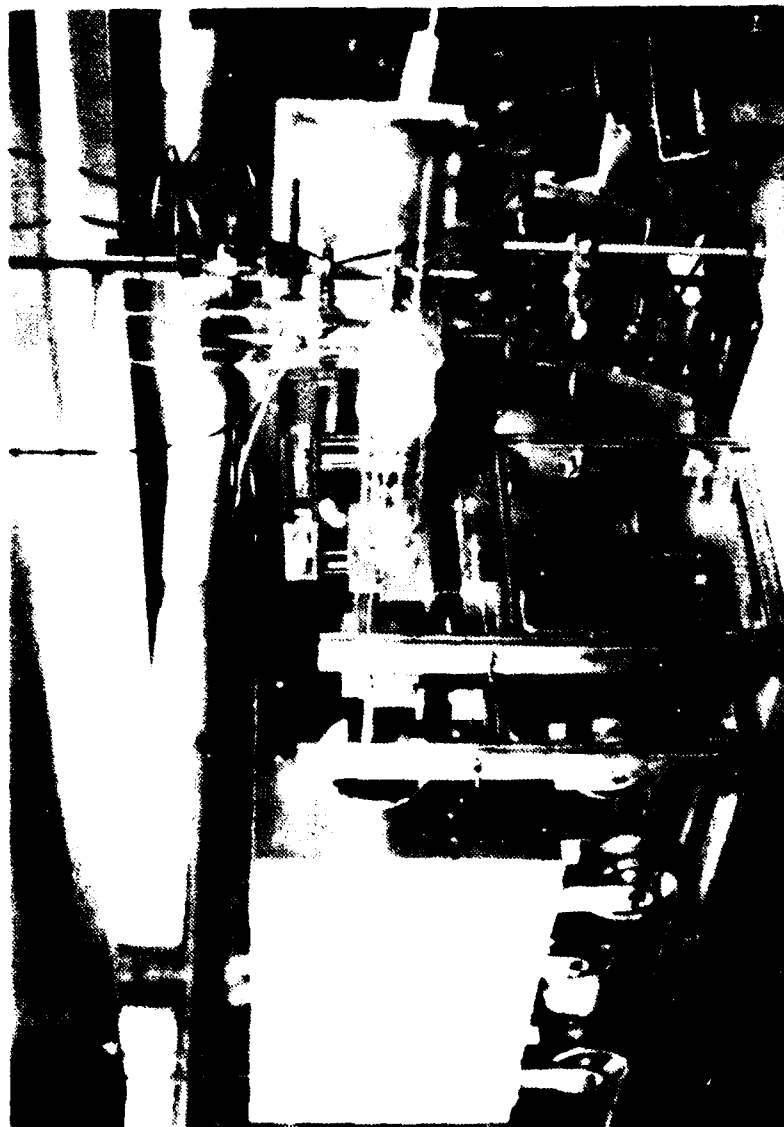


Figure 3.1. Liquid phase epitaxy system.

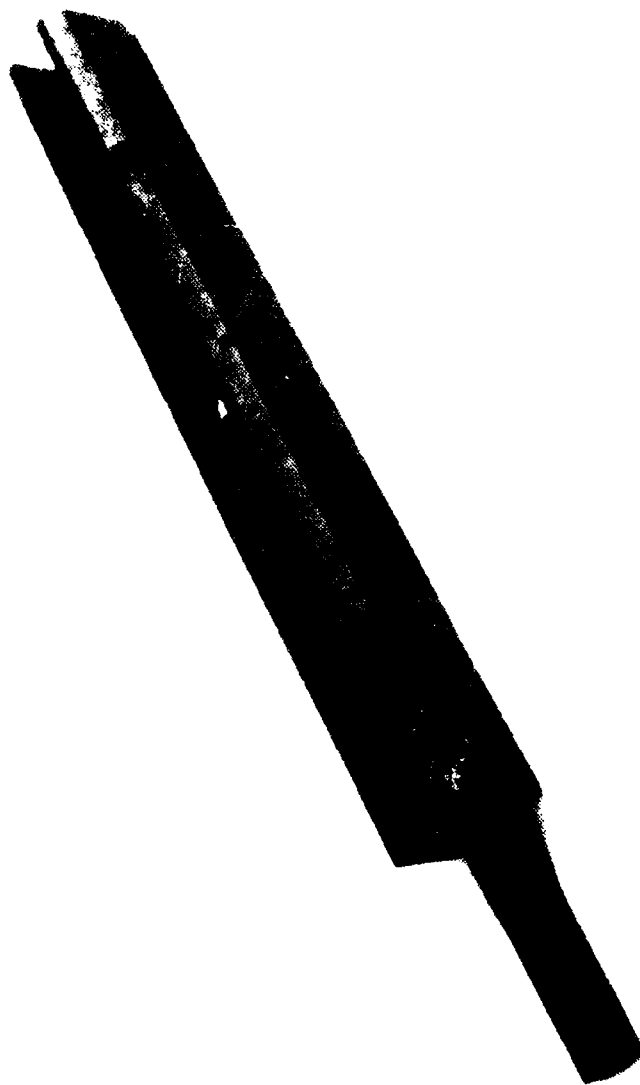


Figure 3.2. The seven-well graphite boat and slider assembly.

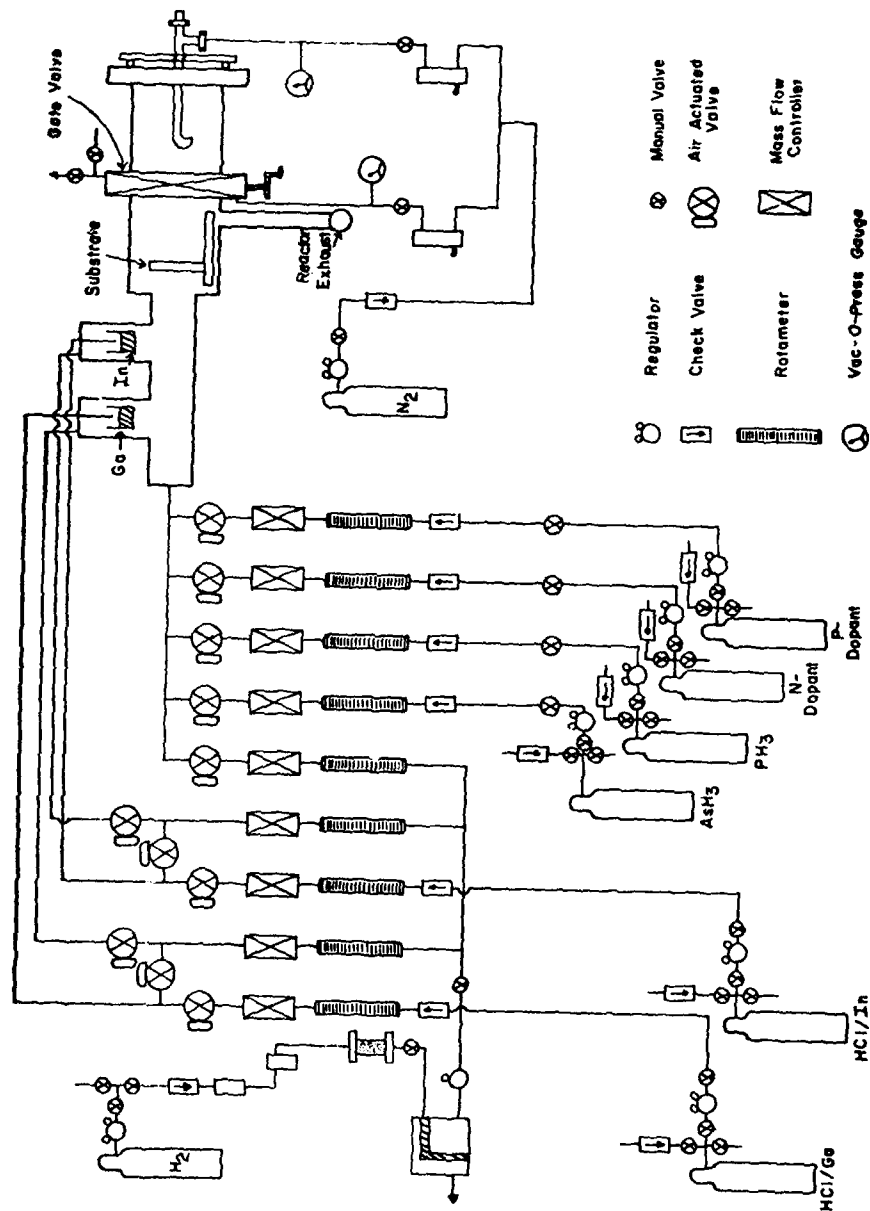


Figure 3.3. GaInAsP VPE system.

3.3 Measurement Techniques

X-ray diffraction has been used to determine the composition of the LPE layers. A Norelco single-crystal diffractometer was used with a copper target tube. For (111) substrates the (444) reflection peak was scanned. With epilayers of several μm in thickness, diffraction peaks from the substrate, as well as the grown layers, can be detected; and from the 2θ location of each peak the corresponding lattice parameter can be deduced. Since Vegard's law applies to these ternary materials, the lattice parameter was used to calculate the layer composition.

The crystalline quality of epitaxial layers can also be qualitatively judged from the sharpness of the diffraction peaks (FWHM). For the GaAs substrates, the Cu $K\alpha_1$ - $K\alpha_2$ doublet with 2θ spacing of 0.8° can be clearly resolved. LPE-grown layers can also resolve this doublet, yielding sharp diffraction peaks with a FWHM approaching that of the substrates. The sharp diffraction peaks indicate good crystalline quality of the epilayers. Electron microprobe analysis was also used to determine the composition of the epitaxial layers, and the results were in good agreement with the X-ray data.

In many cases layer composition was also estimated from photoluminescence (PL) spectra taken at room temperature. The homogeneity of layers across the sample was also checked by probing at several different points across the sample with a laser beam approximately $100\ \mu\text{m}$ in diameter.

The doping density of the layers was measured by standard Hall techniques at both room temperature and liquid nitrogen temperature.

Diffusion length measurements were made on selected samples by use of a γ -ray technique. In this procedure a sample is uniformly illuminated with γ -rays from a Co^{60} source. The generated carriers are then collected at either a p-n junction in the material or at a Schottky barrier at the surface. From measuring the collected current per unit area and estimating the generation rate, a total carrier collection depth can be obtained. For a Schottky barrier this depth equals the depletion layer depth plus the bulk minority carrier diffusion length. For a p-n junction structure the collection depth equals the depletion layer width plus the sum of the diffusion lengths on both sides of the junction. Most of these measurements have been made on p-n junction structures.

3.4 AlGaAs/GaAs Studies

A demonstration cascade solar cell has been fabricated in the AlGaAs/GaAs material system with GaAs used as the bottom cell and AlGaAs used as the top cell and tunnel junction [10,18,19]. The reported cells were fabricated in AlGaAs with bandgaps of about 1.6 eV to 1.7 eV. The demonstration cells, while verifying the cascade solar cell concept, did not achieve the desired high efficiency because the bandgaps of the two cells were not correct for equal short circuit currents.

If the bandgap (1.44 eV) of GaAs is assumed for the bottom cell, then the highest efficiency obtainable in the AlGaAs/GaAs material system is achieved when the AlGaAs bandgap is about 1.8 eV to 1.9 eV; this efficiency is around 24 to 25 percent. Work has continued on this material system under the present contract in an effort to obtain an optimum AlGaAs/GaAs cascade cell. Work on the AlGaAs tunnel junction is reported in Section 3.7 so the discussion here will focus on the bottom cell and top cell research.

A p-n junction in GaAs with a top n^+-p^+ tunnel contact is shown in Figure 3.4. Device structures of this type have been studied in detail as a means of characterizing the properties of the bottom cell while avoiding the interfering effects of the top cell. The GaAs p-n junction

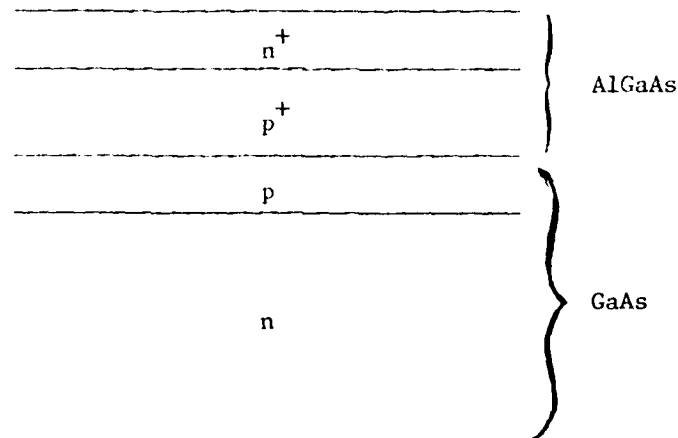


Figure 3.4. Bottom cell in GaAs plus top n^+-p^+ tunnel contact.

has been fabricated both by the growth of a thin p-layer on an n-type GaAs substrate and by impurity diffusion from the p^+ -AlGaAs layer into the n-type GaAs.

Figure 3.5 shows the spectral response of three bottom cell/tunnel contact structures having different AlGaAs bandgaps. Each diode is seen to have a fairly sharp absorption window extending from the bandgap of GaAs to varying upper cutoff wavelengths. From the point at which the spectral response begins to decrease sharply, the bandgap of the AlGaAs layers can be estimated as 1.65 eV, 1.75 eV, and 1.80 eV for the three curves in Figure 3.5. These values are in fairly good agreement with photoluminescence measurements of cell bandgaps.

Spectral response of a cell with a wider bandgap is shown in Figure 3.6. The cell in this figure indicates that optical absorption in the AlGaAs begins to occur at about 1.90 eV. The spectral response of this cell is also reasonably flat over the response band, indicating a good collection efficiency from the GaAs cell.

The onset of strong optical absorption in the n^+-p^+ -AlGaAs layer does not necessarily coincide exactly with the bandgap of the AlGaAs. For example, in a degenerately n^+ -type semiconductor the electron states (or valence states for p^+ material) are filled from the conduction band-edge to the Fermi energy, which may be 0.1 eV or larger, depending on the doping. Strong optical absorption will thus only occur when the photon energy exceeds the bandgap energy plus the Fermi level penetration into the band. This will always be somewhat larger than the bandgap.

Test cells with the structure shown in Figure 3.7 have been fabricated to study the spectral response of the top cell in AlGaAs. Cells have been fabricated with the p-layer either grown by LPE or diffused from the p^+ window layer. The best top junctions have been obtained by diffusion of Be from the window layer, and only these results are reported here.

Figure 3.8 shows the spectral response of a top cell p-n junction with a bandgap of approximately 1.9 eV. The response shows a characteristic rapid increase at the bandgap energy but also exhibits a fairly rapid decrease in response at wavelengths below about 5500 Å. This decrease can be attributed to two reasons. First, the curve has not

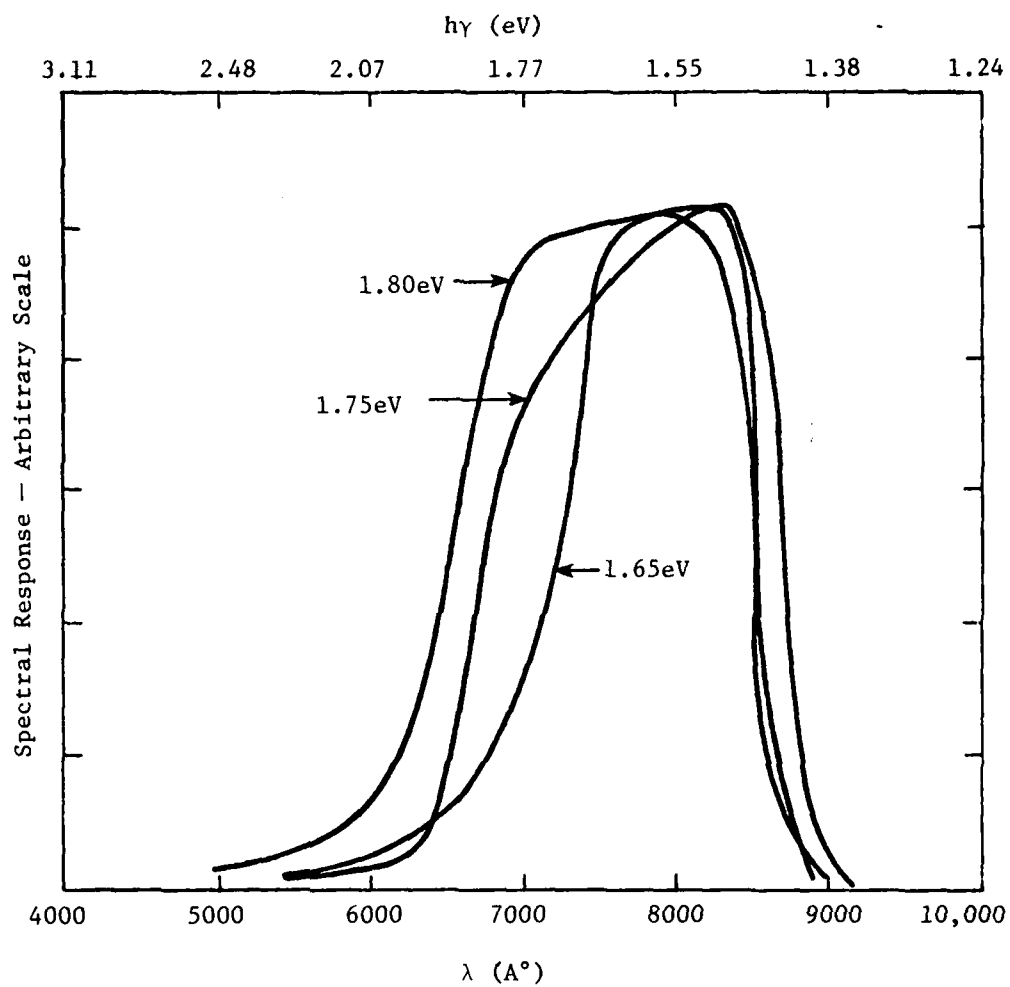


Figure 3.5. Spectral response of three GaAs cells with n^+-p^+ tunnel contacts.

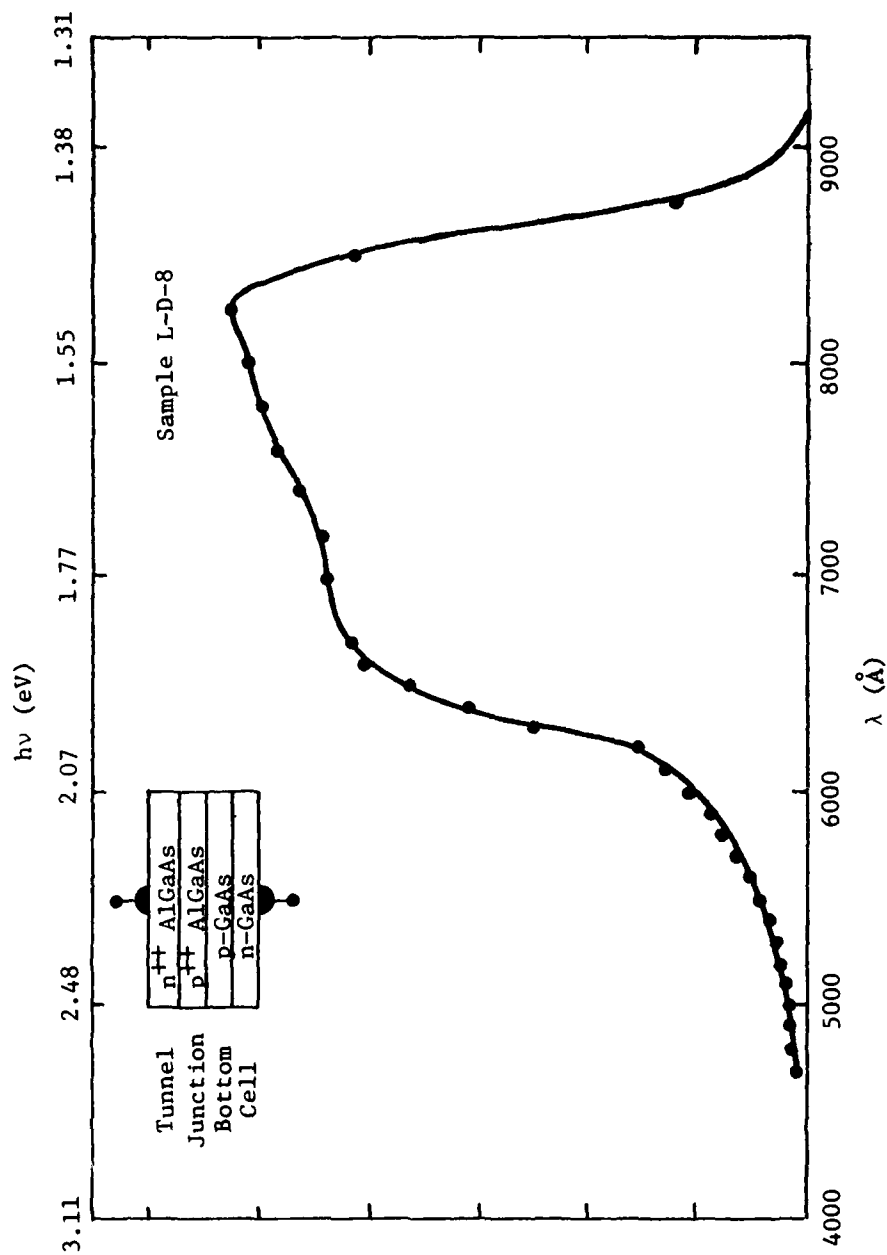


Figure 3.6. Spectral response of GaAs cell with wide bandgap tunnel junction.

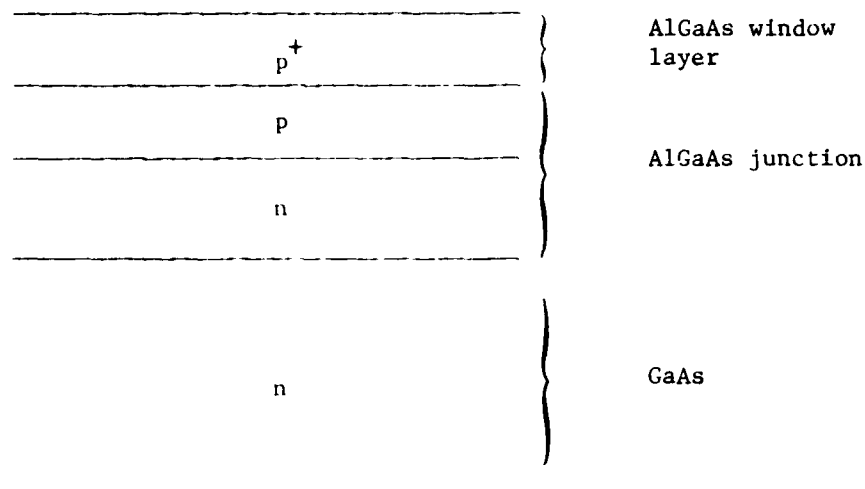


Figure 3.7. AlGaAs structure for tests of top cell.

been corrected for optical reflection, which becomes significant in this spectral region. Second, the window layer thickness of about $1\text{ }\mu\text{m}$ is too thick for low window-layer absorption. It is expected that the short wavelength response will improve considerably for thinner window layers that are also corrected for optical reflection at the surface.

Figure 3.9 shows the spectral response of an AlGaAs cell with a bandgap of about 1.75 eV fabricated by ion implanting Be into the n-type AlGaAs layer.* This cell was fabricated without a window layer. The spectral response is seen to be comparable to that of the diffused p-n junctions with a window layer.

In summary, the individual parts of the AlGaAs/GaAs system have been studied in detail. This has been undertaken to verify the operation as predicted of the bottom cell, tunnel contact, and top cell. The optimized AlGaAs/GaAs cascade cell requires that the top cell and tunnel contact be

* We are grateful to Dr. Jim Comas of NRL, Washington, D.C., for kindly performing the Be ion implantations.

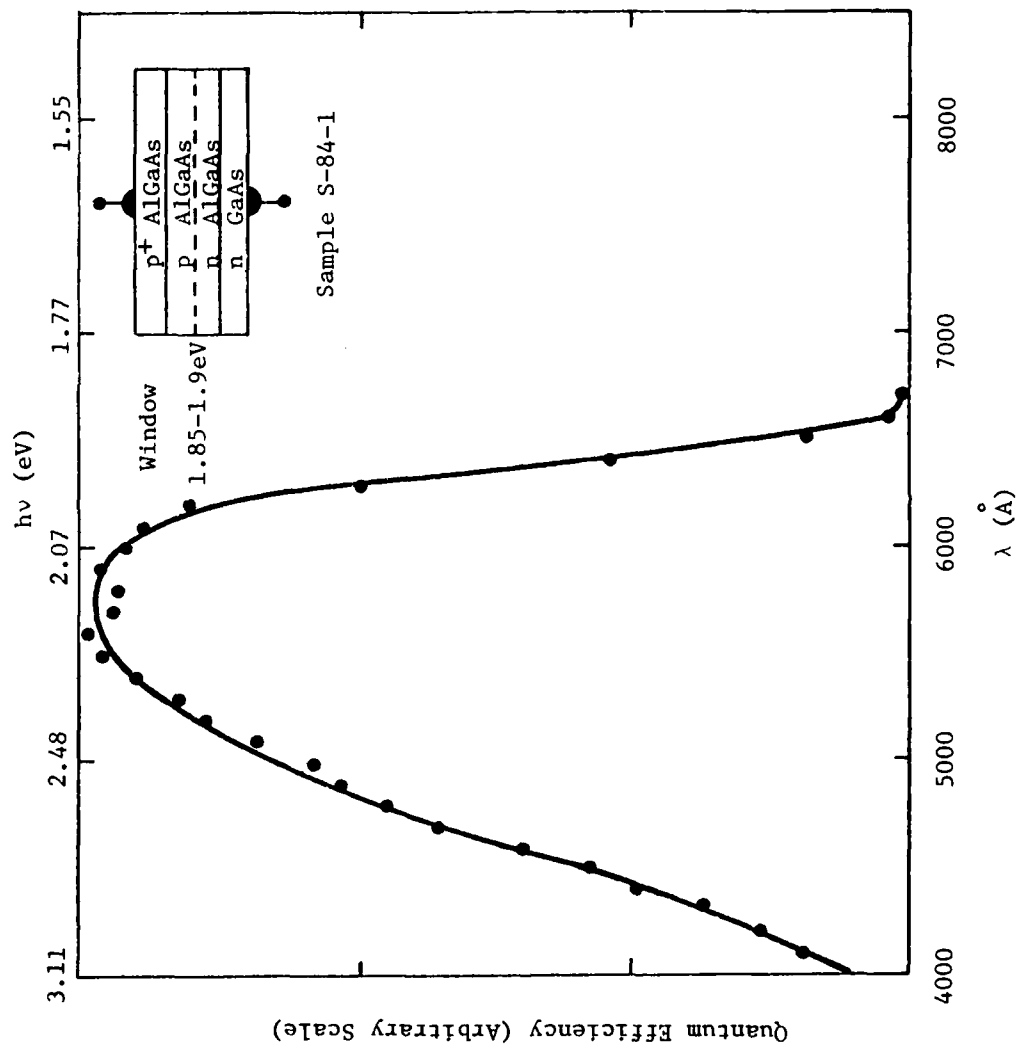


Figure 3.8. Spectral response of AlGaAs top cell.

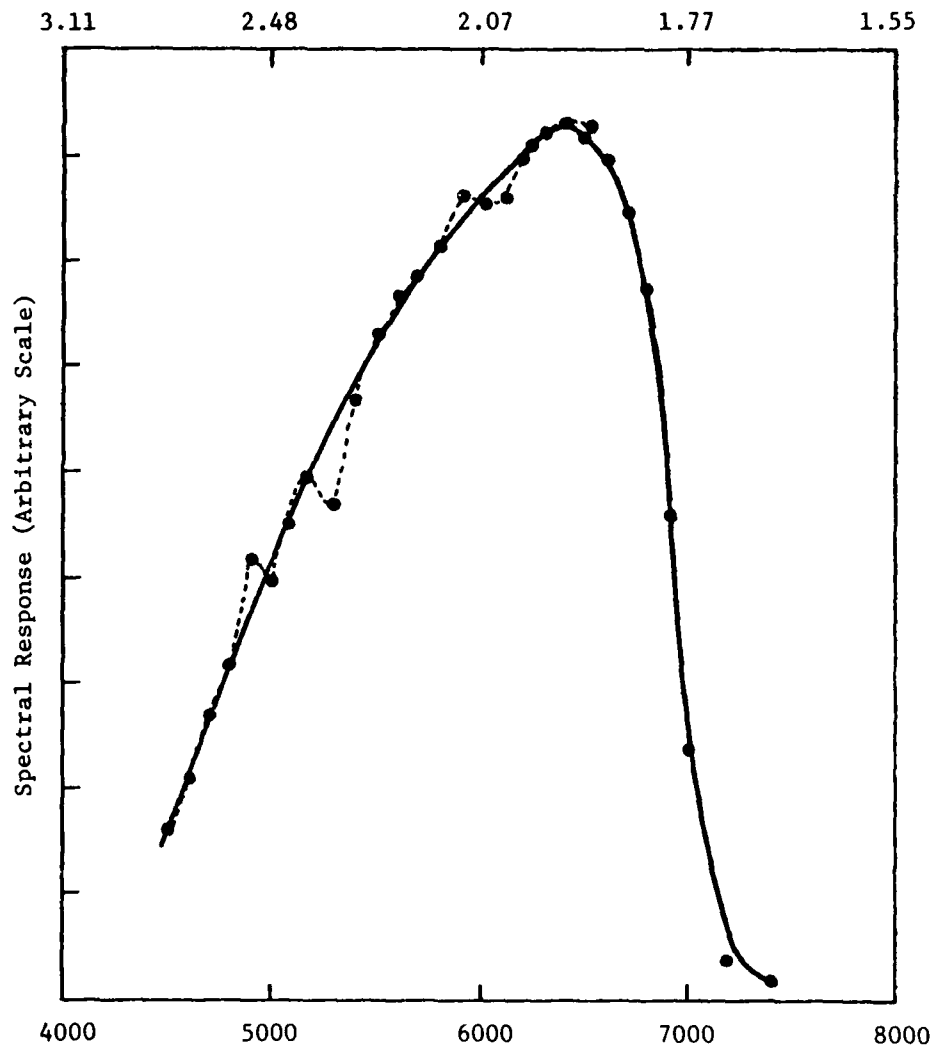


Figure 3.9. Spectral response of Be ion implanted top cell of AlGaAs.

fabricated with a bandgap of about 1.8 eV to 1.9 eV. Low dark current p-n junctions are difficult to obtain by LPE at this bandgap, and the most successful junctions have been diffused junctions. In addition, it has proven difficult to reliably fabricate low impedance tunnel junctions at this large a bandgap. This is discussed in more detail in Section 3.7.

Presently work is continuing on putting together a complete cascade solar cell in the AlGaAs/GaAs material system with a top cell bandgap of 1.8 eV to 1.9 eV. While the AlGaAs/GaAs material system is not quite capable of reaching the 24 percent efficiency goal, the efficiency of such a cell should be above that of pure GaAs and will hopefully demonstrate for the first time a cascade solar cell with an efficiency greater than that of a single-junction cell.

3.5 AlGaAs/GaInAs Studies

Work in this material system has focused on achieving a lower cell bandgap in the optimum range of 0.95 eV to 1.2 eV with an upper cell bandgap in the optimum range of 1.6 eV to 1.8 eV. In this materials system major consideration has to be given to two intrinsic material properties--vis., lattice parameter mismatch and melt-back effects during synthesis via LPE. In $\text{Ga}_{1-x}\text{In}_x\text{As}$ crystals the lattice mismatch increases rapidly with x, being 7.15 percent for $x = 1.0$. For $\text{Al}_y\text{Ga}_{1-y}\text{As}$, the change in lattice parameter is relatively small (approximately 0.14 percent for $y = 1$). Thus the AlGaAs connecting junction and top cell layers have lattice parameters substantially smaller than those of the underlying GaInAs bottom cell layers. Since optimum design requires $x \approx 0.20$, the AlGaAs layers clearly will have a smaller lattice parameter--i.e., a negative mismatch--which is approximately 1.07 percent for an optimized structure. It has been found experimentally that such high negative mismatch leads to many in-grown defects in LPE material. Mainly these defects are in the form of microcracks and dislocations arising from the state of tensile stress of the epilayers. This degrades the crystalline quality of the AlGaAs layers.

The second major consideration for this system is melt-back (or etch-back) during LPE growth. This stems from the fact that an AlGaAs melt is not in thermodynamic equilibrium with the underlying GaInAs

solid phase (epilayer). Melt-back does not occur uniformly over the entire sample area, and this leads to degradation of the AlGaAs/GaInAs interface. It is believed that this process will lead to reduced lower cell collection efficiency through increased interfacial recombination velocity.

Therefore, conventional LPE methods lead to reduced overall cell efficiency by degrading both the top and bottom cells. Because of this, several approaches have been tried to overcome these problems. To reduce melt-back, high cooling rates of up to 100°C/hr have been used. This leads to a higher growth rate for the AlGaAs layers, and the time of contact between the AlGaAs melt and the GaInAs epilayers is reduced. The $\text{Ga}_{1-x}\text{In}_x\text{As}$ layers were grown using the conventional near-equilibrium LPE method. The starting growth temperatures were in the 795 to 800°C range with a cooling rate of 20°C/hr. A step-grading method was used to grow multiple layers with x changing in steps of approximately 5 mole % InAs. Typical growth rates were 2 to 3 $\mu\text{m}/^\circ\text{C}$ of cooling, and growth time was adjusted to yield step-graded layers with a thickness of approximately 6 to 7 μm . At the end of the growth of the last GaInAs layer, the cooling rate was increased, and the substrate was inserted in a supersaturated AlGaAs melt. Growth was continued to yield AlGaAs p-n junction layers with thicknesses in the range of 2 to 3 μm .

This approach has been used to deposit AlGaAs on $\text{Ga}_{1-x}\text{In}_x\text{As}$ with $x \approx 0.15$. It should be noted that melt-back increases with increasing x , and this fast growth method becomes increasingly ineffective. In order to assess the quality of GaInAs bottom cells, some connecting junction/bottom cell structures have been grown. For $x \approx 0.05$, values of $V_{oc} \approx 0.7$ V and $J_{sc} \approx 5$ to 10 mA/cm^2 were obtained in small area mesa-etched devices (≈ 1 sun illumination). For $x \approx 0.15$, however, $V_{oc} \approx 0.4$ V and $J_{sc} \approx 5$ to 10 mA/cm^2 were obtained, indicating degradation due to melt-back.

The quality of the connecting junctions was ascertained by their optical inactivity. The impedance measured across bottom cells with and without connecting junctions showed no measurable change. It should be pointed out that lattice mismatch and the accompanying defects give rise to a shunt impedance across the tunnel diode connection junction, thereby

improving its performance (reducing series impedance). On the other hand, the top cell has to be grown on top of this highly strained connecting junction layer, and here the same effects (shunt impedance and poor quality) are extremely detrimental. In our experiments a top cell made with 1.6 eV bandgap material had $V_{oc} \lesssim 0.2$ V when grown on connecting junctions as opposed to $V_{oc} \approx 1$ V when grown on GaAs substrate material with minimum mismatch problems.

In order to achieve better crystalline quality and hence better top cells, attempts were made to isolate the top cell from the strained connecting junction by growing a buffer layer. Such buffer layers are used extensively in other device structures to improve crystalline quality. The major requirements for this purpose are that the buffer layers have a high bandgap for optical transparency and a low series resistance. Up to three AlGaAs buffer layers have been grown over the connecting junction before growing the top cell. In these cells evidence of cascade solar cell action has been observed. At the same time there is evidence that the top cell performance is still being degraded. From composite cell I-V curves, top cell degradation can be inferred from low J_{sc} and low V_{oc} --i.e., $V_{oc} = 1.1$ V instead of the ≈ 1.8 V expected from bandgap considerations. Similarly, reverse characteristics exhibit "double breakdown" like curves as shown in Figure 3.10. Here it is believed that until the first breakdown the photocurrent is limited by the top cell. There is a substantial photoresponse from the bottom cell, however, indicating that this cell is still performing as designed.

In view of the problems associated with the AlGaAs/GaInAs, it is useful to review all the factors involved. The optimum cell design calls for bottom and top cell bandgaps of ≈ 1.0 and ≈ 1.7 eV, respectively. A 1.0 eV bottom cell can be fabricated by growing GaInAs p-n junctions with ≈ 30 percent InAs, with a corresponding lattice parameter of ≈ 5.77 Å. In order to achieve device quality material, it is imperative to grow several (three to five) intermediate "step grading" GaInAs buffer layers, as described in previous reports [10], with each successive layer having a higher InAs mole fraction. Then to grow an AlGaAs connection junction (two layers) on top of this, a carefully controlled fast growth technique has to be employed. Further, before any device-quality AlGaAs top cell material can be grown on

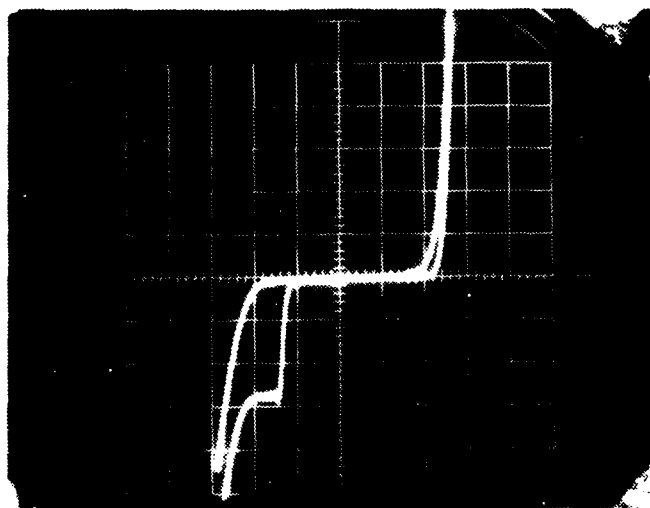


Figure 3.10. V-I characteristics of AlGaAs/GaInAs cascade structure.

top of this, several buffer layers need to be used again. In spite of this tedious and complicated process, it seems doubtful that strain-free, device-quality layers can be synthesized via LPE. Thus the improvement in overall cell efficiency resulting from reducing the bottom cell bandgap (increasing InAs mole fraction) must be weighed against the degradation in overall cell efficiency resulting from the reduced quality of individual cells.

In summary, the quality of AlGaAs/GaInAs structures has been improved considerably during the present contract period. This has been achieved by using fast growth rates to minimize melt-back of the GaInAs layers and by using several wide bandgap buffer layers between the tunnel junction and the active top cell. Cascade solar cell action has been observed for the first time in such AlGaAs/GaInAs cells. However, the performance of the top cell in such structures has been poor, and so far no improvement in cascade solar cell performance has been observed by replacing the GaAs of the bottom cell with a GaInAs layer.

3.6 Inverted GaInAs/AlGaAs Structure

The use of AlGaAs for the top cell and tunnel junction and of GaInAs for the bottom cell is very attractive because of the good electrical properties of individual diodes of AlGaAs and GaInAs. The fabrication of complete cells in this material system is very difficult, however, because of the large lattice mismatch between the AlGaAs and the GaInAs. If the straightforward approach is taken to the two-junction cascade cell, then AlGaAs must be grown on GaInAs, which has a larger lattice constant. The AlGaAs layer is then under tensile stress, and good quality layers are very difficult to grow because of microcracks.

Because of the problems discussed above, the fabrication of an inverted GaInAs/AlGaAs cell has been studied. This structure is shown in Figure 3.11. The cell fabrication sequence consists of growing in sequence on a substrate the window layer, top cell, tunnel junction, and bottom cell. This sequence of growing the layers has several advantages. First, the graded layers between a substrate and the bottom cell are eliminated, and only one lattice mismatched interface occurs. Second, the top GaInAs layers can be grown under compressive stress, eliminating the problem of microcracks occurring in the reversed structure. In this fabrication, the cascade cell would be completed by selectively etching away the GaAs substrate and inverting the cell so that light is incident on the window layer.

As a first step toward realizing this inverted structure, p-n junctions of GaInAs grown on AlGaAs have been investigated. The quality of the GaInAs layers grown on AlGaAs was not as good as layers grown directly on GaAs. A possible explanation is that the In-rich melt attacks the AlGaAs layer, and an intermediate layer of AlGaInAs rich in In is grown first. However, this quaternary shows a miscibility gap for high mole fractions of In; thus this intermediate layer may not grow or may grow with inferior quality. It has been found that a slight degree of supersaturation (few degrees) is helpful in improving the quality of the epitaxial InGaAs on AlGaAs layer.

An InGaAs p-n junction was epitaxially grown on an $\text{Al}_{0.2}\text{Ga}_{0.8}\text{As}$ layer with approximately 10 percent InAs and with $E_g = 1.27$ eV. The layers as grown are n-type, and Mn was used as a p-type dopant. The I-V characteristics

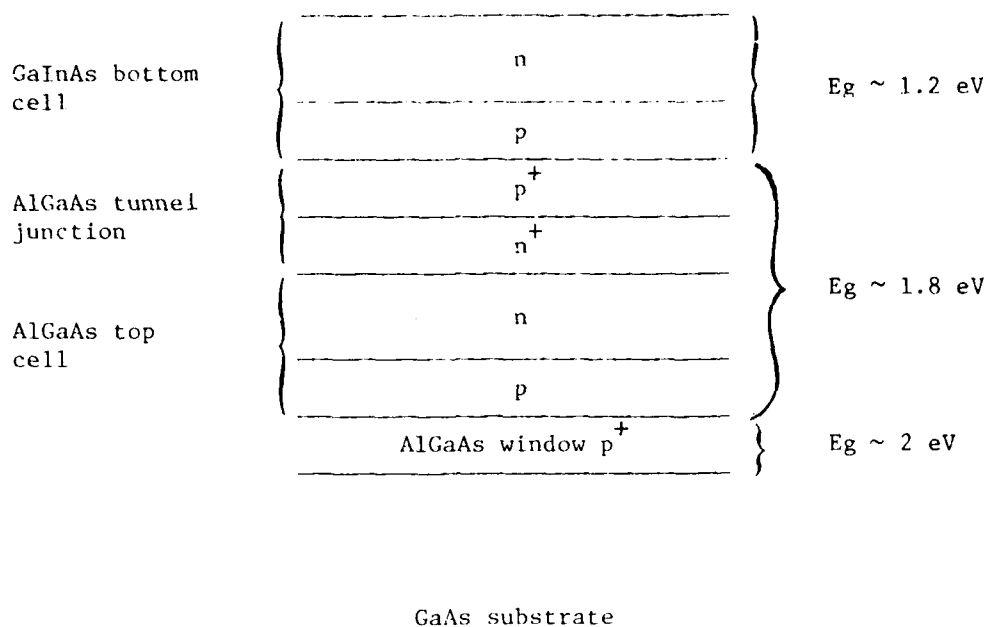


Figure 3.11. Inverted GaInAs/AlGaAs cell structure.

give an open circuit voltage of about 0.4 to 0.5 V. This relatively low V_{oc} may be due to the presence of a low shunt impedance across the InGaAs p-n junction resulting from the relatively high dislocation density from the 0.8 percent lattice mismatch between InGaAs and AlGaAs. Diffusion length (collection depth) measurements by the X-ray technique gave a collection depth of 0.44 μm . This relatively low value also indicates a poor quality layer due to the high degree of mismatch and the relatively poor interface between InGaAs and AlGaAs.

The use of an intermediate lattice matching layer between the GaInAs and GaAlAs may be helpful in avoiding some of the problems stemming from the lattice mismatch at this interface. In addition to providing good lattice matching, a buffer layer material should be optically inactive (nonabsorbing) and should have low electrical series resistance. It is

believed that the quaternary $\text{Al}_{1-g}\text{Ga}_g\text{Al}_{1-x}\text{Sb}_x$ will be useful in this application. Recalling that GaInAs has a higher lattice parameter than AlGaAs, the bottom cell layers will be in a state of compressive strain. In the earlier "up-right" structure where AlGaAs layers were grown on a GaInAs bottom cell, the AlGaAs layer was in tension, leading to material and device quality degradation. In the inverted structure such degradation can be avoided, and this is the major rationale behind this effort. While $\text{Ga}_{1-x}\text{In}_x\text{As}$ layers with small amounts of InAs ($0 < x < 0.07$) can be grown indirectly on AlGaAs connecting junctions in spite of the (positive) lattice mismatch, any further increase in x rapidly degrades material quality. To obtain high efficiency cascade cells, the bottom cell bandgap has to be lowered to ≈ 25 percent InAs. In this situation, however, the bottom cell material cannot be grown directly on AlGaAs connecting junction layers because of the high (≈ 1.8 percent) lattice mismatch. Therefore, it is necessary to include a mechanism to accommodate this mismatch. One method is to use buffer layers for lattice parameter grading. For this purpose we propose to use the AlGaAsSb quaternary system. In LPE growth of this material it is observed that both Al and As have very high distribution coefficients, K_i ($K_i = C_i^s/C_i^l$, where C_i^s is the concentration of element i in solid phase and C_i^l is the concentration in the liquid phase). Thus during LPE growth both Al and As are rapidly depleted from the melt, thereby changing composition of the growing epitaxial layers. With changing layer composition, its lattice parameter also undergoes a continuous change, increasing for the GaSb-rich layer compositions, as indicated schematically in Figure 3.12. The second criterion for selecting this material is that it has a high bandgap, in the indirect region, in this composition range. Thus this grading layer is optically inactive since it is transparent to the photon flux in the wavelength range of interest for the bottom cell. By keeping the Al mole fraction in the graded quaternary layer above approximately 20 percent, it is believed that a high bandgap value can be maintained even after sufficient lattice parameter grading. This variation in bandgap for an inverted structure is depicted schematically in Figure 3.13.

In order to realize this structure experimentally, a substantial amount of work had to be done to grow the AlGaAsSb layers. All these

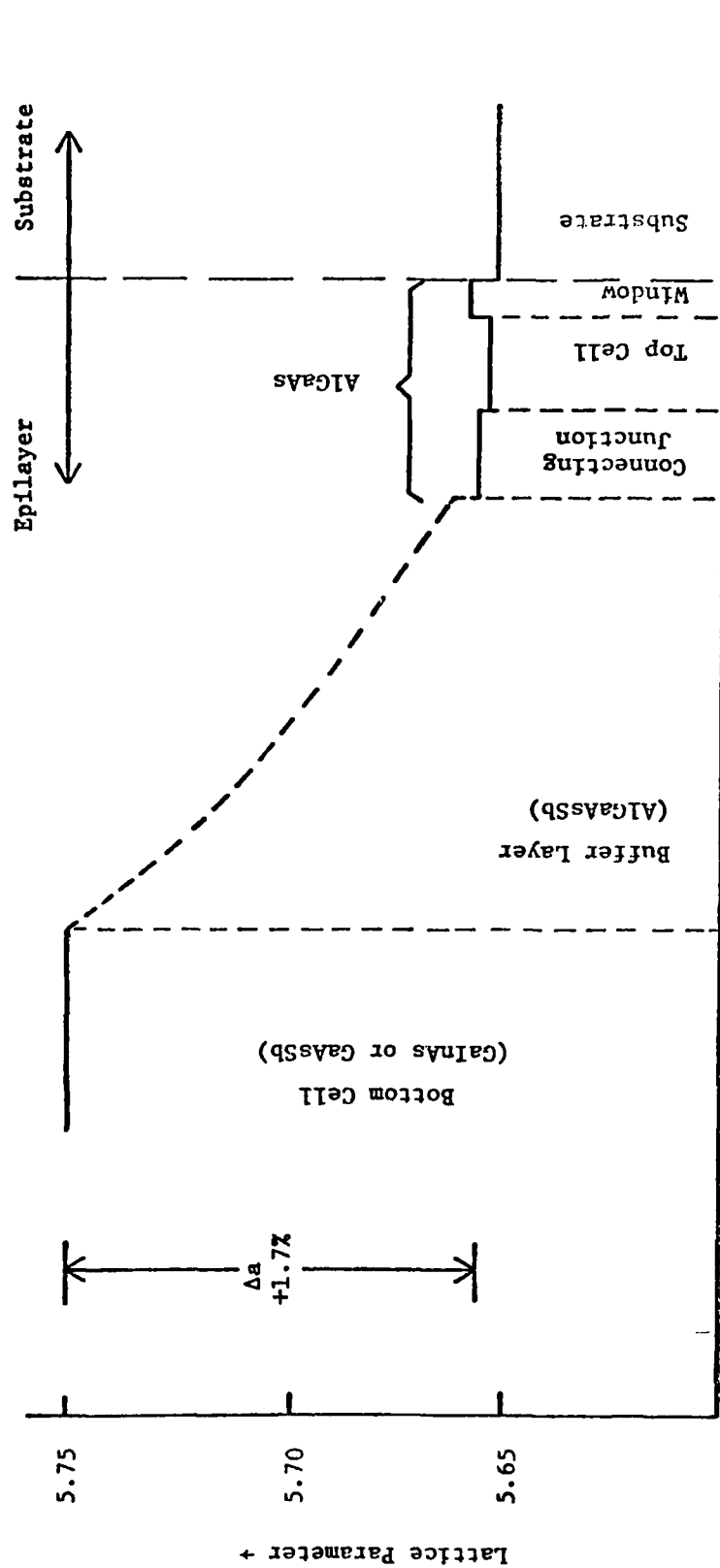


Figure 3.12. Lattice parameter profile for inverted structure.

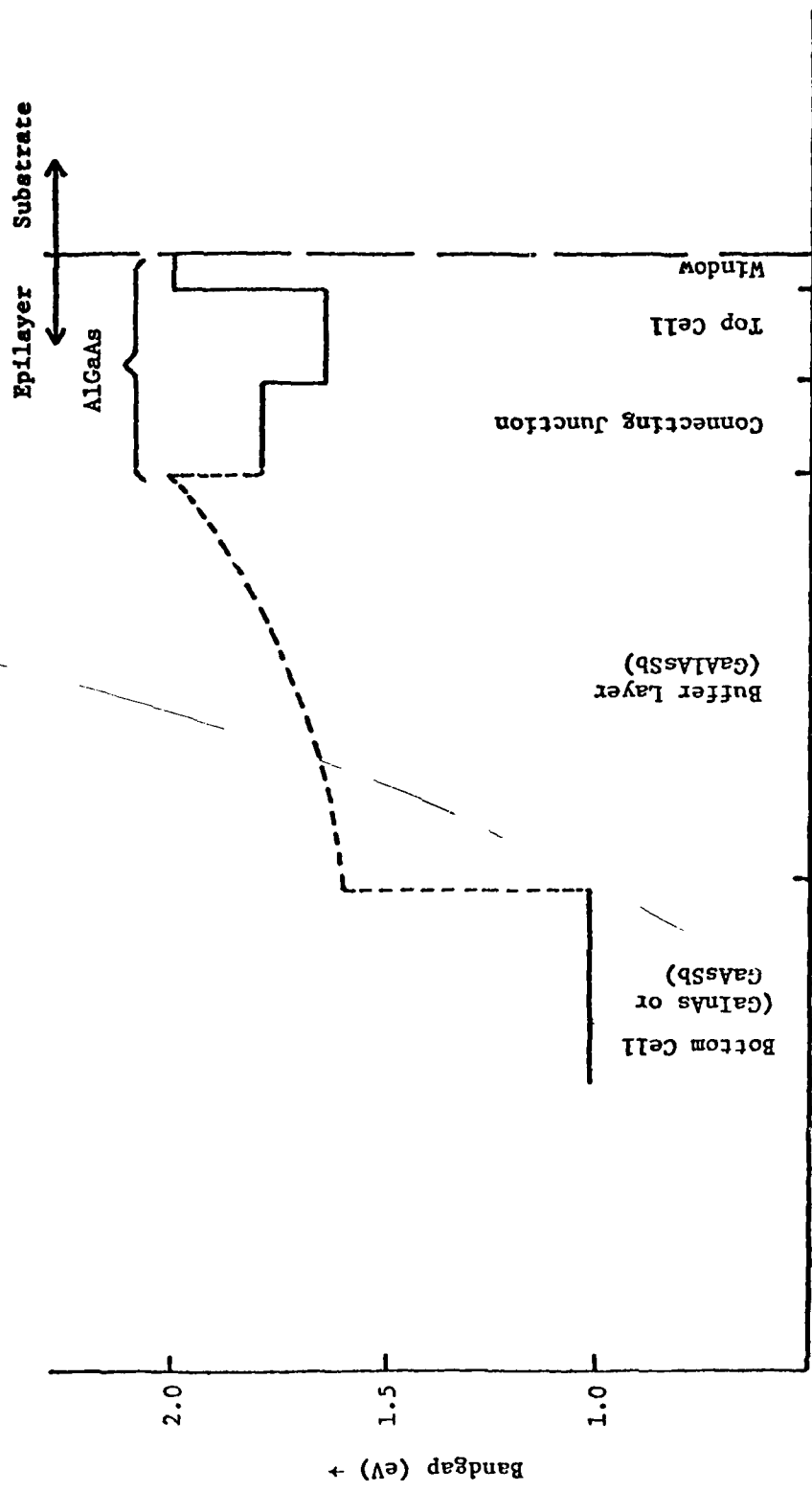


Figure 3.13. Bandgap profile for inverted structure.

epitaxial layers were grown on GaAs substrates with (111) A orientation since this orientation yields better morphology than the (111) B face. In the past some work has been published on this quaternary for the composition range $0.8 \leq g < 1.0$, $0 < l \leq 0.2$. For our purpose, this composition range had to be extended to include higher Al mole fractions. Also, growth temperatures were reduced to $\approx 725^\circ\text{C}$ since in the complete solar cells these quaternary grading layers will be grown on top of the connecting (tunnel) junction and at lower temperatures, and this leads to a faster (steeper) compositional grading in the epitaxial layers.

At the present time, sufficient experimental data have been obtained to allow growth of graded layers with a final composition of up to 15 mole % Al and up to 20 mole % Sb. These layers have a lattice parameter of $A_0 \approx 5.75 \text{ \AA}$ (GaAs $A_0 = 5.653 \text{ \AA}$) so that GaInAs p-n junction layers with up to 20 percent InAs could be lattice matched to this graded layer, yielding a bottom cell with $E_g \approx 1.15 \text{ eV}$.

3.7 AlGaAs Tunnel Diode*

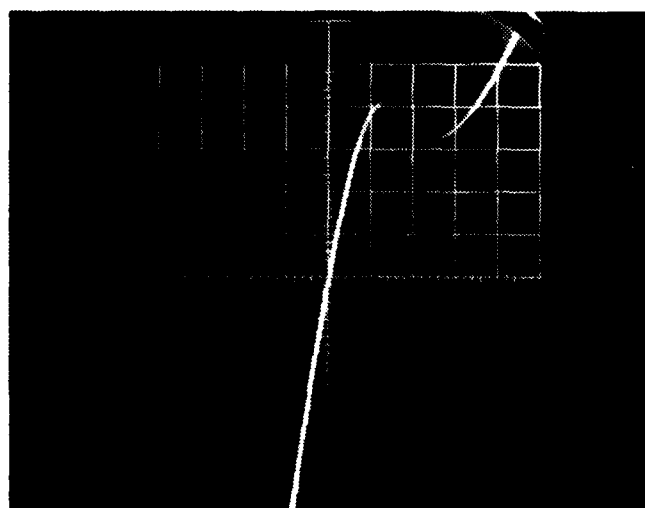
This section reports on the achievement and fabrication of an AlGaAs tunnel diode with a bandgap of about 1.6 eV. This work was motivated by the need to have a wide bandgap, low impedance junction to serve as a low contact interface to two forward biased p-n junctions connected in series in the cascade solar structure [8,11]. This appears to be the first reported tunnel diode epitaxially grown in a ternary III-V compound or in a direct bandgap semiconductor with a bandgap above 1.43 eV. This AlGaAs tunnel junction can also be used in the integrated multijunction photo-detector structure recently reported [20].

Liquid phase epitaxy was used to fabricate the AlGaAs diode. Several n^+ and p^+ dopants were tried, and best results were obtained when using Te and Ge as the n^+ and p^+ dopants, respectively. Carrier concentrations in the upper $10^{18}/\text{cm}^3$ range were obtained. The growth temperature was 800°C with a $1^\circ\text{C}/\text{min}$ cooling rate. The structure consisted of $n \approx 5 \times 10^{17} \text{ cm}^{-3}$ GaAs:Si substrate, with n^+ Te-doped and p^+ Ge-doped AlGaAs layers. The

* Material in this section has been accepted for publication in J. Appl. Phys. with S. M. Bedair as the author.

thickness of the active layers was about one micron each. For electrical evaluation Ag:Mn dots were evaporated on the p^+ layer and Au:Sn on the back side of the GaAs substrate. Mesas with areas in the range 0.02 to 0.2 cm^2 were etched using a Br:methanol solution. A typical I-V characteristic for an individual tunnel diode is shown in Figure 3.14. Ohmic behavior is observed in the forward and reverse tunneling region up to current levels approaching the peak tunneling current of $\approx 40 \text{ mA}$.

The potential application of such a tunnel diode is in the cascade solar cell approach whereby two or more p-n junctions are connected in optical and electrical series. In such a cascade solar cell, the top cell is made of a wide bandgap material and optimized for the high energy photons while the lower cell is made of a narrow bandgap material and optimized to use the photons that are not absorbed by the top cell. The efficiency of two-junction solar cells has been shown to be above 30 percent, with optimum bandgaps at 300 K being around 0.95 eV and 1.6 eV for the two junctions [8,11]. The material considerations for such structures have been previously reported [15].



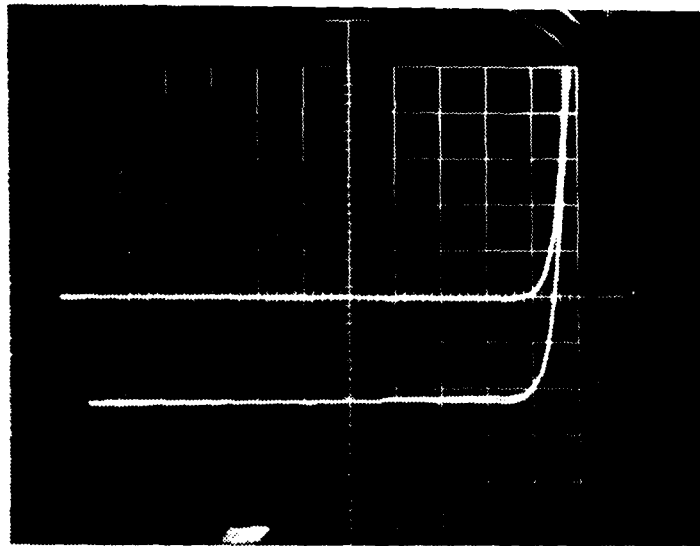
Hor: 0.1 V/Div

Vert: 10 mA/Div

Figure 3.14. Voltage current characteristics of AlGaAs tunnel diode; the diode area is $3 \times 10^{-2} \text{ cm}^2$.

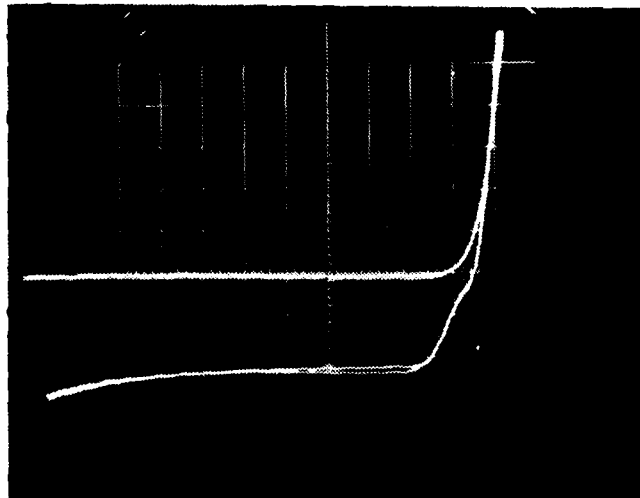
In order to produce a voltage-aiding configuration, an extra connecting p-n junction has to exist between the two cells. The connecting diode plays an important role in the cascade cell and must exhibit several important properties. It should present a low impedance to current flow in both directions, and the voltage drop across it should be as small as possible. It should also have a very low absorption for photons that are transmitted through the top cell so that they can be utilized efficiently by the low bandgap junction. Thus the current generated by both junctions should be equal (which is a necessary requirement) to attain high efficiency. If the connecting junction has a bandgap less than that of the high bandgap junction, a considerable part of the solar spectrum transmitted through the high bandgap junction will not reach the low bandgap junction, and the current passing through the whole cascade structure will be limited. This will result in decreasing the efficiency of the cascade solar cell. One means of obtaining this is to use a heavily doped tunneling junction such as that reported here in a material with a bandgap as large as or larger than the top cell bandgap of 1.6 eV. As a matter of fact, the tunnel junction with high bandgap had appeared to be the stumbling block in achieving high efficiency. A two-junction stacked cell has previously been fabricated with an open circuit voltage of 2 V and a short circuit current density in the mA/cm^2 range [18,19]. Figure 3.15 shows the I-V characteristics of a more recent cascade cell with an open circuit voltage of 2.2 V and a fill factor of about 0.8, indicating the proper action of the connecting diode. However, Figure 3.16 illustrates the effects of a poor connecting junction presenting an appreciably non-linear resistance in series with the solar cell. Such characteristics give a low fill factor and are not acceptable for a cascade solar cell.

From the above consideration, it is seen that the resistance of the tunnel junction is very important if the potential of this cascade solar cell structure is to be realized. The total resistance of the structure shown in Figure 3.14, including the measuring probe, is 1.6Ω . This value can be considered as an upper limit in estimating the series resistance of the tunneling contact interface with an area of $3 \times 10^{-2} \text{ cm}^2$. However, it is apparent from Figure 3.14 that at current density of 30 mA/cm^2 the voltage drop across the junction is on the order of



Hor: 0.5 V/Div Vert: 0.1 mA/Div

Figure 3.15. I-V characteristics of the cascade cell structure with and without light, showing no evidence of any appreciable series resistance due to the tunnel diode.



Hor: 0.5 V/Div Vert: 0.1 mA/Div.

Figure 3.16. I-V characteristics of the cascade cell structure with and without light, showing the tunnel junction is presenting an appreciable nonlinear series resistance.

millivolts. Thus for a cascade cell with an open circuit voltage of 2.2 V, the voltage drop across the tunnel diode would result in negligible decrease in the overall conversion efficiency.

The tunneling process has been observed for diodes with areas up to 0.2 cm^2 ; the peak to valley current ratio, I_p/I_v , decreases with increasing diode area. The relatively low I_p/I_v in Figure 3.14 may be due to excess current arising from tunneling into impurity levels within the bandgap. For example, AlGaAs heavily doped with Ge has been reported to have several levels within the bandgap [21].

It should be mentioned that the junction resistance per unit area is higher than that of the GaAs tunnel junction previously reported [20]. This is mainly due to the fact that in the AlGaAs ternary system, the higher the bandgap, the lower the doping level that can be achieved [22] and thus the higher the junction resistance. For diodes with bandgaps of about 1.7 eV, the negative resistance portion of the I-V characteristics shown in Figure 3.14 starts to disappear without any appreciable changes in the junction resistance. For a bandgap of about 1.8 eV, the I-V characteristic shows only an ohmic behavior, and the junction resistance starts to increase with the bandgap.

In summary, an AlGaAs tunnel diode with a bandgap of approximately 1.6 eV has been fabricated by LPE. This tunnel diode is a suitable connecting junction between the high and low bandgap cells of a cascade solar cell structure. In fact, the I-V characteristics of the tunnel diode are such that it should also be suitable for use with the cascade cell at the high current densities associated with multisun illumination.

3.8 AlGaAsSb/GaAsSb Studies

The $\text{GaAs}_{1-y}\text{Sb}_y\text{As}_{1-x}\text{Sb}_x$ system is attractive for the cascade configuration because the bandgap ranges from $\approx 0.7 \text{ eV}$ (GaSb) to over 2.0 eV (AlAs); hence it is possible to fabricate all the components of the cascade cell in a single material system. The major drawback is the large amount (7.5 percent) of lattice mismatch between GaAs and GaSb. To avoid the problems associated with lattice mismatch, matching schemes are generally used to grow materials with useful bandgaps on GaAs substrates; these schemes employ either step-graded layers [23] or a continuously graded

layer [24]. The use of step-graded layers has been examined, and the use of a continuously graded layer is currently under investigation.

When using step grading in a mismatched system, it is essential to consider the optimum composition change from one layer to the next, more specifically, how much of an Sb increase can be tolerated while maintaining good crystallinity and an adequate surface morphology for growth of subsequent layers. Using full-width-at-half-maximum (FWHM) of an X-ray diffraction pattern and Nomarski optical microscopy to indicate crystallinity and surface morphology, respectively, the most desirable grading layer would not involve more than a 4.5 percent increase in antimony content from one layer to the next. Beyond this value the crosshatch pattern, reported in much of the GaAsSb literature, characteristic of misfit dislocation networks, becomes very pronounced. This 4.5 percent value is consistent with the 3 percent step-graded layers used in Reference 9, for example.

There is a drawback to limiting the graded layers to 4.5 percent. Since the optimum bottom cell would require approximately 24 percent GaSb (i.e., $\text{GaAs}_{0.76}\text{Sb}_{0.24}$) for a bandgap near 1.0 eV, a minimum of four grading layers would be required to get to the 24 percent value. A compromise is to forsake some crystalline quality to gain a reduction in the number of matching layers required; therefore, to increase the grading layers to 6 or 7 percent steps, only three layers are required. Some justification for this can also be found in the literature where workers [25] have reported that diodes with a composition of $\text{GaAs}_{0.94}\text{Sb}_{0.06}$ have electroluminescent efficiencies the same order of magnitude as diodes with $\text{GaAs}_{0.97}\text{Sb}_{0.03}$ in spite of the greater lattice mismatch.

Using this step grading technique, top layer compositions in the range of $0.18 \leq 1 - x \leq 0.24$ were grown. This composition range was reached in both three- and four-layered structures. None of these secondary substrates had particularly good surface morphologies, and the FWHM's of all the X-ray diffraction patterns were fairly broad. Coupled with the diffusion length measurements of 1 μm or less for diodes fabricated using step-graded layers, the above results indicate that $\text{GaAs}_x\text{Sb}_{1-x}$ ($x \approx 0.76$) as the bottom cell may be difficult to realize with optimum material quality.

An alternative to step grading is continuous grading [24] in which the composition on one of the components, antimony in this case, is gradually increased. The aim is to accommodate the lattice mismatch with elastic strain instead of dislocation [26]. The growth of thin, graded bandgap layers has been reported for the $\text{Al}_x\text{Ga}_{1-x}\text{As}$ system [27] using what has been designated the isothermal, etchback-regrowth method [28]. Although previously used to grow thin window layers on solar cells, the approach seemed plausible to grow continuously graded layers on GaAs substrates.

The method was tried, and the results have been very encouraging. Single layers of $\text{GaAs}_{0.88}\text{Sb}_{0.12}$ grown by the isothermal, etchback-regrowth method followed by a normal cooling program have shown FWHM of diffraction patterns almost identical to the GaAs substrate (see Figure 3.17); this is a qualitative indication that the crystalline quality of the epitaxial layer is comparable to the substrate. The surface morphologies of the grown layers are also excellent, and there is a complete absence of the crosshatched patterns characteristic of misfit dislocation networks (see Figure 3.18). Photoluminescence spectra showed the most intense emission of any of the grown antimonide-containing layers.

Attempts at laser annealing to improve the quality of the material met with no success. Several samples of $\text{GaAs}_x\text{Sb}_{1-x}$ with various x values were irradiated with energy densities of 1.0 and 1.5 J/cm^2 . While no changes in the X-ray spectra of the samples were noted before and after exposure, the PL spectra changed drastically. Samples that showed a PL response before exposure showed no response in areas which had been irradiated. Normal response was measured on nonexposed areas. It is assumed that at these laser energies, a thin surface layer was melted and resolidified. This did not affect the X-ray spectra because penetration was too deep. However, the PL response was completely eliminated by non-radiative recombination in this surface layer. In addition, the surface areas affected by the laser showed a milky color characteristic of oxidation. No further work has been done with this technique.

Some work has been done on the phase diagram of the GaAsSb system. The purpose for this was twofold:

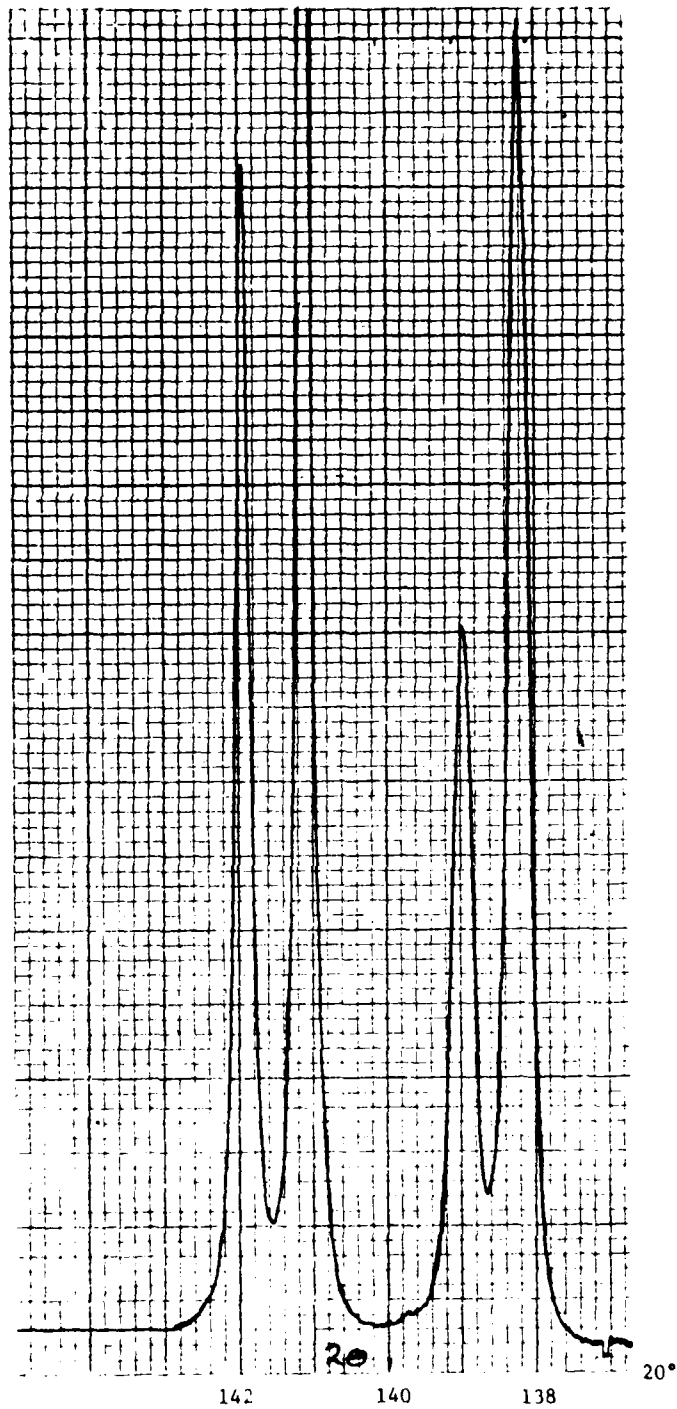
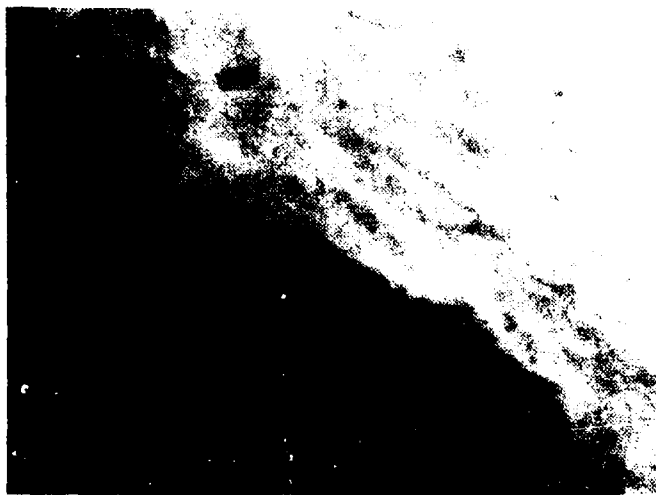


Figure 3.17. Diffraction pattern for layer of $\text{GaAs}_{0.88}\text{Sb}_{0.12}$ grown on GaAs using isothermal, etchback-regrowth method to grow this continuously graded, matching layer.



a) $\text{GaAs}_{0.94}\text{Sb}_{0.06}$ single layer grown on GaAs.



b) $\text{GaAs}_{0.9}\text{Sb}_{0.1}$ layer grown on continuously graded layer.

Figure 3.18. Demonstration of efficacy of continuously graded layers. a) 6% GaAs grown on GaAs showing cross-hatched pattern of misfit dislocation networks. b) 40% GaSb grown on GaAs with continuously graded layer by isothermal technique. Note absence of cross-hatching in spite of greater lattice mismatch.

1. Most published data in this system are the result of theoretical computation, and
2. There is some question as to the complete miscibility of the system.

The results shown in Figure 3.19 are experimentally derived points and are compared with the theoretical work of Nahory, et al. [23]. While the shapes of the curves appear similar, the antimony incorporation in the solid is greater than predicted by the model. In the composition range involved ($0 \leq 1 - x \leq 0.24$), there does not appear to be any problem with miscibility at the growth temperature of $\approx 750^\circ\text{C}$. At lower temperatures this may not be the case.

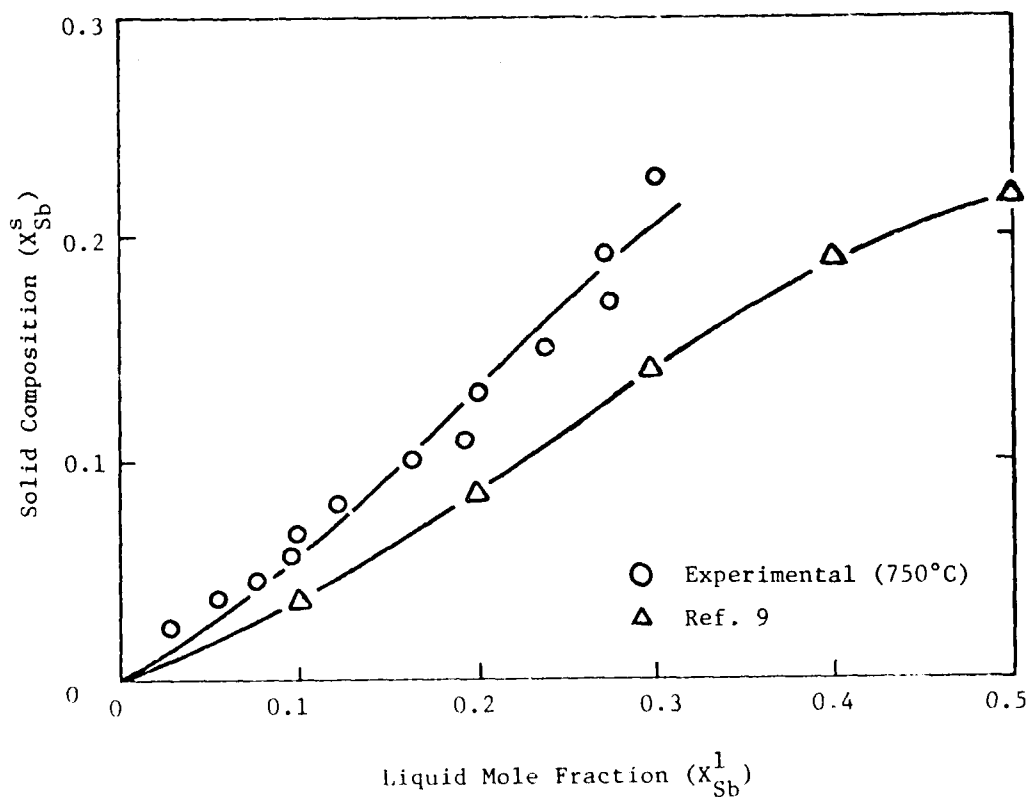


Figure 3.19. Portion of GaAsSb phase diagram.

Studies of several device structures have been made in the GaAsSb and AlGaAsSb material systems. Most of these studies have been made on devices grown on the step-graded layers. The use of the continuously graded layers is very recent in the research program, and device studies on these layers are just now beginning.

Three step-graded layers of GaAsSb (GaSb = 4, 7, then 12 percent) were grown on (111) GaAs, As-face substrates. The lattice constant of the top layer was 5.708 Å as measured by X-ray diffraction, and the band-gap was 1.23 eV as determined by photoluminescence measurements. Also, GaAsSb layers with lattice constants of 5.7218 Å (≈ 20 percent GaSb) and $E_g \approx 1.1$ eV have been grown by five step-graded layers. Figure 3.20 shows the X-ray diffraction pattern of these five step-graded layers. Photoluminescence of GaAsSb samples has given a broad peak (see Figure 3.21) with relatively low intensity, which indicates a poor lifetime and/or high density of lattice defects. These layers are n-type as grown. Junctions have been obtained by Ge doping. The I-V characteristics have shown open circuit voltages of 0.5 V to 0.6 V, as depicted in Figure 3.22, for material with about 1.2 eV bandgap. This low V_{oc} may be due to a high density of dislocations resulting from the step grading technique. Figure 3.23 shows an I-V plot that has a central region with a diode factor near unity. Diffusion length measurements by the gamma ray technique on similar diodes have given a value of ≈ 0.2 μm for the carrier collection depth. Such a low value is not acceptable for the present solar cell structure. Efforts are underway to improve the quality of these layers and to obtain better values for the diffusion length. The step-grading process is being replaced by the continuous grading of AlGaAsSb, where the Al content in the epilayer decreases with the layer thickness and the lattice constant thus increases.

A few diodes have been grown using the isothermal, etchback-regrowth method to lattice match the junction to the GaAs substrate. Measured collection depths are given below:

Sample No.	V_{oc}	I_{sc}	Collection depth
T-48-A	0.40 V	0.1 mA	0.56 μm
T-49-A	0.45 V	0.12 mA	0.61 μm
T-50-A	0.50 V	0.25 mA	0.75 μm

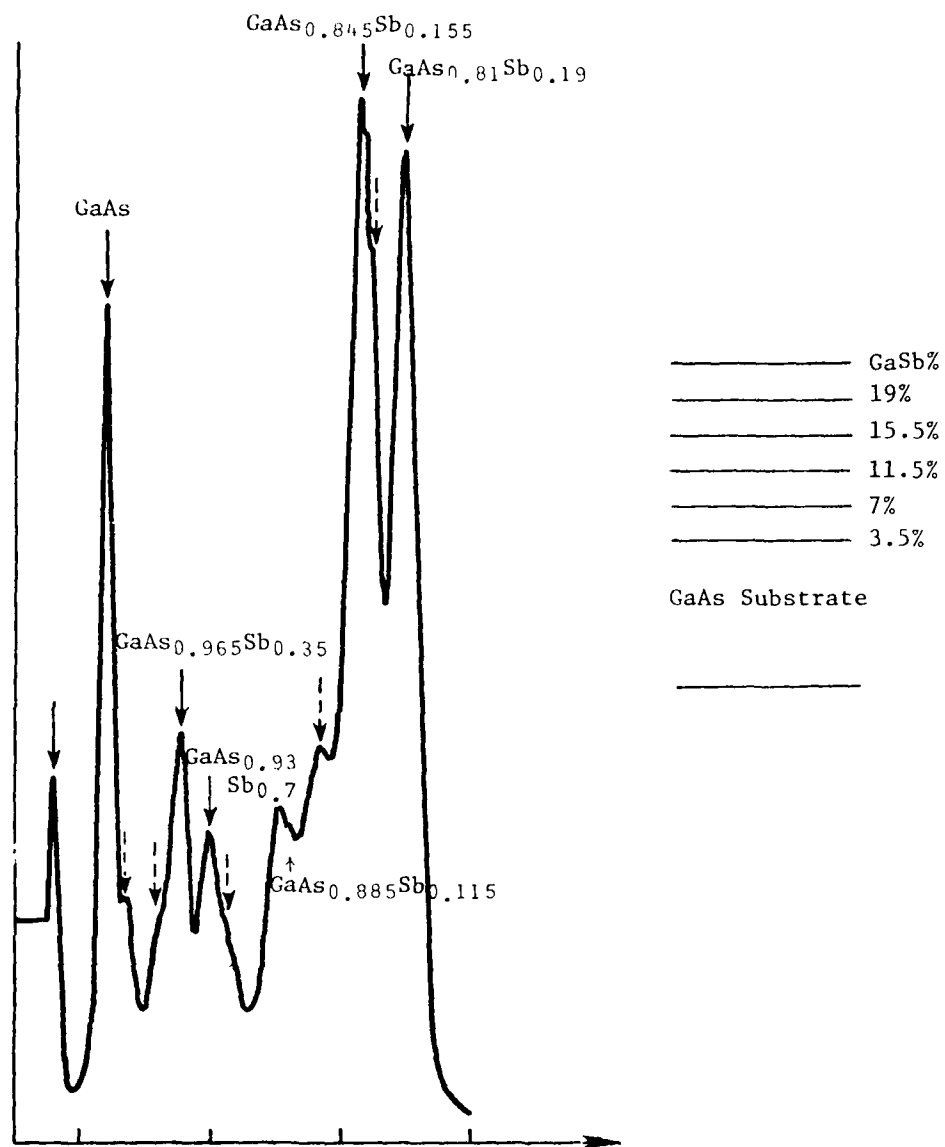


Figure 3.20. X-ray diffraction pattern for GaAsSb five step-graded layers on GaAs substrate.

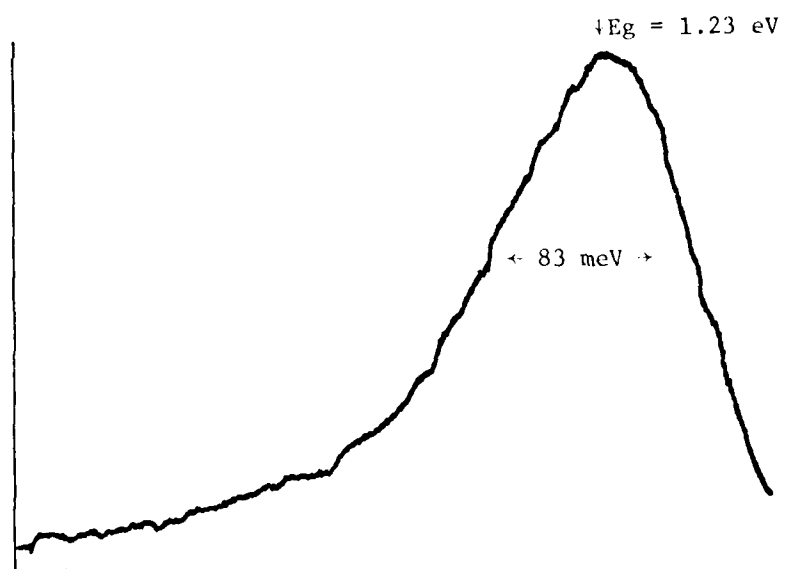
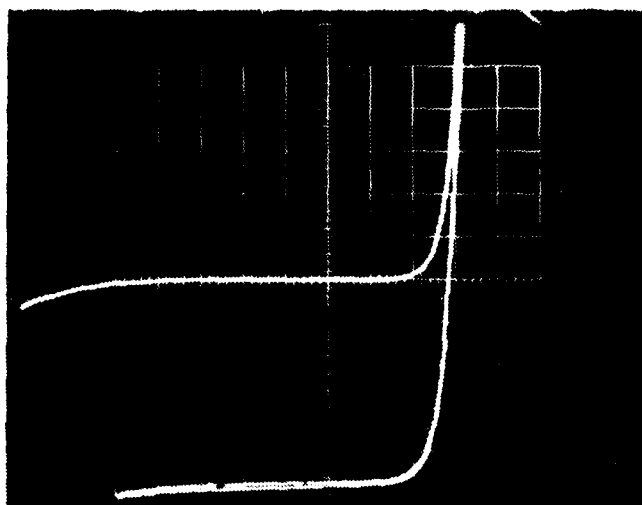


Figure 3.21. Photoluminescence spectra for GaAsSb sample.



Hor: 0.5 mA/Div

Vert: 0.2 V/Div

p	}	GaAs _{0.88} Sb _{0.12}
n		GaAs _{0.88} Sb _{0.12}
n	}	GaAs _{0.93} Sb _{0.07}
n		GaAs _{0.96} Sb _{0.04}
n	}	GaAs

Figure 3.22. V-I characteristics of GaAsSb p-n junction.

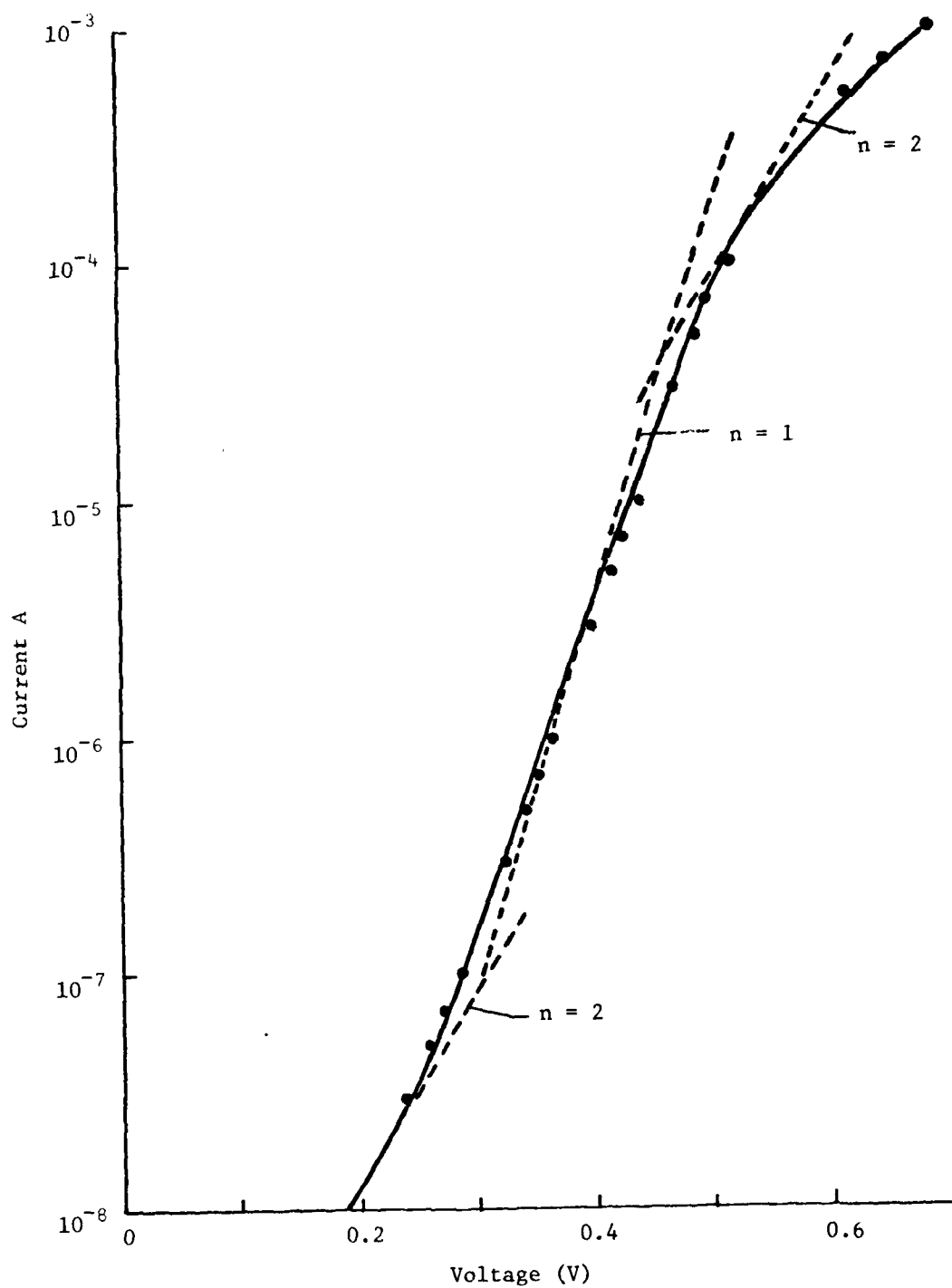


Figure 3.23. V-I characteristic for GaAsSb diode.

The composition of these diodes is $\text{GaAs}_{0.92}\text{Sb}_{0.08}$, and the bandgap is approximately 1.27 eV as determined by photoluminescence techniques. The good crystalline quality of these samples is indicated by the narrow FWHM of the X-ray diffraction pattern (Figure 3.24) of three grown GaAsSb layers on a GaAs substrate. It is noteworthy that each succeeding diode yielded larger V_{oc} values and deeper collection depths, implying perhaps that impurities are being depleted from the melts. If this is the case, bakeout of the antimony and gallium could eliminate the impurities that have been limiting the diffusion lengths in the grown material. This has been tried, and the results are summarized in Table 3.1. Collection depths, the sum of hole and electron diffusion lengths and the junction depletion width, as high as 10.4 μm have been measured. All the samples were grown from melts made with prebaked components; however, the correlation of slow cooling rate and long collection depths seems quite obvious--i.e., the slower the growth, the better the collection depth. These diodes had V_{oc} values of about 0.5 V, which is slightly lower than expected based on the 1.23 eV bandgap (determined by photoluminescence). This low value may be the result of several effects, including surface recombination and bulk recombination in the relatively thick (≈ 10 to 11 μm) junction layers.

Table 3.1. Effect of Growth Cooling Rate on Collection Depth of $\text{GaAs}_{x-1}\text{Sb}_x$ Diodes.

Sample	Collection depth (μm)	Cooling rate ($^{\circ}\text{C}/\text{min}$)
T56A	2.1	0.1
T57A	1.9	0.2
T58A	1.7	1.0
T60A	7.8	0.07
T61A	8.4	0.07
T62A	7.8	0.07
T63A	10.4	0.07

NOTE: Collection depth is sum of hole and electron diffusion lengths and junction depletion widths (≈ 0.3 to $0.4 \mu\text{m}$ in these diodes).

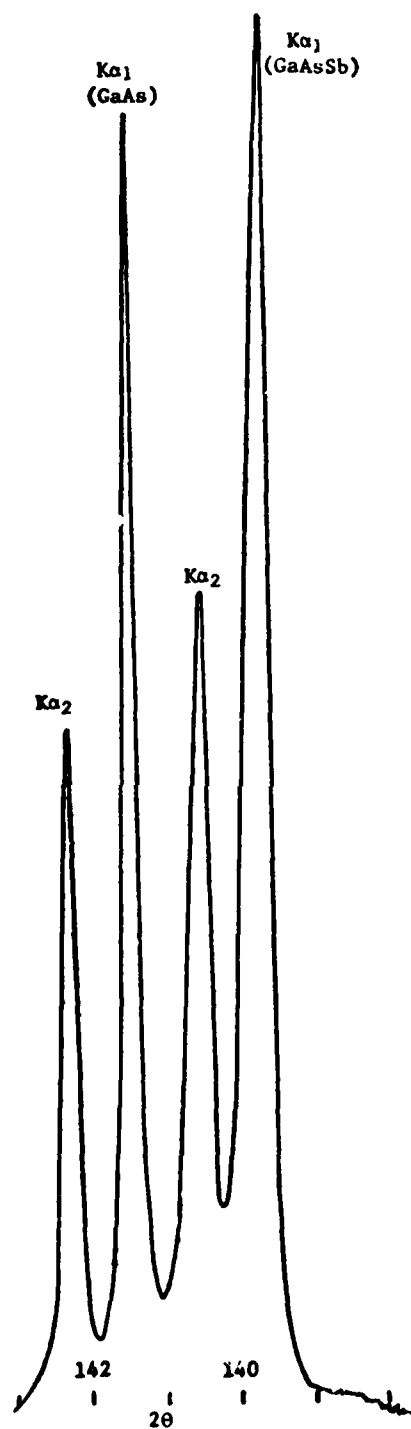


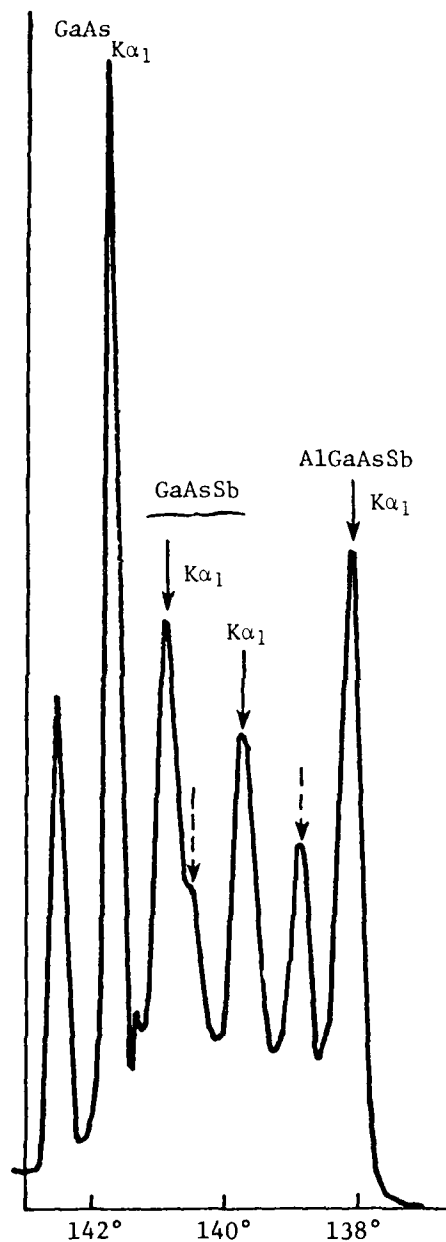
Figure 3.24. X-ray diffraction scan of T50A showing FWHM of three grown layers comparable to GaAs substrate.

Efforts are currently underway to determine the relative contributions of prebaking melt components, growth rate, and the isothermal, etchback-regrowth method to the markedly increased collection depths.

Another feature, beside impurities and interface phenomena, that might limit collection depth is a native defect. In pure GaSb, it has been shown that Sb vacancies may be the predominant native impurity, and workers have shown the importance of Sb partial pressure during LEP growth of this compound. Thus by placing pure Sb in one well of the graphite boat, the Sb pressure in the growth system should increase, particularly at low H_2 flow rates, and hence reduce the tendency of Sb to escape from the melt. The diodes grown in this fashion had collection depths on the order of 2 μm . For GaAsSb, As has a higher distribution coefficient than either Ga or Sb--i.e., it has higher activity. Thus it is possible that the poor collection depths observed with fast cooling rates as shown in Table 3.1 are related to the rapid depletion of As in the melt that will result in a nonstoichiometric epilayer. Hence a slow cooling rate coupled with an As overpressure during the growth cycle may result in more improvements in the collection depth.

AlGaAsSb quaternary layers for the top cell have been epitaxially grown on GaAsSb step-graded layers. Figure 3.25 shows the X-ray diffraction pattern for one particular epitaxial AlGaAsSb layer on GaAsSb. The lattice mismatch for this particular combination is about 0.5 percent; however, other layers have been grown with a mismatch of about 0.2 percent between the GaAsSb and the AlGaAsSb. The composition of this quaternary layer as determined by the electron microprobe is Al = 10 percent, Ga = 40.5 percent, As = 42.8 percent, and Sb = 6.5 percent. For these layers the bandgap is 1.45 eV as measured by photoluminescence.

The layers as grown are n-type, and p-n junctions have been obtained by Ge doping of the upper layer. The I-V characteristic of one AlGaAsSb diode, as shown in Figure 3.26, gives an open circuit voltage of about 0.7 V. Again, this is a relatively low V_{oc} for a material with a bandgap of 1.45 eV. This may be a result of a high density of defects due to the step grading process and/or the presence of 0.5 percent lattice mismatch between the AlGaAsSb and the GaAsSb. Work is underway to obtain a better quality AlGaAsSb p-n junction with a bandgap of about 1.7 eV.

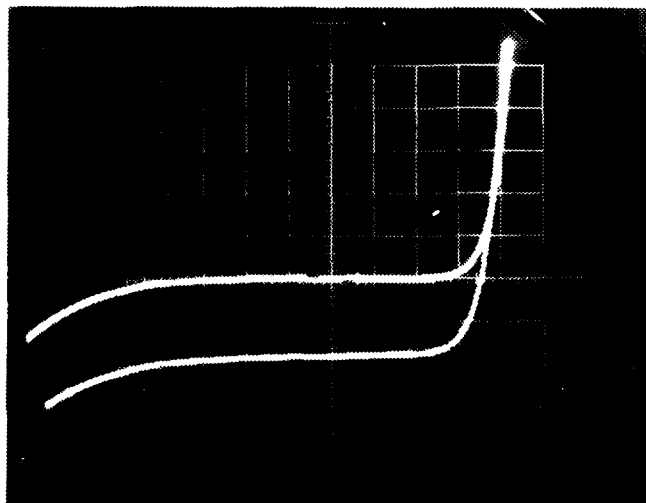


AlGaAsSb
GaAs _{0.92} Sb _{0.08}
GaAs _{0.96} Sb _{0.04}
GaAs

Electron Microprobe Data
on the AlGaAsSb

Al = 10.1%
Ga = 40.5%
As = 42.8%
Sb = 6.5%

Figure 3.25. X-ray diffraction pattern for AlGaAsSb on GaAsSb.



Hor: 0.2 V/Div

Vert: 0.1 mA/Div

P	}	$\text{Al}_{0.2}\text{Ga}_{0.8}\text{As}_{0.87}\text{Sb}_{0.13}$
n		
n	}	GaAsSb
n		
n	}	GaAs

Figure 3.26. V-I characteristics of AlGaAsSb p-n junction.

No work has been done on the AlGaAsSb connection junction, but Ge and Te seem to be very suitable candidates for the p^+ and n^+ dopants.

AlGaAsSb with 60 percent AlAs and 10 percent GaSb has been epitaxially grown on a step-graded GaAsSb layer. This quaternary alloy, which should have a bandgap of about 2 eV in the indirect region, is being considered as a window for the antimonide system and also for several other proposed systems. Detailed electrical evaluations of these layers have not yet been made.

In summary, one of the major problems initially experienced with Sb layers was the low diffusion lengths observed. The combination of isothermal, etchback-regrowth, prebaking melt components, and very slow growth has enabled this problem to be overcome; and the GaAsSb remains a viable candidate for the bottom cell.

3.9 GaInP Studies

Considerable effort has been directed towards $Ga_{1-x}In_xP$ materials growth in the 1.6 to 1.7 eV range using the HCl-hydride open tube VPE technique. The VPE system being used employs some major design changes in the Ga and In source reaction zones. The growth system was designed to have a fast response so that abrupt (100 to 200 Å) junctions could be synthesized merely by changing dopant type while the growth is in progress. This is also expected to minimize composition changes or the introduction of defects at the junction.

GaInP layers have been grown successfully over a wide range of compositions. Figure 3.27 illustrates the photoluminescence spectra obtained on a 1 μ m layer having an InP composition of approximately 53 percent. The strong peak at 1.86 eV is indicative of a layer of relatively good quality. The small peak at 1.43 eV is attributed to the GaAs substrate, which is apparently being excited through the thin GaInP epilayer.

As-grown GaInP layers were n-type with carrier concentrations ranging from $6 \times 10^{16} \text{ cm}^{-3}$ to $7 \times 10^{16} \text{ cm}^{-3}$ as determined by Hall effect measurements. An electron mobility of $440 \text{ cm}^2/\text{V sec}$ was measured in a 1 μ m layer.

A GaInP p-n junction was successfully fabricated by growing an n-type layer and then introducing Cd and S into the growth system to form a p-type upper layer. The structure, shown in Figure 3.28, was grown at 600°C.

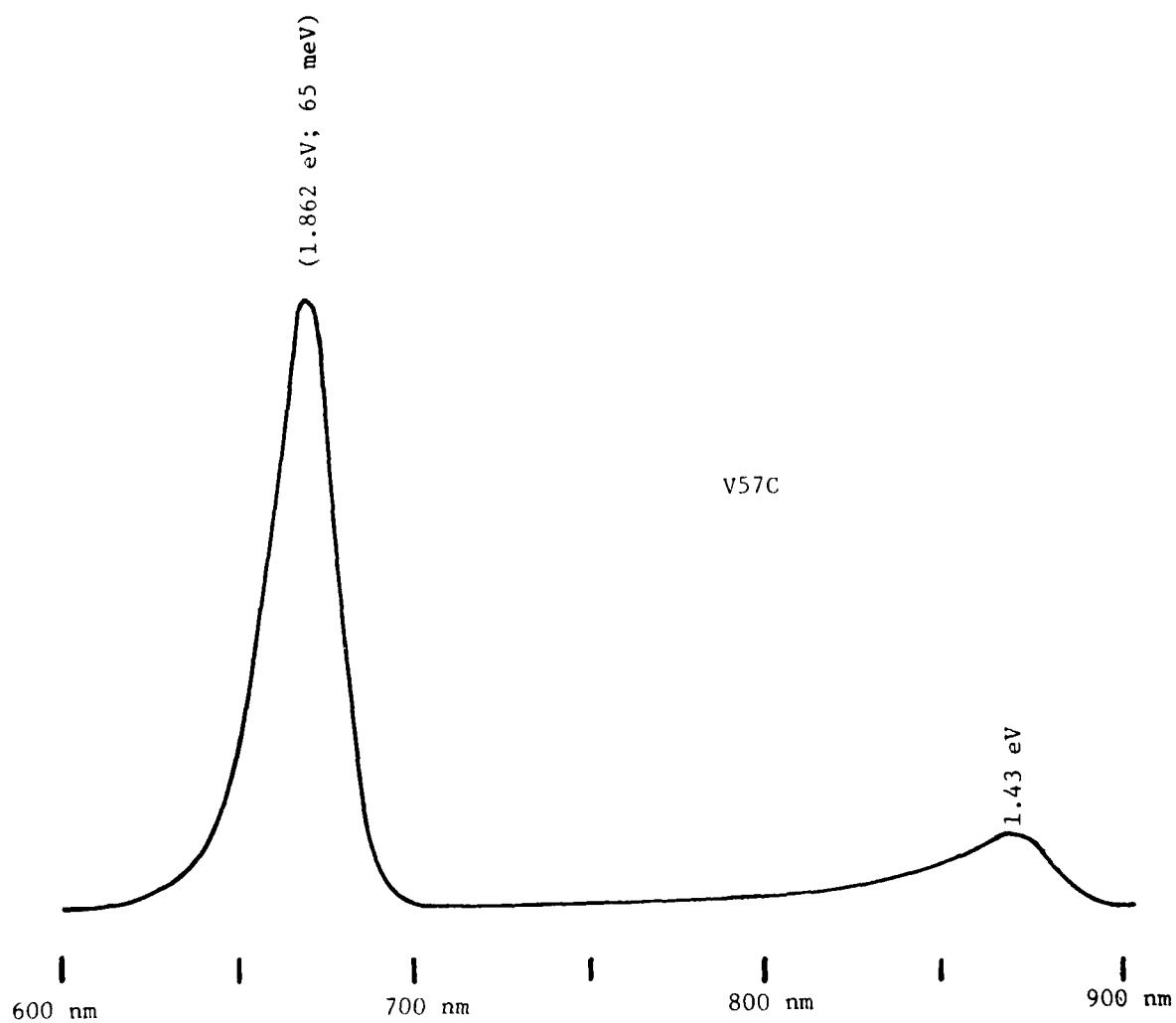


Figure 3.27. Photoluminescence spectra of GaInP sample.

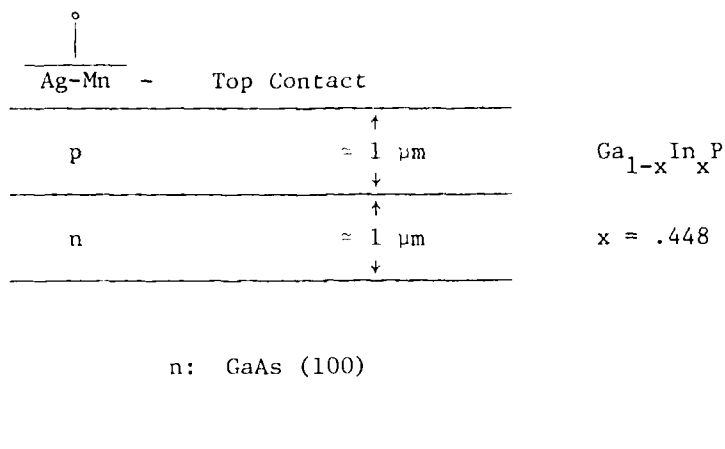


Figure 3.28. GaInP sample configuration.

The composition was less than the desired 60 to 70 percent InP (1.6 to 1.7 eV) due to In boat depletion. The In boat was recharged, and compositions again returned to the nominal 63.5 percent InP. The individual layers were approximately 0.8 to 1.0 μm thick, and the contact used for the top layer was Ag-Mn. V-I characteristics of this structure are shown in Figure 3.29.

Subsequent p-n junctions were grown in which the p-type dopant flow rate was systematically reduced. This, however, resulted in greater difficulties in obtaining ohmic contacts. Higher alloying temperatures (≈525°C), which were required, resulted in short circuits and were thought to be due in part to the thin layers used in the junctions.

In order to alleviate the ohmic contact problems, a heavily doped p⁺ capping layer is currently being deposited on the p-layer to form a p⁺/p/n structure. The thickness of each of these layers has also been increased to approximately 2 μm each.

Some difficulty has been recently experienced in obtaining reproducible GaInP layers and is believed to be the result of several small leaks in the VPE system and possibly contaminating source gases.

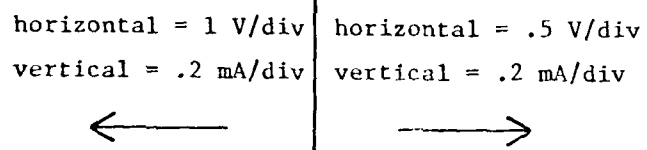


Figure 3.29. V-I characteristics for GaInP sample (44.8% InP in GaInP).

4.0 PREDICTED CASCADE SOLAR CELL PERFORMANCE CHARACTERISTICS BETWEEN 83 K and 600 K

4.1 Introduction

An analytical method and a companion computer program have been developed to optimize cascade solar cell design for performance under a given set of operating conditions [8,29-31]. The operating conditions under which optimization studies have been conducted are usually prescribed by the values assigned to air mass, operating junction temperature, and solar concentration. For space applications the design has been optimized for operation at 300 K, AM 0, and unity solar concentration. The device performance characteristics have been obtained over an 83 K to 600 K temperature range.

The analytical method used in this work considers the excitation of the total solar spectrum in the linear continuity equation. The solution of the minority carrier concentration is obtained in closed form by making the assumption that the mobility is independent of position or is an average value in those cases where the bandgap and/or impurity concentration is variable. It is also assumed that either the built-in field is independent of position or it has an average value.

The other assumptions used in the analysis are that the thermal diffusion contribution to dark current is large compared to space charge recombination and excess tunnel current components; the minority carrier recombination rate is linearly proportional to excess carrier concentration; the surface recombination velocity is 10^6 cm sec⁻¹; reflectivity and recombination at heterojunction interfaces are negligible; efficiency is not corrected for grid contact shadowing or for power loss from joule heating arising in the structure's series resistance; and reflectivity at the window is 5 percent. In all calculations of carrier concentration, Fermi-Dirac statistics are used.

Figure 4.1 shows the bandstructure parameters used to construct the mathematical model in the analysis of the monolithic, two-junction cascade solar cell. It consists of two homojunctions on either side of a tunnel junction and a window layer. The homojunctions are fabricated from material of differing bandgap values, but the tunnel junction bandgap is

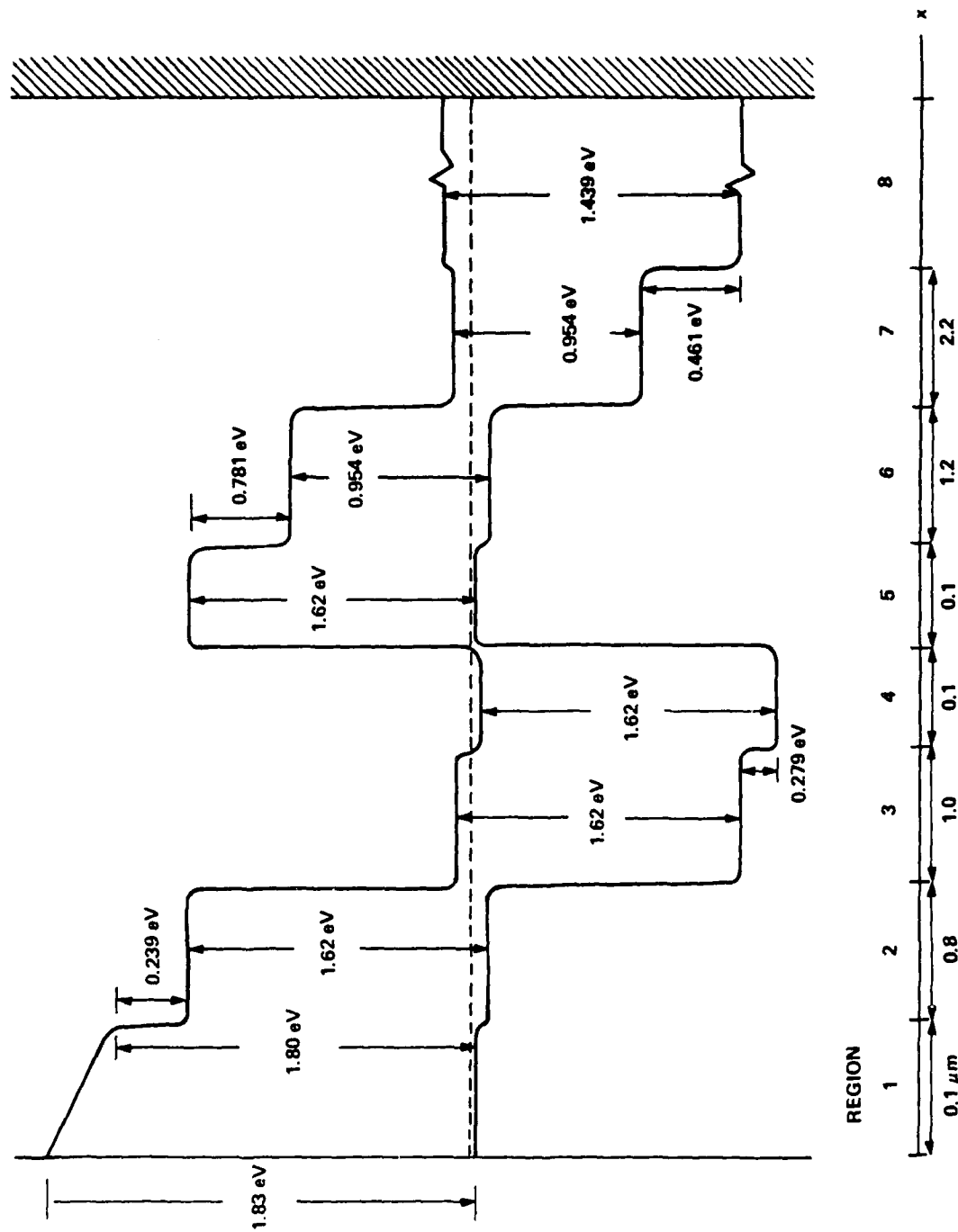


Figure 4.1. Bandstructure of a two-junction, voltage aiding, two-terminal cascade solar cell optimized for operation at 300 K, AM 0, 10^6 cm sec^{-1} surface recombination velocity, and unity solar concentration ratio.

equal to or greater than either homojunction material to ensure that it is optically inactive. The wider bandgap cell is closest to the surface and capped with a window layer while the bottom cell has a smaller bandgap and is placed below the tunnel junction. For maximum efficiency, the bandgap combination used for the top and bottom cells is carefully chosen along with other material and structural parameters. Regions 1 through 5 use AlGaAs, Regions 6 and 7 use GaInAs, and the substrate, Region 8, is GaAs.

Imposed on the structure in all these calculations are a window layer thickness of $0.1 \mu\text{m}$ with 10^{18} cm^{-3} acceptor concentration and a linear bandgap grading as required to establish a 3000 V cm^{-1} built-in field in the window layer. The impurity concentrations in Regions 1, 3, 6, 7, and 8 are assumed to be 10^{17} cm^{-3} [8,29-31].

4.2 Computer Modeling Results

The device performance characteristics in the 83 K to 600 K temperature range obtained from computer modeling for a cascade cell design represented in Figure 4.1 are presented and discussed in this section. Figure 4.2 shows the cascade cell family of V-I curves, with temperature a parameter. The open circuit voltage is 1.55 V at 350 K, increasing to 2.5 V at 83 K and decreasing to about 0.67 V at 600 K. The short circuit current decreases slightly with decreasing temperature. As a result of the significant increase in photovoltage and the small decrease in short circuit current, the areas under the V-I curves increase with decreasing operating temperature. The increased area under the V-I curve represents an increase in conversion efficiency.

In Figure 4.3 the behavior of the conversion efficiency with temperature is shown for the cascade cell and for each of the component cells. These calculations show that the efficiency is 46.5 percent at 83 K and decreases to 32 percent at 300 K. This results in a temperature coefficient of $0.069 \text{ \%}/^{\circ}\text{C}$ and a normalized temperature coefficient of $0.0022/^{\circ}\text{C}$. (The normalized temperature coefficients of conversion efficiency and photovoltage are defined as the change of efficiency or voltage divided by the temperature change and this slope normalized with respect to the corresponding value at 300 K.) These values are approximately 18 percent

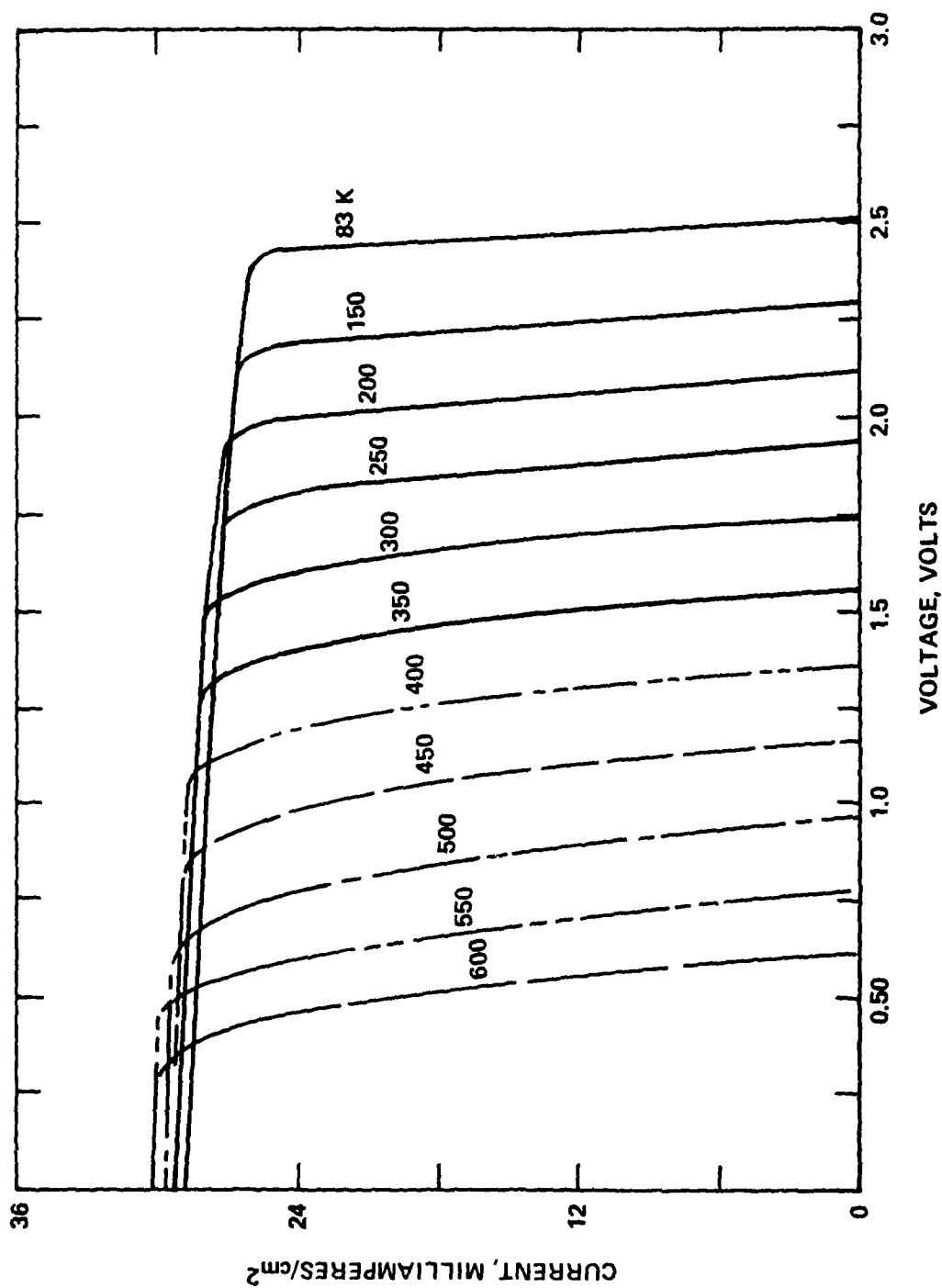


Figure 4.2. Cascade solar cell V-I family of curves with temperature a parameter; conversion efficiency maximized for operation at 300 K, AM 0, unity solar concentration ratio, and 10^6 cm sec⁻¹ surface recombination velocity.

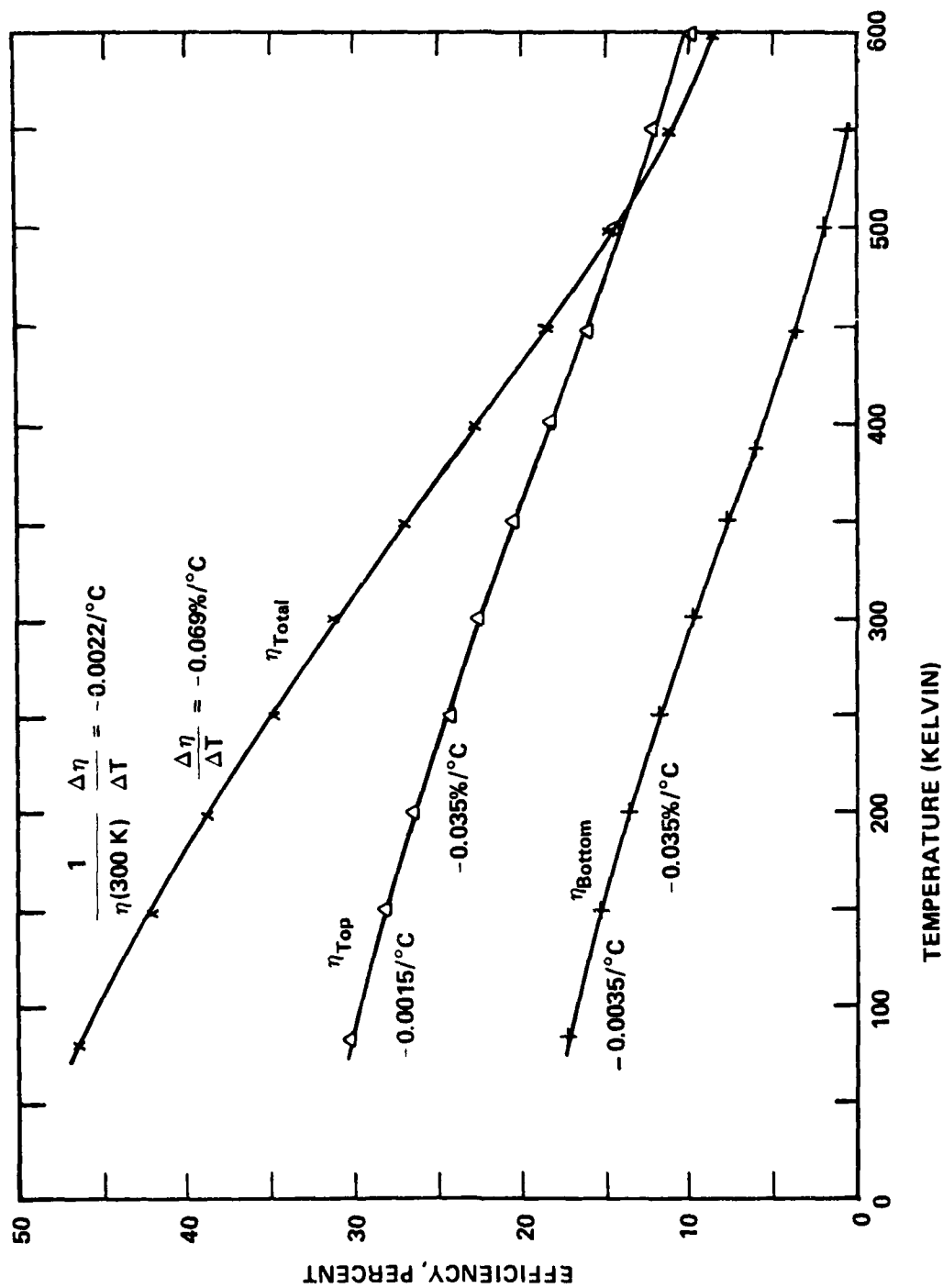


Figure 4.3. Conversion efficiency vs. temperature of a cascade cell designed for maximum efficiency under the operating conditions of 300 K, AM 0, unity solar concentration ratio, and 10^6 cm sec^{-1} surface recombination velocity.

lower than the corresponding values over the 300 K to 600 K range. The same statement can be made for the coefficients of the top and bottom cells. The relative behavior of efficiency of the top and bottom cells is similar to the behavior over the 300 K to 600 K range. The temperature coefficient of the top cell is seen to be slightly higher than the bottom cell value.

These results show that the efficiency markedly increases with decreasing temperature, approaching 50 percent at 83 K. The marked improvement obtained for operating temperatures below 300 K suggests that it may be advantageous to design solar panels on space vehicles so that cell temperature is as low as possible.

The temperature behavior of the photovoltages at the maximum power point on their respective V-I curves of the cascade, top, and bottom cells are shown in Figure 4.4. The three photovoltages increase significantly with decreasing temperature. This type behavior is also observed in conventional single-junction solar cells. The temperature coefficient with both top and bottom cells operating as a unit is $-4 \text{ mV}/^\circ\text{C}$ while for the individual cells it is $-2.3 \text{ mV}/^\circ\text{C}$. The normalized temperature coefficient is smallest for the top cell and highest for the bottom cell. This arises because the larger bandgap of the top cell results in a smaller dark current than for the bottom cell, which has a smaller bandgap. The normalized temperature coefficient for the cascade cell takes on a weighted average value between the values of the component cells. The photovoltage normalized temperature coefficients are significantly greater in magnitude than the corresponding values for efficiency given in Figure 4.3.

Table 4.1 lists the efficiency and photovoltage normalized temperature coefficients and their ratios for the 83 K to 350 K and 300 K to 600 K temperature ranges. In general, the ratios obtained in the 83 K to 350 K investigation deviate further from unity than do the ratios in the 300 K to 600 K study. Moreover, the cascade ratio for the 83 K to 350 K case is less than unity while for the 300 K to 600 K case it is greater than unity. This shows that the photovoltage normalized coefficient is larger in magnitude than the efficiency value for the 83 K to 350 K case while the opposite is true for the 300 K to 600 K case. The

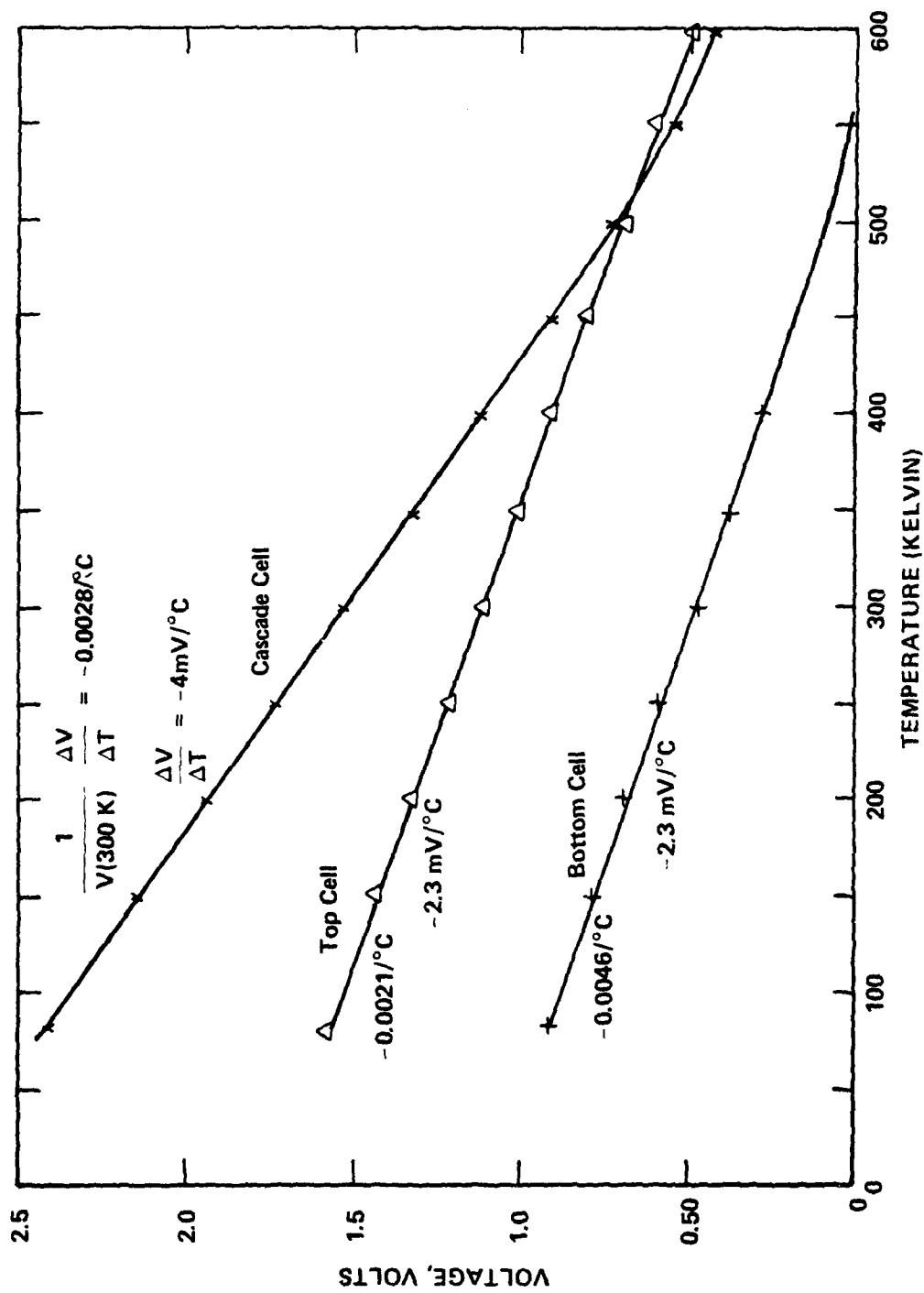


Figure 4.4. Voltage at the maximum power point of the cascade cell V-I curve vs temperature of a cascade cell designed for maximum efficiency under the operating conditions of 300K, AM 0, unity solar concentration ratio, and $10^6 \text{ cm}^{-1} \text{ sec}^{-1}$ surface recombination velocity.

Table 4.1. The efficiency and photovoltage normalized temperature coefficients and their ratios in the 83K to 350K and 300K to 600K temperature ranges.

	83 K -- 350 K			300 K -- 600 K [10]		
	Efficiency	Photovoltage	Efficiency Photovoltage	Efficiency	Photovoltage	Efficiency Photovoltage
Cascade	-0.0022/°C	-0.0028/°C	0.786	-0.0027/°C	-0.0026/°C	1.038
Top	-0.0015/°C	-0.0021/°C	1.667	-0.0019/°C	-0.0018/°C	1.056
Bottom	-0.0035/°C	-0.0046/°C	0.761	-0.0040/°C	-0.0041/°C	0.976

reason for the difference in the ratios between the two temperature ranges is a complex function of the internal competing electronic process: dark current decreasing at different rates in the top and bottom cells with decreasing temperature, particularly for the 83 K to 350 K case, giving increasing current mismatch between the top and bottom cells; while the fill factor changes in the 300 K to 600 K range, it is relatively constant in the 83 K to 350 K range; the photon absorption distribution changes which occur as bandgap changes with temperature.

The dark currents for the top and bottom cells are shown in Figure 4.5. These results show that while the top cell dark current decreases monotonically with decreasing temperature, the bottom cell dark current does not exhibit a monotonic behavior. Surprisingly the dark current value at 83 K is slightly higher than the value at 350 K. This suggests that the current mismatch between top and bottom cells is significantly greater in the 83 K to 350 K case than it is for the 300 K to 600 K case. In addition, one may conclude that the terminal current is limited by the top cell which results in the operating point on the bottom cell V-I curve being closer to the open circuit voltage point than to the short circuit current point.

The contributions to the total spectral response of the optimized cascade cell structure are shown in Figure 4.6. The electron contributions to the total response of each cell is higher than the hole contribution because the solar radiation is first incident on the p-region of each cell. This results in greater photon absorption in the p-regions, and consequently, there is a higher concentration of excess electrons produced.

The electron and hole contributions, as well as the total spectral response, shift to longer wavelengths with increasing temperature as a result of bandgap narrowing. While this shift takes place, their shapes remain very nearly the same, and the areas under the curves are also nearly the same. There is a decrease in response with increasing temperature between 0.2 and 0.75 μm due to increasing surface recombination loss. This is partially or totally compensated by the shift to longer cut-off wavelengths. These results are consistent with the V-I curves in Figure 4.2, which show that the short circuit current is relatively insensitive to temperature.

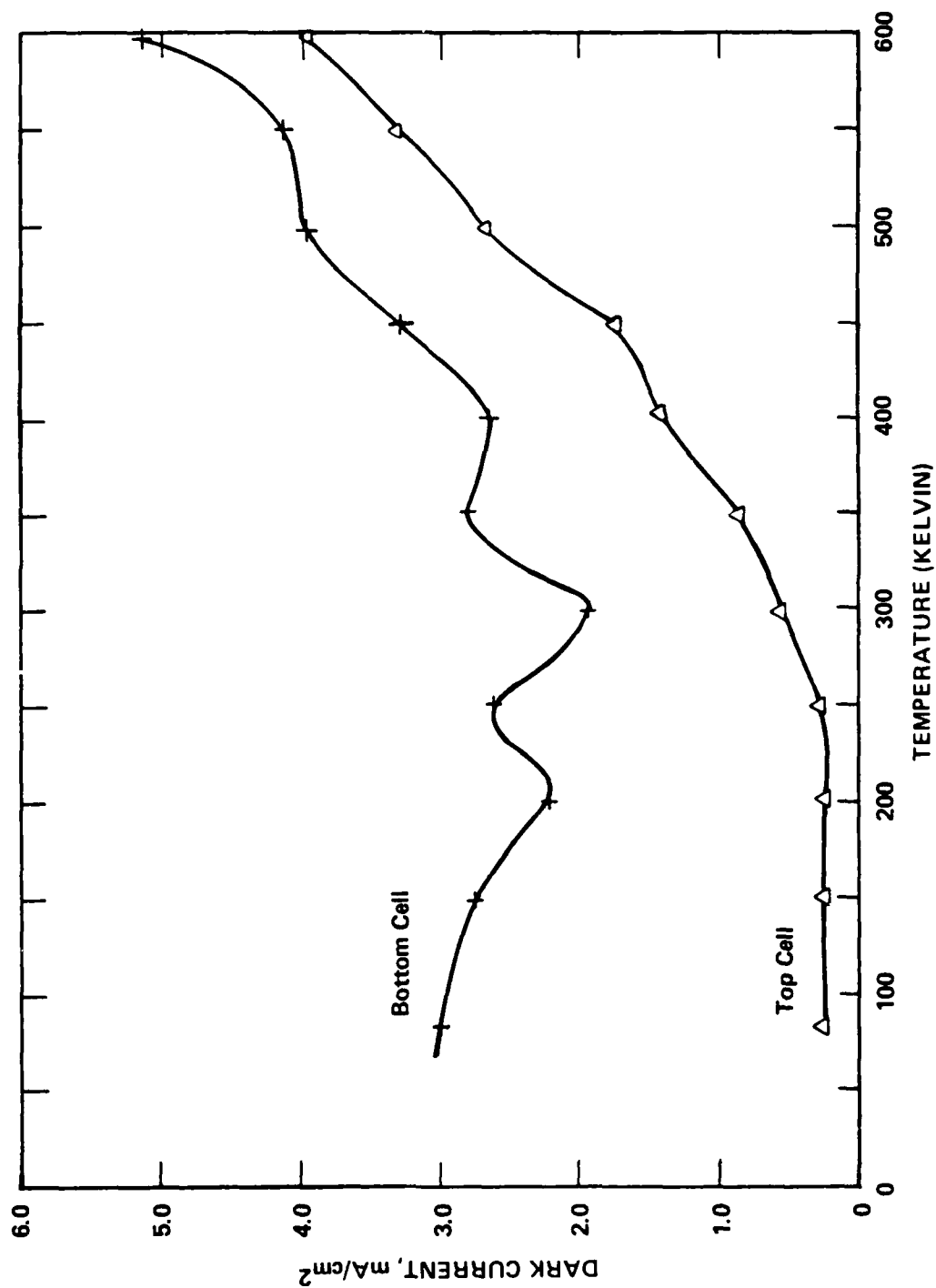


Figure 4.5. Dark current of the top and bottom cells vs temperature of a cascade cell designed for maximum efficiency under the operating conditions of 300K, AM 0, unity solar concentration ratio, and 10^6 cm sec^{-1} surface recombination velocity.

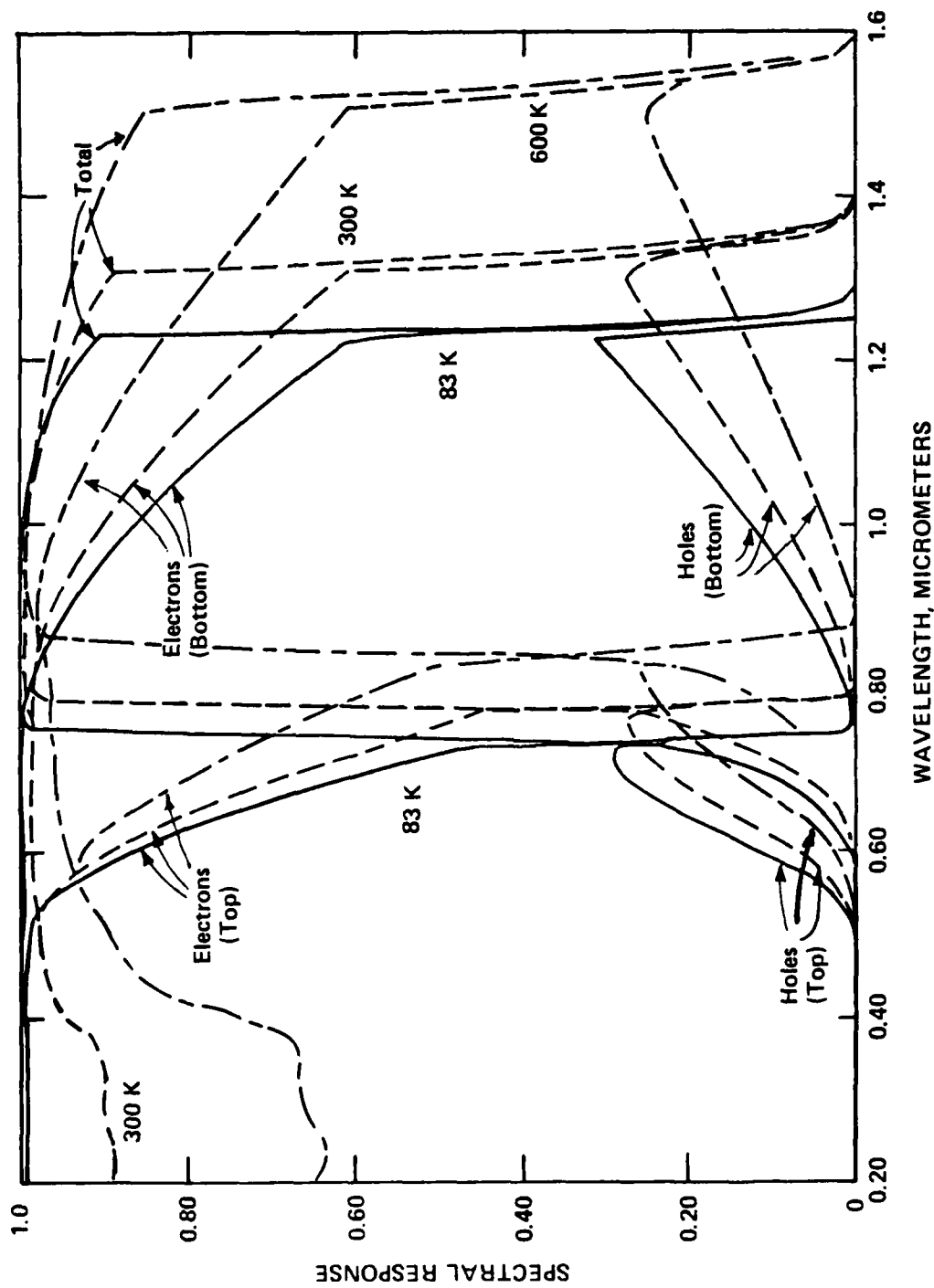


Figure 4.6. Spectral response of electrons and holes for top and bottom cells and the total spectral response of the cascade cell at 83 K and 300 K of a cascade cell designed for maximum efficiency under the operating conditions of 300 K, AM 0, unity solar concentration ratio, and 10^6 cm sec^{-1} surface recombination velocity.

5.0 REDUCED EQUIVALENT CIRCUIT OF A TWO-JUNCTION SOLAR CELL

5.1 Introduction

In this section a simplified V-I equation and an equivalent circuit are developed for a two-junction, monolithic cascade photovoltaic detector. The V-I equation and equivalent circuit are placed in forms that may be interpreted as representing a single-junction detector, which is in agreement with the theory and computer modeling developed for cascade solar cells. Two methods are presented to obtain the reduced forms.

Although the development of the cascade solar cell is in the early stages, circuit applications are being considered; in such applications it is useful to represent the cascade cell by a simple, convenient equivalent circuit and a corresponding voltage-current equation. The description of device performance characteristics by means of an equivalent circuit over a range of load values and over a temperature range is most desirable, but not always achieved. Equivalent circuits are only capable of describing some terminal characteristics, are almost never derived to describe internal processes, and typically do not accurately describe the V-I terminal behavior over the entire load range from zero to infinity. Therefore, appropriate approximations are made that best describe the behavior in the load region of major interest and the V-I behavior over a narrow temperature range.

It has been shown experimentally [18,19] and analytically [29-31] that cascade solar cell performance characteristics are similar to those of single-junction devices. For example, the V-I curve of a cascade cell has a shape similar to that of a single-junction cell. Ideally the short circuit current density is the same for both cells and the open circuit voltage is indicative of a cell having a bandgap value equal to the sum of the top and bottom cell bandgaps [29-31]. The cascade equivalent dark current takes on a value between the values of the separate top and bottom cells. The temperature coefficients of conversion efficiency and photovoltage are weighted averages of the top and bottom cells. With increasing temperature, the increase in surface recombination loss in the short wavelength region is compensated by the increase in spectral response in the long wavelength region due to the shrinkage of the bandgap in the top and

bottom cells. This results in the short circuit current being relatively insensitive to temperature, as it is in single-junction cells (see Section 4.0).

An equivalent circuit of a cascade cell may be constructed from the series connection of the individual equivalent circuits of three junctions: two solar cells and a tunnel junction [20]. A corresponding V-I relationship may be deduced that is equally unwieldy. However, the experimental data and analytical results suggest that a simpler V-I cascade cell equation may be derived and a corresponding reduced equivalent circuit deduced. These are similar in form to a single-junction solar cell. The simplified V-I equation and reduced equivalent circuit represent a significant reduction in complexity in contrast to the three-junction series connection configuration.

In this section a V-I equation is obtained; it is similar in form to that for a single-junction cell and describes the cascade cell terminal performance characteristics. Both an exact solution and an approximation method are used to obtain equations that represent the cascade cell terminal characteristics. As one would expect, the V-I equation obtained by using the approximate method is more convenient to use than the equation obtained using the exact analysis. However, both methods imply a reduced equivalent circuit that is similar in form to that for a single-junction solar cell. Such an equivalent circuit, of course, has great utility when modeling complex series-parallel combinations of cells in an array.

5.2 Reduced Equivalent Circuit

The bandstructure of a two-terminal, two-junction cascade solar cell (or photodetector) and its equivalent circuit, which is composed of the individual equivalent circuits for each of the component solar cells and the tunnel junction, are shown in Figures 5.1(a) and 5.1(b), respectively. The subscripts sc , D , sh , s , L denote short circuit current, dark current, shunt resistance, series resistance, and load resistance, respectively. The subscripts T and B refer to the top (wide bandgap) and bottom (narrow bandgap) cells, respectively, and TJ refers to the tunnel junction. In the following discussion it will be shown that neglecting the shunt resistance, the equivalent circuit shown in Figure 5.1(b) can be simplified, and a reduced equivalent circuit can be obtained as shown in Figure 5.1(c).

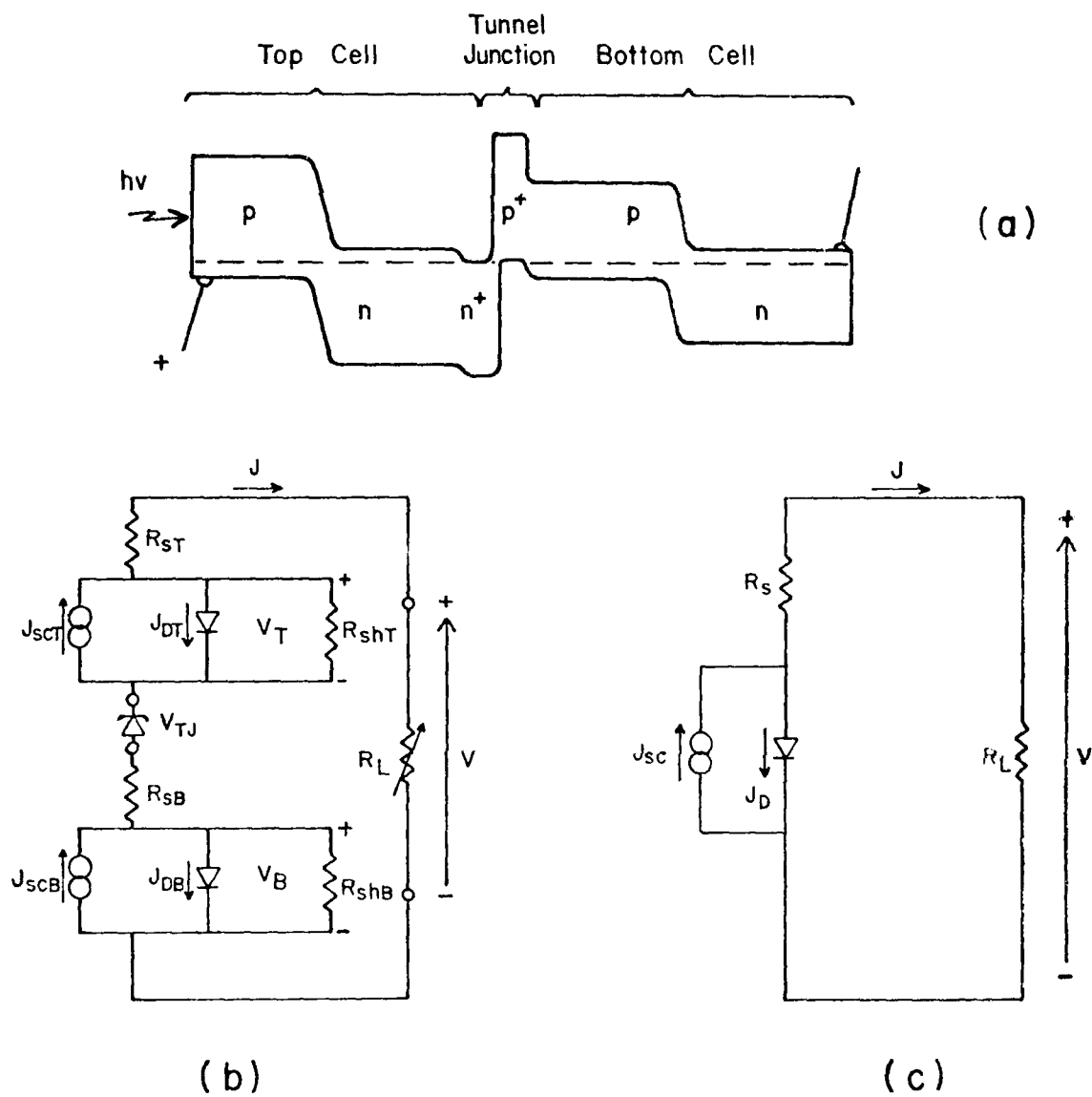


Figure 5.1. (a) Energy bandstructure of a two-junction, monolithic, cascade solar cell; (b) equivalent circuit of two-junction cascade solar cell; (c) reduced equivalent circuit.

energy band-structure in Figure 5.1(a) is for a semiconducting structure shown in Figure 5.1(b). In Figure 5.1(a), the device consists of top (wide bandgap) and bottom (narrow bandgap) junctions that are responsive to different portions of the solar spectrum and a connecting tunnel junction. The photo-generated carriers in each of these junctions are transferred to the tunnel junction which serves to join the top and bottom junctions. The tunnel junction has a very small voltage drop when it is conducting. In an optimized cascade cell the terminal current assumes values at the maximum power points of the individual V-I curves of the top and bottom cells. Furthermore, the tunnel junction is optically inactive and its voltage is selected to be equal to or slightly greater than the voltage of the top cell.

Design and optimization of individual materials relative to the top and bottom junctions and the tunnel junctions are necessary for a detailed comparison of the various devices. It must be carried over into the analysis to obtain the optimum design. In fact [15-17], the first of these requires that the junctions be made of each of the p-n junctions and heterojunctions be made of the same material. Other circuit criteria are that the photo-voltages of the top and bottom cells are additive, the tunnel junction is optically inactive so that it does not generate a photovoltage, and the voltage drop across the tunnel junction due to the conduction of the carriers must not be subtracted from the sum of the photo-voltages. Figure 5.2 shows the results of this analysis and computer modeling results shows that the maximum efficiency of the top and bottom cells of the cascade structure are described in the form of the well-established V-I characteristics that is applicable to the junction cells. The individual V-I characteristics (neglecting shunt resistances)

$$I = I_0 \left(\exp \left(\frac{qV}{kT} \right) - 1 \right) \quad (1)$$

$$I = I_0 \left(\exp \left(\frac{qV}{kT} \right) - 1 \right) \quad (2)$$

of the top and bottom cells, respectively, are used in the determination of the reduced equivalent circuit. The nonideality factor (A_i) in the coefficient β_i of the argument of the exponential is

$$\beta_i = \frac{q}{A_i kT} \quad (3)$$

where $i = 1, 2$.

The symbols q , k , and T represent the usual quantities. The voltages V_T and V_B represent the photovoltages of the top and bottom cells, respectively. Similarly, I_{SCT} and I_{SCB} , and I_{DT} and I_{DB} represent the short circuit and saturation currents of the top and bottom cells, respectively. The saturation currents, I_{DT} and I_{DB} , are given by the well-known relationship obtained for a p-n homojunction in which the minority carrier diffusion length is greater than the distance over which carriers must diffuse to be collected by the junction [32].

The net terminal photovoltage, V , obtained from a cascade cell shown in Figure 5.1 is given by

$$V = V_T + V_B - IR_S, \quad (4)$$

$$R_S = R_{TJ} + R_{ST} + R_{SB}, \quad (5)$$

where the forward bias tunnel junction has been represented by resistance, R_{TJ} , and the voltage drop when conducting the terminal current, I , by IR_{TJ} . This is a realistic approximation because in a tunnel junction operating at 300 K and at current density less than 40 mA/cm^2 , the value of IR_{TJ} is on the order of 0.025 V. Equation (4) assumes that the tunnel junction is optically inactive and that a photovoltage is not generated by it.

The terminal voltage can be written from Eqs. (1), (2), and (4) as

$$V = \frac{A_1 kT}{q} \ln \left(\frac{I_{SCT} - I - I_{DT}}{I_{DT}} \right) + \frac{A_2 kT}{q} \ln \left(\frac{I_{SCB} - I - I_{DB}}{I_{DBY}} \right) - IR_S. \quad (6)$$

In a slightly different form this becomes

$$\frac{q}{kT} (V + IR_S) = A_1 \ln \left(\frac{I_{SCT} - I - I_{DT}}{I_{DT}} \right) + A_2 \ln \left(\frac{I_{SCB} - I - I_{DB}}{I_{DB}} \right). \quad (7)$$

For the most general case of $A_1 \neq A_2$, this equation cannot be put in the form of a single-junction solar cell and a simple equivalent circuit such as Figure 5.1(c) is not obtained. However, several special cases are of interest. First, consider the dark I-V characteristics ($I_{SCT} = I_{SCB} = 0$) of the cascade cell when $I_F = -I \gg I_{DT}$ or I_{DB} . Equation (7) then becomes

$$\frac{q}{kT} (V - I_F R_S) = (A_1 + A_2) \ln I_F - A_1 \ln I_{DT} - A_2 \ln I_{DB}. \quad (8)$$

This can be written in the form

$$I_F = I_D \exp \left[\frac{q}{AkT} (V - I_F R_S) \right], \quad (9)$$

$$\text{where } A = A_1 + A_2 \quad (10)$$

$$I_D = I_{DB}^{\sigma_2} I_{DT}^{\sigma_1} \quad (11)$$

$$\text{with } \sigma_1 = \frac{A_1}{A_1 + A_2} \quad (12)$$

$$\sigma_2 = \frac{A_2}{A_1 + A_2}. \quad (13)$$

The form of Eq. (9) is the same as for a single-junction with a diode factor equal to the sum of the individual cell diode factors and a saturation current factor I_D , which is given by Eq. (11).

A second special case is that in which the short circuit currents of the two cells are equal--i.e., $I_{SCT} = I_{SCB} = I_{SC}$, and $I_{SC} - I \gg I_{DT}$ or I_{DB} . In this case Eq. (6) can be simplified to the form

$$I = I_{SC} - I_D \exp \left[\frac{q}{AkT} (V + IR_S) \right], \quad (14)$$

where A and I_D are again defined as in Eqs. (10) and (11). This is the most important special case of the general cascade solar cell since an ideal cascade solar cell has equal short circuit currents from the top and bottom cells. The cascade cell equivalent circuit thus simplifies to that of a single junction solar cell as shown in Figure 5.1(c).

A final special case is that in which $A_1 = A_2$, and Eq. (6) can be written in the form

$$\frac{q}{A_1 kT} (V + IR_S) = \ln \left[\frac{(I_{SCT} - I - I_{DT})(I_{SCB} - I - I_{DB})}{I_{DT} I_{DB}} \right] . \quad (15)$$

An equivalent form of this equation is

$$I = \left(\frac{I_T + I_B}{2} \right) - \left[\left(\frac{I_T - I_B}{2} \right)^2 + I_{DT} I_{DB} \exp \left\{ \frac{q}{A_1 kT} (V + IR_S) \right\} \right]^{1/2} , \quad (16)$$

$$\text{where } I_T = I_{SCT} + I_{DT} \quad (17)$$

$$I_B = I_{SCB} + I_{DB} \quad (18)$$

If the two individual cells are further matched such that $I_T = I_B$, then the equation further simplifies to

$$I = \left(\frac{I_T + I_B}{2} \right) - \sqrt{I_{DT} I_{DB}} \exp \left[\frac{q}{A kT} (V + IR_S) \right] , \quad (19)$$

$$\text{where } A = 2A_1 = A_1 + A_2 . \quad (20)$$

This form of the equation is also obtained at large voltages where the exponential term dominates the square root expression in Eq. (16). It is also noted that this agrees with Eq. (14) for the identical conditions of $A_1 = A_2$.

5.3 Summary

In this work the general I-V equation for a cascade solar cell has been considered as a function of the terminal voltage and current values. If the most general solar cell case is excluded and one considers only cascade cells with equal diode factors for the individual cells or cascade cells with equal short circuit currents, the terminal I-V characteristic can be reduced to the same form as that of a single p-n junction solar cell. Important conclusions from this are that the diode factor of the equivalent cell is the sum of the individual cell diode factors and the equivalent short circuit current factor is between that of the individual cells.

The equivalent series resistance of the cascade cell is the sum of that from the individual cells and the tunnel junction.

The dark I-V characteristic of the composite cell under forward bias can always be expressed in the form of a single-junction cell regardless of the diode factors, and the equivalent diode factor is the sum of the individual cell diode factors.

6.0 PREPARATION AND EVALUATION OF GaAs EPILAYERS ON Ge SUBSTRATES

6.1 Introduction

Germanium substrates are of interest for cascade solar cell applications for several reasons. First, Ge substrates can be obtained in larger areas with better crystalline perfection than GaAs substrates; they offer the potential for greater cost reduction when used with flat plate solar collector systems. Second, the potential exists for forming an additional junction within the Ge substrate material and depending on the upper layer materials, improving the overall conversion efficiency of the cascade structure.

During this work a subcontract was initiated with TRW to prepare GaAs layers on Ge substrate materials. The objective of the subcontract was to obtain high quality epitaxial GaAs layers on single-crystal (111) Ge substrates. Laser annealing was investigated as a technique for improving the crystalline quality of the GaAs layers [33].

The quality of the GaAs layer and of the GaAs/Ge interface is determined by three parameters:

- (1) autodoping of Ge
- (2) cross-diffusion of Ge, Ga, and As
- (3) misfit dislocation density.

The misfit dislocation density was studied by etching and optical microscopy which is described below. Qualitative information about autodoping and cross-diffusion can be obtained summarily by spreading resistance measurements.

6.2 Spreading Resistance Measurement

Autodoping is the dissolution of Ge by the carrier gas in the epitaxial furnace and subsequent deposition in the epitaxial layer. In the case of GaAs epitaxial layers Ge atoms are electrically active, hence the term autodoping. It affects the impurity profile, and therefore can be detected by any technique measuring the impurity profile. Cross-diffusion refers to the diffusion of Ga or As atoms into the Ge lattice or of Ge into the GaAs lattice while the wafer is at elevated temperatures in the epitaxial furnace. Cross-diffusion also affects the profile of

electrically active impurities. Cross-diffusion is confined to a narrow layer around the interface of the heteroepitaxial layers while autodoping can affect the impurity distribution in the entire epitaxial layer.

The spreading resistance (SR) profile of one of the GaAs/Ge wafers is shown in Figure 6.1. The SR is constant for the first 6 μm below the surface, then falls off smoothly by two orders of magnitude between 6.0 and 9.2 μm . Between 14 and 18 μm depth the SR increases again from 20 to 30 Ω , and stays constant at this value for greater depths.

Obviously the abrupt SR change between 9.2 and 9.6 μm represents the heteroepitaxial interface. The abrupt increase of the SR at 9.6 μm is quite remarkable and suggests that cross-diffusion of Ga or As into the Ge substrate is insignificant. On the other hand, the smooth SR increase between 6.0 and 9.2 μm indicates some additional active impurities in this layer. These may have been introduced by autodoping or diffusion of Ge into the GaAs lattice. A single SR measurement cannot distinguish between these two phenomena. The backsides of the Ge wafers were coated with polycrystalline silicon to reduce autodoping.

In summary, the Ge substrate appears to be unaffected by the epitaxial growth process. The epitaxial layer itself is degraded within the layer about 3 μm from the GaAs/Ge interface. The top 6 μm of the epitaxial layer has a constant resistivity.

6.3 Etching/Dislocation Experiment

The intent of the laser annealing of the GaAs/Ge wafers was to reduce the density of misfit dislocations which are expected to be present in the GaAs layer due to the small but nonvanishing lattice mismatch.

In silicon heteroepitaxial wafers misfit dislocations can be brought out by certain etches. For GaAs/Ge wafers there are no reports of successful etching to make misfit dislocations observable. Nevertheless, an etching experiment was formed in order to search for some other linear defect intersecting at the surface using the A/B etch recommended by Stirland and Straugham [34] consisting of

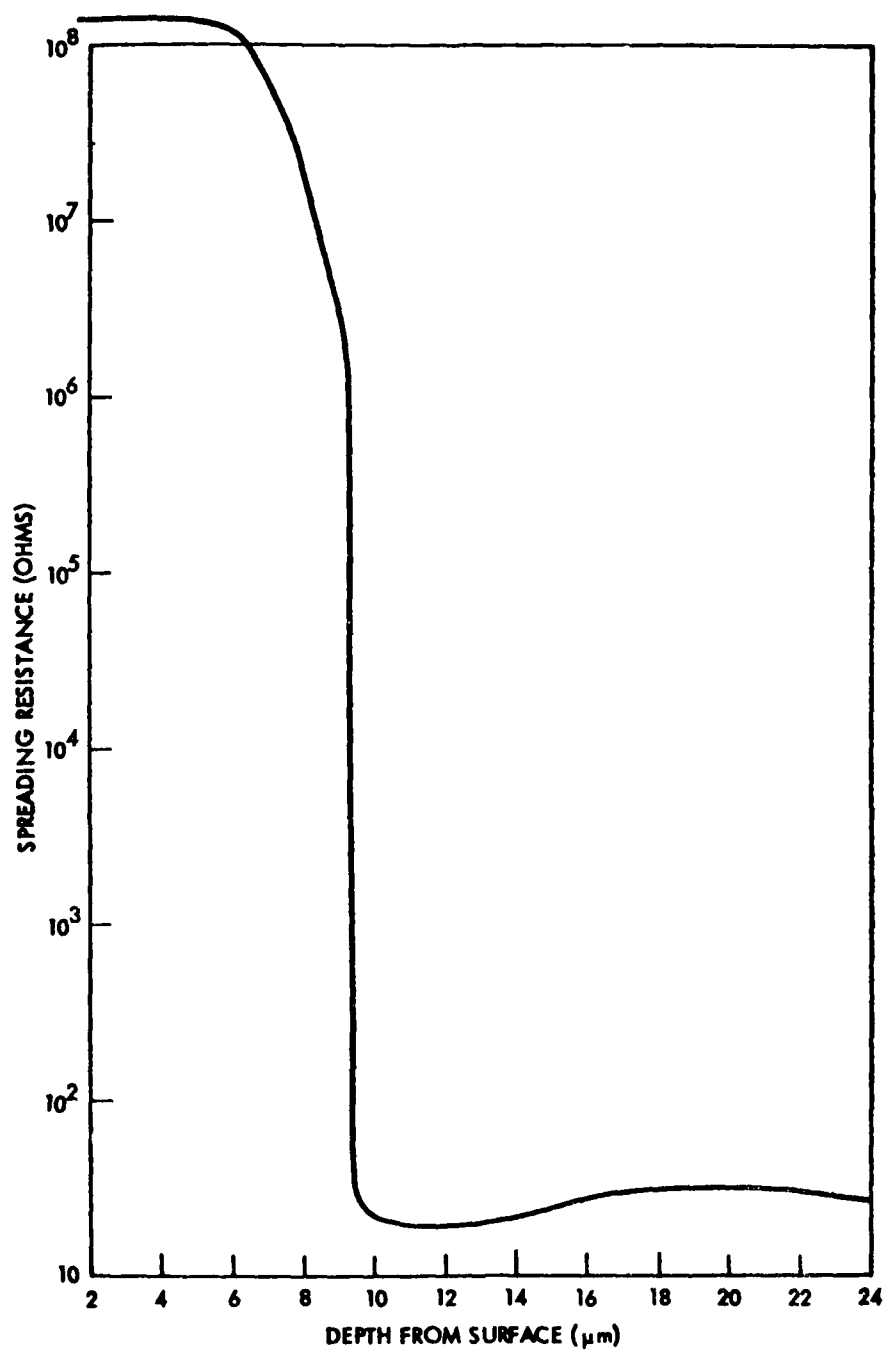


Figure 6.1. Spreading resistance curve of GaAs/Ge heteroepitaxial wafer. The stepsize was $\Delta x = 10 \mu\text{m}$, the slope of the bevel was 50:1, so that each step represents a depth increment of $\Delta d = 0.2 \mu\text{m}$.

8 mg	AgNO ₃
2 ml	H ₂ O
1 g	CrO ₃
1 ml	HF

Mix, stir, and apply for 30 seconds.

Etching was done on (1) some as-received wafers, (2) some wafers laser annealed with ruby laser pulses between 0.5 and 4.0 j/cm² pulse energy, and (3) one wafer that prior to laser annealing had been ion-implanted with 5×10^{15} As⁺/cm² at 200 keV. This dose and energy of ion implantation is well above the threshold at which silicon becomes amorphous. The majority of the successful laser experiments in silicon are reported for amorphous material. The question arose whether the laser annealing of GaAs/Ge wafer may be helped by first driving the wafer amorphous, and it was hoped that the above dose and energy of implantation was sufficient to convert the top of the GaAs layer into the amorphous state.

The microscope observations after etching of the three types of wafers are summarized in Tables 6.1 and 6.2.

A summary of the effects of laser annealing is presented in Figure 6.2. In the non-ion-implanted wafer for ruby laser pulse energies above 0.75 and below 2.5 j/cm², the surface is covered with an array of cracks. They probably prohibit the use of these wafers for device applications. Above 2.5 j/cm² the surface shows wrinkles. This suggests that the surface has been molten and has re-solidified nonuniformly.

The observations of the ion-implanted wafers were the same except that the limits between the three regimes are shifted downward. The regime with cracks starts at about 0.5 j/cm² and extends to 1.5 j/cm². Below 0.5 j/cm² no visible alteration was observed of the laser anneal; about 1.5 j/cm² cracks are absent and the surface is covered with wrinkles.

In summary, the etching revealed the following:

- (1) There is a regime of laser pulse energies for which the surface of the GaAs/Ge wafers is covered with cracks.
- (2) At higher energies the surface is covered with wrinkles, and the boundary of each laser pulse impact area is covered with cracks.

Table 6.1. Effect of Ruby Laser Anneal on As-Received GaAs/Ge Wafers. The wafers were A/B etched for 30 sec and studied by optical microscopy.

Laser Anneal Energy (j/cm ²)	Effect
(As received)	Individual and linear arrays of triangular-shaped dislocation growth planes (DGPs). The 1-d defect arrays appear to originate from scratches at the interface.
0.5	No discernible difference to as-received wafers except possibly some DGSs are molten.
1.0	DGPs appear the same as in the 0.5 j/cm ² anneal area. Area is covered with fine cracks, which may obscure wrinkling.
1.5	Area covered with a dense array of heavy cracks. DGPs appear to be molten. A small fraction of the non-DGP surface is molten.
2.0	All DGPs are molten but not dissolved. Non-DGP surface about 50% molten. No cracks except at the laser pulse boundary.
3.0	Entire surface is molten. Cracks in the transition region only. Some DGPs dissolved.
4.0	Entire surface is molten. Heavy array of cracks in the transition region. Few DGPs appear to be partially dissolved. Wrinkles are higher than in the 3.0 j/cm ² area, particularly around the edges.

Table 6.2. Effect of Laser Anneal on Ion-Implanted (5×10^{15} As⁺/cm², 200 keV) GaAs/Ge wafers. The wafers were A/B etched for 30 sec and studied by optical microscopy.

Laser Anneal Energy (j/cm ²)	Effect
0	Undistinguishable from non-implanted, non-annealed surface.
0.4	Most of the area is covered with cracks. Track density lower towards edge than in the center. No sign of melting, also not within DGPs.
0.6	Crack density higher than in 0.4 j/cm ² area. No melting; DGP not affected.
0.8	Cracks very dense. No melting; DGPs not affected.
1.0	Cracks very dense, seen without etching. Small fraction (~2%) of surface molten. Some DGPs also possibly molten.
1.5	Surface 75% molten. Cracks only in non-molten areas; wrinkles in molten areas. Some DGPs molten.
2.0	Entire surface molten; heavy cracks at boundary. All DGPs molten, not dissolved.
2.5	Like 2.0 j/cm ² area, surface more wrinkled, edges cracked.

GaAs/Ge

SUMMARY OF LASER ANNEAL WAFERS

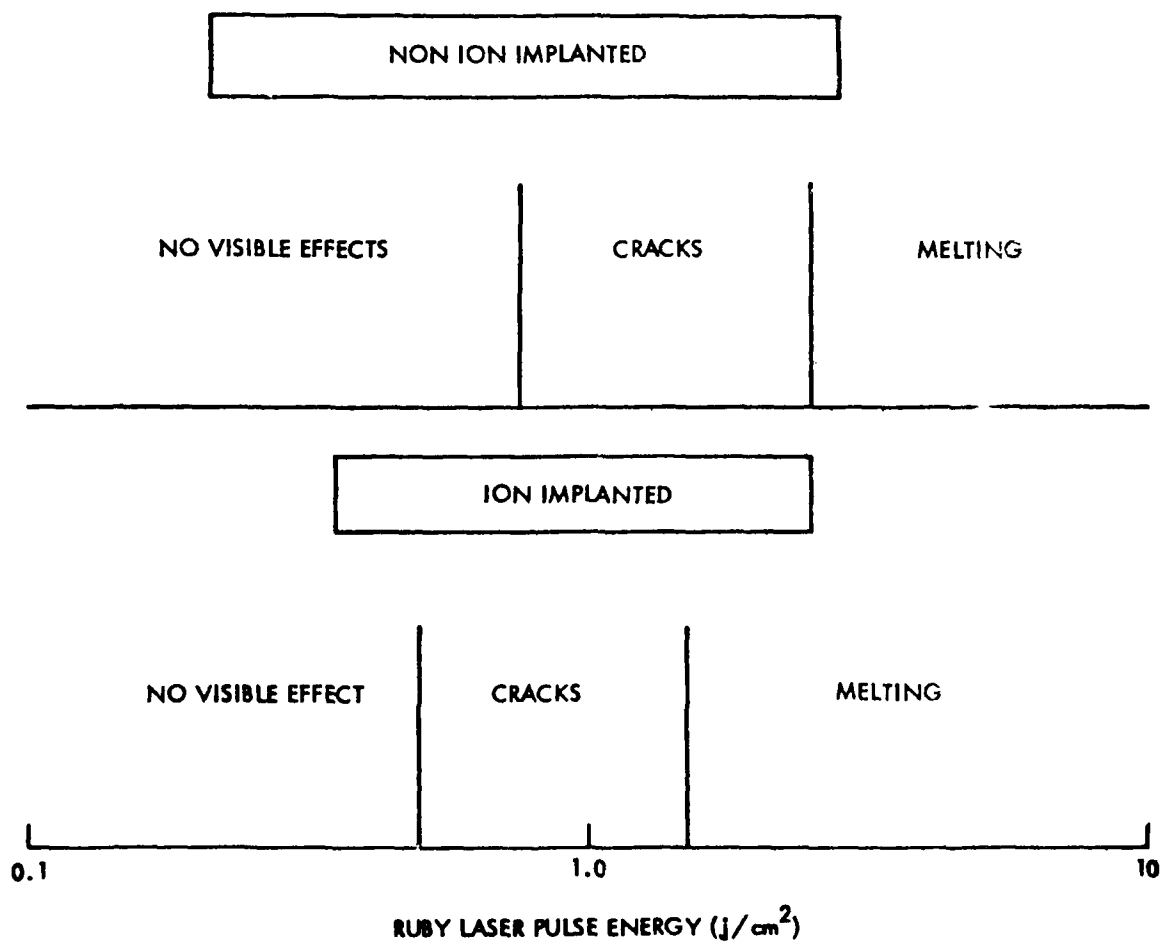


Figure 6.2. Ruby laser pulse energy (J/cm^2)

- (3) At the node of each DGP there is a dislocation that probably extends downward to a defect at the GaAs/Ge interface.
- (4) The triangular defects (DGPs) were not dissolved by the laser annealing, not even at the high energies at which the entire surface was molten. The dislocation at the node of some DGPs appears to be dissolved at the highest laser energy used.
- (5) No general statement can be made about the density and reduction of the misfit dislocations.

6.4 Discussion

The results of the study suggest that laser annealing of GaAs/Ge wafers should be done at energies below about 0.75 J/cm^2 . At higher energy densities the surface is covered with cracks, and at even higher energies melting sets in, leaving the surface wrinkled and each laser pulse impact area surrounded by a strip of cracks. These cracks alone probably make the use of these wafers impossible for device applications. Moreover, as suggested by other workers [35], actual crystal damage may have occurred at these high energy densities. Ion implantation per se does not seem to alter these results significantly. In particular, ion implantation does not seem to offer any advantage to the laser annealing process.

It has been found that at power densities above 20 MW/cm^2 laser pulses damage the GaAs wafer [35]. Uneven solidification and damage of the crystal lattice was seen for single crystals as well as for ion-implanted samples and was attributed to loss of arsenic at high power densities. The authors used a frequency-doubled Nd:YAG laser, radiating at 2.34 eV. The absorption coefficient of single-crystal GaAs at 2.34 eV is higher than at ruby laser wavelength by about a factor of two. This difference may account for a higher threshold for lattice damage when a ruby laser is used. Assuming a pulse length of $\tau = 15 \text{ nsec}$ for our experiments, the quoted threshold is 20 MW/cm^2 . This suggests that in cases where a wrinkled surface was observed, a loss of arsenic may have occurred and the gallium-rich liquid may have recrystallized in a disordered lattice.

Unfortunately, misfit dislocation could not be observed in our study. The purpose of the laser annealing was to reduce the number of misfit dislocations, which are often present in heteroepitaxial wafers. It is hoped that this purpose has been achieved, but this cannot be verified.

These laser anneal and etching experiments represent a first step into an unknown direction. More experiments are needed in order to develop this technique. Inferring from the impressive successes of laser annealing silicon wafers, the prospects for crystalline improvement of GaAs/Ge heteroepitaxial wafers by laser annealing are good and warrant further effort. It is recommended that further work be done in conjunction with a technique by which misfit dislocations can be observed directly.

6.5 RTI Evaluation of GaAs/Ge Samples

6.5.1 Surface Characteristics

Sample surfaces appeared shiny but had a very high density of pits. Laser-annealed samples looked cloudy, indicating some permanent damage to the surface resulting from the annealing process. Due to the presence of these pits, such samples are probably not adequate as substrates for device-quality epitaxial layers.

GaAs epilayers were uniform in thickness: about 10 μ thick for one set of wafers and 5 μ thick for another set. A cross-sectional view of a cleaved and stained sample is shown in Figure 6.3. Chemical testing of the sample surface indicates that the As-face is up and the Ga-face is at the interface with the Ge substrate.

6.5.2 X-Ray Diffraction

X-ray diffraction and back Laue diffraction patterns were used to study the orientation and crystalline quality of the GaAs epilayer. The back Laue pattern shows diffraction spots without any diffraction rings, indicating that the GaAs layer is a single crystal. The diffraction pattern from the diffractometer is shown in Figure 6.4 and indicates that the GaAs is epitaxially grown on the (111) Ge substrate. The K_{11} and K_{12} peaks of the GaAs are resolved, indicating good crystalline quality. Also, the width at half maximum of the GaAs peaks are comparable to that

AD-A083 092

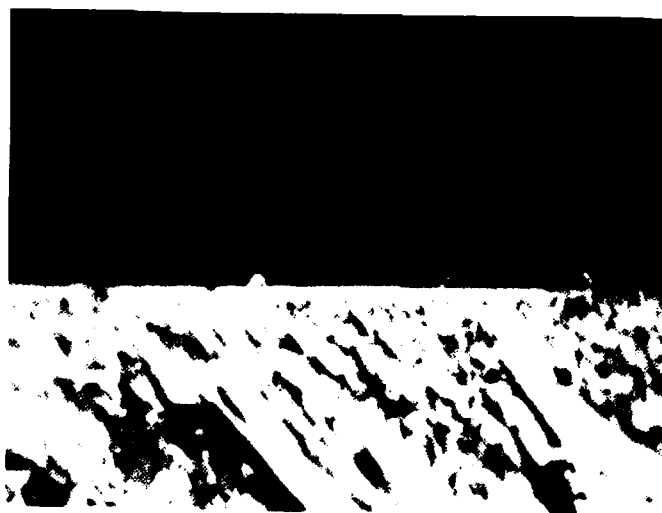
RESEARCH TRIANGLE INST RESEARCH TRIANGLE PARK N C F/G 10/2
DEVELOPMENT OF HIGH EFFICIENCY STACKED MULTIPLE BANDGAP SOLAR C--ETC(U)
OCT 79 S M BEDAIR, J R HAUSER, M F LAMORTE F33615-78-C-2077
RTI-41U-1678 AFAPL-TR-79-2116 NL

UNCLASSIFIED

242
AL
AUGUST



END
DATE
FILMED
5 80
DTIC



← 5 μ GaAs Layer

← Ge Substrate

A-B ETCH TRW9 Ge(111)GaAs ep. $\sim 5.0\mu$

Figure 6.3. Cleaved and strained cross-section of GaAs/Ge wafer.

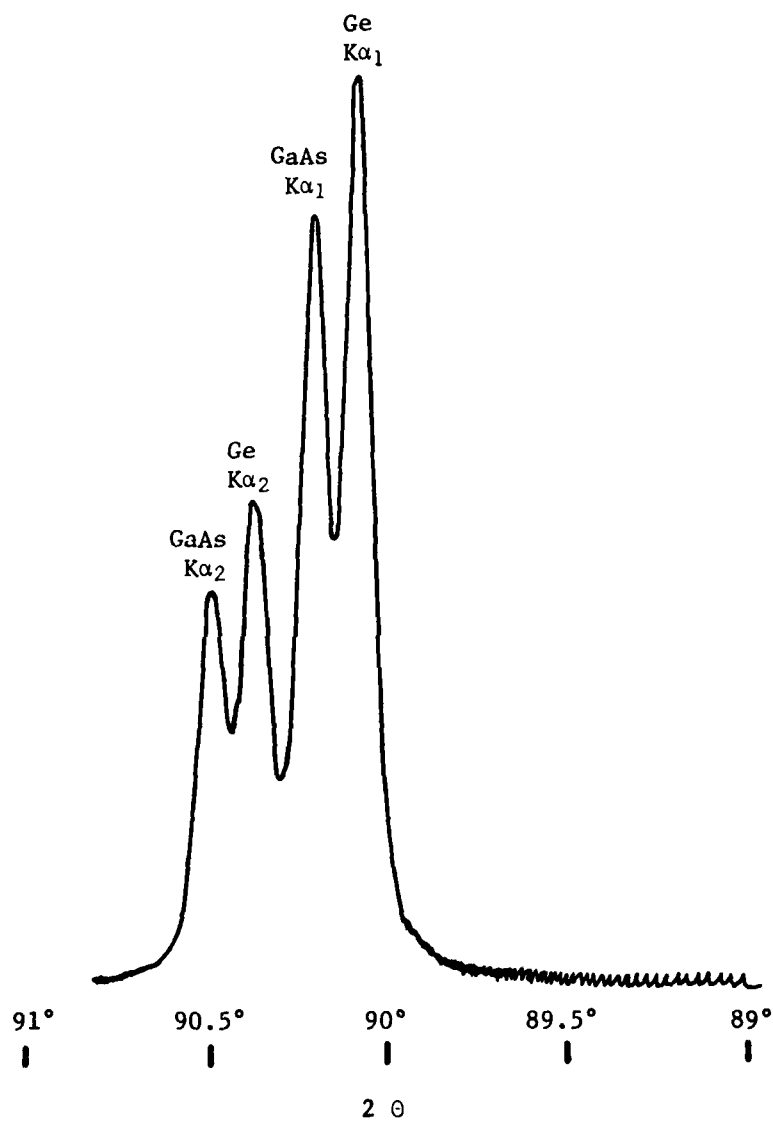


Figure 6.4. Diffraction pattern for GaAs/Ge as-grown samples.

of the substrates, indicating that the GaAs layer is uniform in composition. For those wafers that had gone through the laser annealing cycle, the same results were mainly obtained.

6.5.3 Photoluminescence

Photoluminescence measurements were made at room temperature for both as-grown and laser-annealed samples, and the results are given below.

<u>Sample</u>	<u>PL Peaks</u>	<u>FWHM</u>	<u>Relative Intensity</u>
As-grown	1.42	77	194
	1.04		5
Laser-annealed	1.411	51	34
	1.04		3

The main peaks in both cases correspond to GaAs; however, the laser-annealed samples exhibited poor luminescence in comparison with the as-grown one. This may be a result of the excessive laser power density. This high power density can result in local melting of the top surface of the GaAs layer or introduce a high density of lattice defects that will degrade the lifetime. There is a secondary peak observed at 1.04 eV in both samples; however, its origin is uncertain.

6.5.4 Summary

In summary, the samples supplied by TRW are epitaxially grown GaAs on Ge substrate in the (111) orientation. Sample surfaces are very pitted, and this makes them unsuitable for use as substrates for epitaxial growth of device-quality material.

The laser annealing process used seems to be inadequate. However, an attempt will be made to grow GaAs p-n junctions on these samples.

REFERENCES

1. J. J. Foferski, *J. Appl. Phys.* 27:96 (1956).
2. J. J. Wysocki and P. Rappaport, *J. Appl. Phys.* 31:571 (1960).
3. H. J. Hovel, "Solar Cells," Vol. II, *Semiconductors and Semimetals*, A. C. Beer and R. K. Willardson, Ed., Academic Press, Inc., New York, N.Y. (1976).
4. P. M. Dunbar and J. R. Hauser, *Solid-State Elec.* 19:95 (1976).
5. J. R. Hauser and P. M. Dunbar, *IEEE Trans. on ED*, ED-24:305 (1977).
6. H. J. Hovel, *IBM J. Res. Dev.* 22:112 (1978).
7. J. E. Sutherland and J. R. Hauser, *IEEE Trans. on ED*, ED-24:363 (1977).
8. M. F. Lamorte and D. Abbott, *Proc. Thirteenth Photovoltaic Spec. Conf.*, 874 (1978).
9. L. M. Fraas and R. C. Knechtli, *Proc. Thirteenth Photovoltaic Spec. Conf.*, 886 (1978).
10. *Novel Concentrator Photovoltaic Converter System Development*, Final Report under Sandia Contract 07-7149, Research Triangle Institute, Research Triangle Park, N.C. (March 1979).
11. R. L. Moon, L. W. James, H. A. VanderPlas, T. O. Yep, G. A. Antypas, and Y. Chai, *Proc. Thirteenth Photovoltaic Spec. Conf.*, 859 (1978).
12. K. W. Mitchell, *Technical Digest*, IEEE International Electron Devices Meeting, 254 (1978).
13. J. E. Andrews and M. A. Littlejohn, *Study of II-IV-V₂ Chalcopyrite Semiconductors for Solar Cell Applications* (March 1979).
14. G. M. Olsen, C. J. Nuese, and R. T. Smith, *J. Appl. Phys.* 49:5523 (1978).
15. S. M. Bedair and M. F. Lamorte, *Extended Abstracts*, 154th Electrochemical Society Meeting, Pittsburgh, PA, 779 (1978).
16. G. B. Stringfellow, *J. Appl. Phys.* 43:3455 (1972).
17. A. G. Sigai, C. J. Nuese, R. E. Enstrom, and T. Zamerowsbi, "Vapor Growth of InGaP for P-N Junction Electroluminescence," *J. Electrochem. Soc.* 120(7):947 (1973).

18. S. M. Bedair, M. G. Lamorte, J. R. Hauser, and K. W. Mitchell, *Proc. Int. IEEE Elec. Devices Meeting*, Washington, D.C., 250 (1978).
19. S. M. Bedair, M. F. Lamorte, and J. R. Hauser, *Appl. Phys. Lett.* 34:38 (1979).
20. M. Ilegems, B. Schwartz, L. A. Koszi, and R. C. Miller, *Appl. Phys. Lett.* 33:629 (1978).
21. K. K. Shih and G. D. Pettir, *J. Electron. Mat.* 391 (1974).
22. A. J. Springthorpe, F. D. King, and A. Becke, *J. Electron. Mat.* 4:101 (1975).
23. R. E. Nahory, M. A. Pollack, J. C. DeWinter, and K. M. Williams, "Growth and Properties of Liquid Phase Epitaxial $\text{GaAs}_{1-x}\text{Sb}_x$," *J. Appl. Phys.* 48(4):1607-1614 (April 1977).
24. R. L. Moon, G. A. Antypas, and Y. G. Chai, "Continuous Compositional Grading by LPE in Al-Ga-V Quaternary Alloys," *Inst. Phys. Conf. Ser.* 45:78-88 (1979).
25. S. K. Brierly and C. G. Fonstad, "Silicon-Doped Gallium Arsenide Antimonide Electroluminescent Diodes Emitting to 1.06 μm ," *J. Appl. Phys.* 46(8):3678-3680 (August 1975).
26. H. Kressel and J. K. Butler, *Semiconductor Lasers and Heterojunction LED's*, Academic Press, New York, NY, 301 (1977).
27. P. Kordos, R. A. Powell, W. E. Spicer, and G. L. Pearson, "Growth and Properties of Graded Bandgap $\text{Al}_x\text{Ga}_{1-x}\text{As}$ Layers," *Appl. Phys. Lett.* 34(6):366-368 (March 1979).
28. J. M. Woodall and H. J. Hovel, "LPE Growth of $\text{GaAs-Ga}_{1-x}\text{Al}_x\text{As}$ Solar Cells," *J. Crystal Growth* 39:108-116 (1977).
29. *Solar Cell Design Study*, Final Report AFAL-TR-77-74, Contract No. F33615-76-C-1283, Research Triangle Institute, May 1977.
30. M. F. Lamorte and D. Abbott, "Analysis of a Two-Junction Monolithic Solar Cell in a Structure Using $\text{Al}_u\text{Ga}_{1-u}\text{As}$ and $\text{Ga}_v\text{In}_{1-v}\text{As}$," *Twelfth IEEE Photovoltaic Spec. Conf.*, Baton Rouge, LA, November 15-18, 1976.
31. M. F. Lamorte and D. Abbott, "Analysis of AlGaAs-GaInAs Cascade Solar Cell under AMO-AM5 Spectra," *Solid State Elec.* 22:467-473 (1979).
32. J. P. McKelvey, *Solid State and Semiconductor Physics*, Harper Row, New York, NY, 1966.
33. W. K. Hojber, et al., "Laser Irradiation of Silicon Containing Misfit Dislocations," *Appl. Phys. Lett.* 34(10):690, May 15, 1979.

34. D. J. Stirland and B. W. Strangham, "Review of Etching and Defect Characterization of Gallium Arsenide Substrate Material," *Thin Solid Films* 31:139 (1976).
35. Raphael Tsu, et al., "Laser Induced Recrystallization and Damage in GaAs," *Appl. Phys. Lett.* 34(2):153, January 15, 1979.